University of Southampton

Final Thesis

Mechatronics Engineering Group

Cell based applications of acoustofluidic assisted interactions at surfaces

Author:
Filip Plazonic

Supervisors:
Dr. Peter Glynne-Jones
Prof. Martyn Hill
Dr. Dario Carugo

December 17, 2019

Abstract

This thesis looks at development of acoustic devices that utilise ultrasound and its interaction with particles near surfaces. The devices are aimed at application in three fields: detection, diagnosis, and eradication. To capture pathogens and cells for capture, a thin-reflector device was combined with a specific antibody coating applied to the boundary between the reflector and fluid layers. The device was optimised and found to have a strong resonance that can push even small 1 µm sized objects to the surface to be captured. A suitable substitute in the detection experiments for anthrax was chosen in *Bacillus globigii* (BG) spores. They were stained with a fluorescent dye and used to find the limit of detection of the device. The system was also evaluated for the capture of basophils, providing insight into the possibilities of using the same device for allergy diagnosis. The aim was to capture as many basophils as possible in the shortest amount of time, all while maintaining ease of use. For biofilm eradication, a new device was constructed that can create ultrasonic travelling waves that push a microbubble and antibiotic solution into a biofilm, which was then analysed to find what proportion of bacteria survived. A variety of important parameters were considered and tested to find the optimal strategy for improving antibiotic performance with ultrasound stimulated microbubbles.

Contents

List of Figures

List of Tables

Declaration of authorship

I, FILIP PLAZONIC, declare that this thesis titled "*Cell based applications of acoustofluidic assisted interactions at surfaces*" and the work presented in it are my own. I confirm that:

- This work was done wholly or mainly while in candidature for a research degree at this University.
- Where any part of this thesis has previously been submitted for a degree or any other qualification at this University or any other institution, this has been clearly stated.
- Where I have consulted the published work of others, this is always clearly attributed.
- Where I have quoted from the work of others, the source is always given. With the exception of such quotations, this thesis is entirely my own work.
- I have acknowledged all main sources of help.
- Where the thesis is based on work done by myself jointly with others, I have made clear exactly what was done by others and what I have contributed myself.
- Parts of this work have been published as:
  - D. Carugo, B. Hammarström, U. Jonnalagadda, J. Lei, F. Plazonic, W. Messaoudi, Z.I. Shaglwf, P. Glynne-Jones & M. Hill (2017). *Acoustofluidic manipulation of biological bodies: Applications in medical and environmental diagnosis.* The Journal of the Acoustical Society of America, 141, 3504-04. doi:10.1121/1.4987340
  - D. Carugo, B. Hammarström, U. Jonnalagadda, J. Lei, F. Plazonic, W. Messaoudi, Z.I. Shaglwf, P. Glynne-Jones & M. Hill (2017). *Acoustofluidic manipulation of biological bodies: Generation, visualization, and stimulation of cellular constructs.* The Journal of the Acoustical Society of America, 141, 3504-04. doi:10.1121/1.4987340

- C.G. Rose, F. Plazonic, H. Morgan, E. Eren, X.L. Zhang, D. Carugo, P. Glynne-Jones, L.C.K. Lau, M. Hill & A.F. Walls (2017). *Development of an Acoustofluidic Platform for Rapid Basophil Enrichment.* Journal of Allergy and Clinical Immunology, 139, AB125-AB25.
- F. Plazonic, D. Carugo, M. Hill & P. Glynne-Jones. *Acoustophoretic manipulation for use in particle detection*, in The 13th Conference on Acoustofluidics, DTU, Lyngby, Denmark, 2016
- F. Plazonic, C. Rose, X. Zhang, A. Walls, M. McDonnell, D. Carugo, M. Hill & P. Glynne-Jones. *Particle capture and detection using acoustophoresis and antibody binding*, in The 14th Conference on Acoustofluidics, University of California San Diego, USA, 2017
- F. Plazonic, C. Rose, L. Lau, X. Zhang, A.F. Walls, D. Carugo, M. Hill & P. Glynne-Jones. *Basophil purification using a thin-reflector acoustic resonator*, in The 15th Conference on Acoustofluidics, Université de Lille, France, 2018
- F. Plazonic, C. Hind, M. Gray, M. Hill, E. Stride, P. Glynne-Jones, M. Sutton & D. Carugo. *Ultrasound-activated microbubbles enhance the activity of low-concentration gentamicin against Pseudomonas aeruginosa biofilms*, in The 23rd European Symposium on Ultrasound Contrast Imaging, Rotterdam, Netherlands, 2018

Signed: _____

Date: 28.10.2019.

Acknowledgements

I would like to thank my supervisors Peter Glynne-Jones, Martyn Hill, and Dario Carugo for providing guidance and many interesting discussions during this long period. Without their help, patience, and willingness to tolerate numerous impromptu meetings this thesis would not be where it is today.

I am grateful to the opportunities and help that was provided by the team at Public Health England which includes Charlotte Hind and Mark Sutton. This also extends to Gareth Lutheryn for stepping in to help at the final moments of the project.

I would also like to acknowledge my other collaborators, Chloe Rose, Andrew Walls, and Laurie Lau, all of whom have helped bring the basophil project to where it currently is.

This research was made possible by the grants provided by EPSRC and NAMRIP, and for that I say: "Cheers."

I have my friends to thank for all the ridiculous interactions we had throughout. They made this part of my life a lot more enjoyable.

My family has always provided me with all the support I can hope for and more. I am immensely grateful to my Mom and Dad for giving me the opportunity to study in this PhD and encouraging me to push myself further, and to my brother who has been my no. 1 fan since this whole endeavour started.

Above all else, to my wife, Valerija: thank you for the love and support and an amaying sense of humour you have provided throughout our life together. They have carried me over every obstacle and always managed to put a smile on my face. And to our cat Freddie, who's indecisiveness and unwarranted interruptions provided hours of fun whether needed or not.

Abbreviations

AB Antibiotic

ABS Acrylonitrile butadiene styrene

AMR Anti-microbial resistance

BAT Basophil activation test

BSA Bovine serum albumin

CAD Computer aided design

CF Cystic fibrosis

CFU Colony forming unit

CNC Computer numerical control

DAPI 4',6-diamidino-2-phenylindole

DBPCFC Double-blind, placebo-controlled food challenge

DFU Diabetic foot ulcer

DMSO Dimethyl sulfoxide

DSEPC 1,2-dioleoyl-*sn*-glycero-3-ethylphosphocholine

DSPC 1,2-distearoyl-*sn*-glycero-3-phosphocholine

EDTA Ethylenediaminetetraacetic acid

EPS Extracellular polymeric substances

FACS Fluorescent activated cell sorting

FEA Finite element analysis

FFT Fast Fourier transform

FITC Fluorescein isothiocyanate

FMLP Formyl-methionyl-leucyl-phenylalanine

FSC Forward scatter

GTR Glass carrier layer thin reflector resonator

HW Half wave

HW/TR Half-wave/thin-reflector

IDT Intradermal test

KIT Karlsruhe Institute of Technology

MACS Magnetic-activated cell sorting

MB Microbubble

MIC Minimum inhibitory concentration

MTR Mirror thin reflector resonator

NO Nitric oxide

NPV Negative predictive value

OD Optic density

PBS Phosphate-buffered saline

PDMS Polydimethylsiloxane

PE Phycoerythrin

PEG40s Polyoxyethylene (40) stearate

PLA Polylactic acid

PNP Peak negative pressure

PP Polypropylene

PPV Positive predictive value

PRF Pulse repetition frequency

PS Polystyrene

PSF Point-spread funtion

PT Provocation test

PVC Polyvinyl chloride

PVDF Polyvinylidene fluoride

PZT Lead zirconate titanate

QS Quorum sensing

QSI Quorum sensing inhibition

QW Quarter wave

R1 Region one

RT Real-time

SAW Surface acoustic wave

SD Standard deviation

sIgE Serum immunoglobulin E

SPT Skin prick test

SS Stainless steel

SSC Side scatter

SWNT Single-wall carbon nanotubes

Th1 Type 1 helper T-. cells

Th2 Type 2 helper T-. cells

TR Thin-reflector

TSB Tryptic soy broth

TXRED Texas red

US Ultrasound

USW Ultrasound standing wave

WAO World Allergy Organisation

WHO World Health Organisation

Symbols

a Radius of particle

$u_{average}$ Average velocity

B Bulk modulus

c Speed of sound

c_0 Speed of sound in surrounding fluid

ρ Density

ρ_0 Density of surrounding fluid

$\tilde{\rho}$ Density ratio

ρ_p Density of particle

d Particle diameter

E_{kin} Kinetic energy density

E_{pot} Potential energy density

f Frequency

f_1, f_2 Correction factors

F_{rad} Radiation force

g Gravitational acceleration

k Wavenumber

κ Compressibility

κ_0 Compressibility of surrounding fluid

$\tilde{\kappa}$ Compressibility ratio

κ_p Compressibility of particle

p Pressure

p_{max} Pressure amplitude

p_{tot} Total pressure of both waves

R Half of channel height

r Distance from centreline

S Siemens

s_0 Displacement amplitude

s_1 Displacement of incident wave

s_2 Displacement of reflected wave

s_{tot} Total displacement of both waves

t Time

u_{max} Terminal velocity

U Force potential

u, v Velocity

V Volume

μ Dynamic viscosity

V_{pp} Peak-to-peak voltage

λ Wavelength

x Position along the wave

Chapter 1

Introduction

This thesis explores three related applications of the interactions of ultrasound with biological particles close to and in contact with surfaces. The three applications (Chapters 4, 5, 6 respectively) are:

a) The capture of anthrax spores from a suspension for rapid detection using a thin reflector acoustic mode and an antibody coating.

b) The capture of (much larger) Basophils from blood samples for allergy testing.

c) The disruption of bio-films through mechanical forces derived from bubbles actuated ultrasonically at a surface. Initially similar acoustic devices of the sort described and characterised in Chapter 3 were planned for all three applications, however further device development is also described in chapter 6.

1.1 Pathogen detection

1.1.1 Water-borne pathogens

Poor water quality is estimated to be a cause of 3.1 % deaths [1] and is a considerable cost in healthcare [2]. Rapid detection of pathogens in water is vitally important, not only for the public health [3], but for industry as well [4]. Furthermore, pathogens inside water can compromise the quality of a product in several disperse industries (food, pharmaceutical, chemistry, textile, etc.) [5, 6]. Fast pathogen detection is essential for early prevention of water spread diseases that could lead to a loss of lives, livelihood, and capital.

There are well over 30 pathogens that are commonly the cause of water-borne diseases. Some of the most common and dangerous are: dysentery, cholera, and *Escherichia coli*, each shown in figure 1.1. Each of them can be very dangerous and lethal to humans, especially if there is no access to healthcare facilities. The bacteria responsible for dysentery is *Shigella dysenteriae*. Infection doses are very low, only between 10 and 100 organisms are

needed may lead to infection, whose symptoms are cramps, fever, and watery diarrhoea in the early stages of the disease. As it progresses it may lead to ulceration which leads to bloody diarrhoea and a high concentration of neutrophils in the stool. It eventually leads to death. Each year, over 2 million infections occur, of which 600, 000 result in death, most of which in developing countries. Children under 10 years of age are at most risk [7, 8]. Cholera is the result of a bacteria called *Vibrio cholerae*, and its symptoms include loose, watery, mucus-flecked stools which can cause a patient to lose as much as 10-15 litres of liquid per day. Cholera outbreaks still continue to occur in many areas of the developing world where as many as 60 % of untreated patients may die. If, however, treated, the mortality rate drops to below 1 % [7, 9]. *E. coli* strains can cause diarrhoea that is, in most cases, mild and non-bloody, but in up to 7 % of the cases it can become highly bloody and can lead to death by developing haemolytic uraemic syndrome which causes acute renal failure and haemolytic anaemia. Children below the age of 5 are at most risk, and only 100 organisms are needed to develop an infection [7, 10]. From these three examples it can be seen how without the presence of proper treatment facilities, such as in the developing world, the infection and mortality rates are much higher [7].

In the more developed and populated areas of the country, there are enough resources to ensure enough samples are taken through the day and processed in a nearby lab to provide a relatively quick and constant throughput of safety data [12]. But even when all of the resources are available it can take anything between 6-24 hours to get a result on the most common pathogens, due to the methods that are used and prescribed by the World Health Organisation (WHO) [7, 13]. During this time people can potentially be exposed to a pathogen and in very populated areas that can lead to numerous infections. In low-income countries and areas that do not have access to state-of-the-art laboratories or means to provide constant and continuous monitoring, infections are more common and can greatly spread before they are detected. A big reason for this is poor sanitation, but until that is improved quick detection is key. The majority of water-disease related deaths comes from these areas and it is expected that by 2025 half of the world population will not have access to clean, safe water [14].

The goal of water-borne pathogen detection is a quick and cheap device that could provide results in less than an hour, and is easy to use so people with all backgrounds could understand how to operate it and how to interpret the results. Currently the most established methods, recommended by WHO [7] are based on cell culturing, the oldest detection method, which can provide a very low detection limit but may take up to a week to give a positive result [6, 15], and on various immunoassay methods which, while faster, require a certain expertise to operate [16].

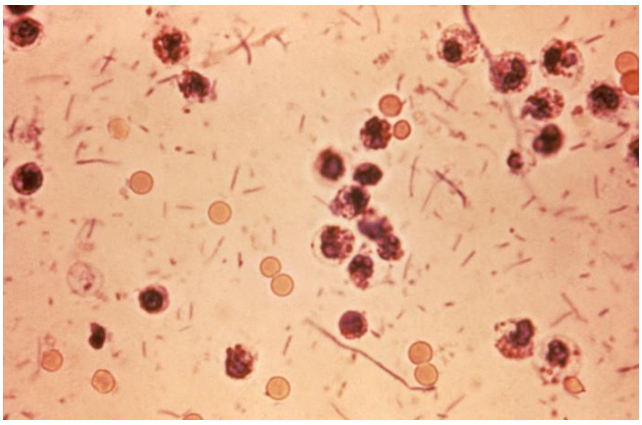

(a) Shigella dysenteriae *in a stool sample [11]*

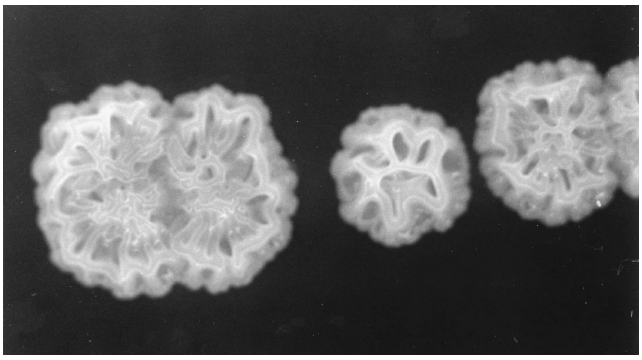

(b) Vibrio cholerae *colony on agar [9]*

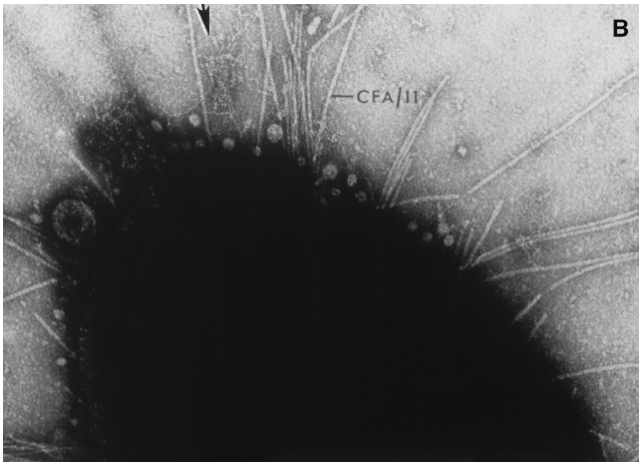

(c) Escherichia coli *through transmission electron miscroscopy [10]*

Figure 1.1: Images of some common water-borne pathogens

1.1.2 Anthrax detection

Bacillus anthracis is a large oblong shaped Gram-positive, non-motile, aerobic bacteria from the *Bacillus* family. It is, on average, 1.42 μm long and 0.81

μm wide [17], and is non-haemolytic on horse's and sheep's blood agar. When the bacteria is situated in nutrient-poor conditions it forms resistant spores which can survive in soil for decades. The species got its name for the ability to cause black, coal-like cutaneous eschars (the name comes from the Greek word *anthrakis* which stands for coal) [18]. Figure 1.2 shows the bacteria in its spore form (1.2a), in both solitary form and as part of a chain (1.2b), and embedded in human tissue (1.2c).

Throughout most of history, anthrax as a disease has been associated with people who work with livestock, or with industries where inhalation is an issue (wool or leather processing plants). Since the attacks that followed the September, 11 terrorist attacks, that mailed dry anthrax spores in envelopes, anthrax become more associated with bioterrorism again [1] which gave a renewed interest in anthrax research and a sense of urgency for developing a rapid testing tool [18]. Anthrax infection can occur in three different form: cutaneous, gastrointestinal, and inhalation anthrax. The first, cutaneous, is by far the most prevalent and accounts for over 90 % of all cases. The anthrax enters the body through a cut, or a lesion, and in a period of 1 - 19 days a ring of vescicles followed by ulceration and the characteristic black eschar occurs [22]. Ten days after the original appearance the eschar begins to resolve itself even without any human interaction [23]. This form has a very low mortality of <1 % . Gastrointestinal anthrax is the rarest of all three forms and is only present in some parts of Africa and Asia, and is obtained by ingestion of improperly prepared meat [18]. Inhalation anthrax is the form associated both with industries that work in processing animal parts like wool and leather, but also with bioterrorism [24]. The spores can lay dormant for up to five days before any signs begin to show. Initially the symptoms are "flu-like" in nature, with mild fever, fatigue, malaise, and a non-productive cough. This phase abruptly ends and is replaced by dyspnoea, stridor, fever and cyanosis, with also a possibility of tachycardia and pleural effusion. By the end the pulse becomes extremely rapid and faint, the patient becomes extremely disoriented, which is quickly followed by coma and death [21, 25]. The mortality rate for this type of anthrax exposure used to be very high, with >95 %, but in recent years, with good access to antibiotics and medical care the rate has dropped to around 45 % [26]. In all forms, anthrax kills from severe septicaemia [18].

Testing for the presence of *B. anthracis* has several problems. In its structure, it is very similar to another *Bacillus* species, that of *B. cereus* [27, 28], which occupies the same environment as *B. anthracis* [29]. With so many shared characteristics and protein chains it is difficult to differentiate between the two. Most testing occurs in specialised labs equipped to deal with the pathogen, where nasal swabs or blood samples (if taken from humans), or environmental samples are taken and the bacteria are grown on agar plates, after which a myriad of tests are performed to confirm the presence of *B. anthracis*

[1] Even during the first and second world wars, both alliances were considering using anthrax as a method of damaging the enemy

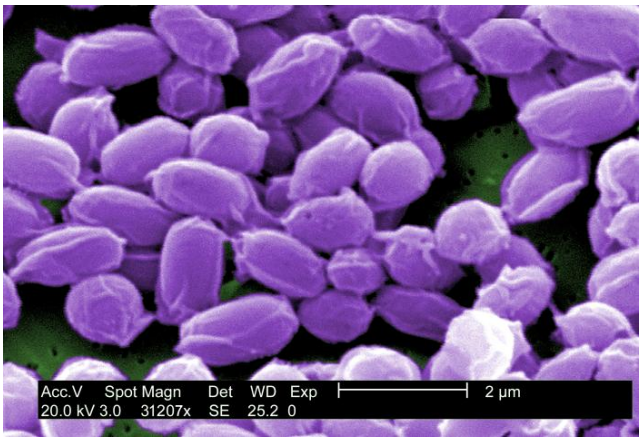

(a) B. anthracis *spores [19]*

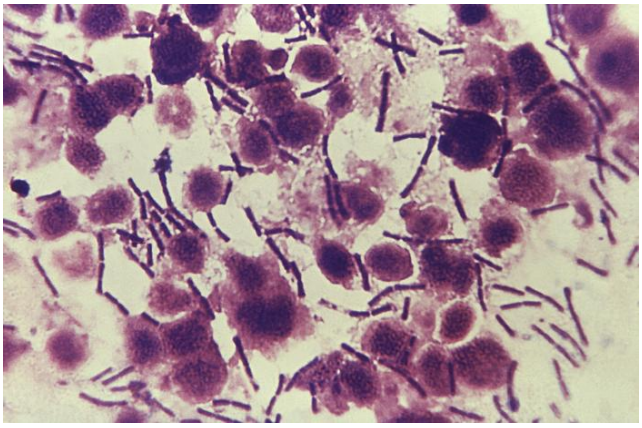

(b) B. anthracis *bacteria, some linked into chains, and some solitary [20]*

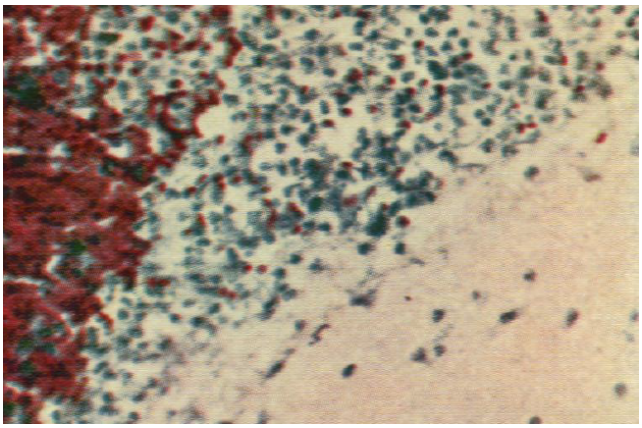

(c) B. anthracis *bacteria embedded in meninges tissue [21]*

Figure 1.2: Images of B. anthracis *in various forms*

[30]. Alternatively, there are commercial biosensors available that can give a result within 15 minutes from sample collection, but they have a very high

limit of detection and can give false negatives which might give a false sense of security to the on-site responders [31]. Anthrax detection can be really difficult on-site as the number of spores present can be quite small, especially in the collected air samples. There is a need for better, and quicker on-site detection [32].

1.1.3 Biosensors

Despite the mentioned failings of the traditional methods there is a lot of new development happening in pathogen detection but there is an overall resistance to industry acceptance, as there was a perception that the legislation and standards would not follow quickly enough the adoption of new, better, methods [33].

Biosensors are defined as: "device incorporating a biological sensing element either intimately connected to or integrated within a transducer" [34]. The aim is to produce a signal that in some way quantifies the amount of chemicals or pathogens present on the sensor. There are many combinations of biological elements and transducers possible (as seen in table 1.1), a few of which have not even been explored.

Table 1.1: Components that may be used to construct a biosensor (from [34])

Biological elements	Transducers
Organisms	Potentiometric
Tissues	Amperometric
Cells	Conductometric
Organelles	Impedimetric
Membranes	Optical
Enzymes	Calorimetric
Enzyme components	Acoustic
Receptors	Mechanical
Antibodies	'Molecular' electronic
Nucleic acids	
Organic molecules	

These biosensors, due to the rapid growth in their development [33], have already solved some of the issues present with the traditional methods (such as glucose sensors for daibetics [35]), but also might be the solution to other, still unsolved, problems in today's methods (like sensitive real-time pathogen detection).

1.2 Allergy diagnosis

1.2.1 What is allergy?

The term "allergy" was first coined by von Pirquet in 1906 to describe a harmful result to a hypersensitive reaction to re-exposure of a substance. He contrasted this to "immunity", which he explained as a protective reaction to a substance [36, 37]. While allergies can cover a broad spectrum of response mechanisms (there are four different types in total) [37], in modern times, the term has come to be more associated with IgE-mediated allergic disease, which are the subject of this thesis [38].

A healthy individual, when in contact with an allergen, mounts a low-grade immunologic response with the production of allergen-specific IgG antibodies and only a moderate proliferation of type 1 helper T- (Th1) cells. On the other hand, a person with an allergy has an exaggerated response in which they produce allergen-specific IgE antibodies, and a high amount of type 2 helper T- (Th2) cells [39]. The excess serum IgE antibodies attach themselves to mast cells or basophils and initiate a release of histamine. Histamine is a compound most associated with an allergic reaction as it is responsible for the inflammation of the affected area as it increases the permeability of capillaries to white blood cells in order to combat the foreign pathogen [40].

According to a survey done by the World Allergy Organisation (WAO), around 22 % of the world's population may be affected by allergy [41]. The most common allergens include: house-dust mite, cats, pollen, latex and peanuts. The cost of treating allergies has risen dramatically, with the US spending around $ 6 billion per year for treating asthma [42]. Overall, allergies represent the most common cause of chronic problems in developed countries, and most of them are not equipped to deal with the problems this presents. An example of the rising incidence of allergies and its links to the western lifestyle can be found in the data from Germany around the time of reunification. Seasonal allergic rhinitis and asthma were less common in East Germany than they were in West Germany before reunification [43]. After, however, the percentage of atopy and hay fever incidence has increased among children who spent their early childhood in East Germany, but not that of asthma [44]. A hypothesis has been proposed that in Western countries a developing immune system is deprived of microbes that stimulate the Th1 cells, as a consequence of a relatively clean environment due to the use of antibiotics for even minor illnesses in early life [45]. Furthermore, there is compelling evidence that the type of bacteria present in the gut may have a significant influence on allergic reactions and a presence of certain, "good", bacteria can indicate less problems with allergies further in life [2] [46].

[2] A study on chlidren in Estonia and Sweden found a smaller incidence of allergies in Estonian children which has a gut flora dominated by Lactobacilli and eubacteria, while the Swedish chlidren, which has a much higher allergy incidence, had higher levels of aerobic bacteria [46, 47].

An allergic disease can manifest itself in many forms. Asthma is the most common allergy disease that affects over 300 million people worldwide. Its symptoms include airway inflammation, mucus hyper secretion and airway hyper responsiveness [48]. Histamine blocker do not have a noticable effect on asthma [38], therefore other treatments, like corticosteroids are required. Allergic rhinitis is characterised by nasal congestion, sneezing and rhinorrhea, caused by the allergen provoking inflammation inside the nose [49]. Despite its mild symptoms, up to 80 % of patients have reported insomnia, depression, irritability and an adverse influence on work performance due to the condition. Currently affecting more than 20 % of the population of UK rhinitis is a considerable health cost to the NHS [50]. Urticaria is another well known allergy disease, commonly reffered to as hives. It is characterised by the appearance of red wheals on the surface of the skin which can last for over 6 weeks (chronic urticaria). It is caused by the release of histamine from basophils and mast cells. There are multiple treatments present, most prominent being antihistamines, but also trigger allergen avoidance, and in some cases even exposure therapy [51]. Food and drug allergies are a way of grouping common allergens, but who's prevalence and treatment differ from case to case. It depends on the patient and the allergen how successful the detection is going to be, and what course of action is to be taken [52]. The most prevalent food allergy currently is that to peanuts where in the past 10 years the number of people allergic to them in the UK and the western countries has doubled from 1.4 to 3.0 %. This pattern is also seen in Africa and Asia [53]. A WAO report from 2011 has shown that up to 10 % of the world's population has adverse drug reaction effects, with the number going up to 20 % for hospitalised patients [54]. Drug allergies have a specific problem when tested for, as many drugs cannot be produced in solid state for binding which rules out serum immunoglobulin E (sIgE) testing [55]. Anaphylaxis is a severe allergic reaction that can potentially lead to death. The most common causes are IgE-mediated sensitivity to foods like peanuts, nuts, fish, etc., bee and wasp stings, drugs and latex. It is caused by a systemic release of histamine and is characterised by laryngeal edema, lower-airway obstruction and hypotension. Currently, the treatment involves administering epinephrine which reverses the action of histamine within minutes. Epinephrine syringes for self-administration are an option to the patient [56]

1.2.2 Basophils

Basophils are the least abundant group of white blood cells, and is one of two types of cells (the other being mast cells) responsible for allergic reactions and the release of histamine [57]. Basophils were discovered by Paul Ehrlich in 1878 [58]. They originate and mature in the bone marrow, are 5 - 7 μm in size, have a bi-lobed nucleus, have a lifespan of approximately 60 h, and can be seen with basic dyes under microscope [59]. In a healthy adult, basophils

make only 0.4 % of all white blood cells [60] which translates to only around 45 basophils per μl of blood, or around 200 million cells in circulation at any time [61]. Due to them being the rarest of white blood cells and their physical and chemical similarity to other blood cells, basophils are very difficult to study, and their isolation from the whole blood sample can be extremely challenging [60]. Figure 1.3 shows a photomicrograph of a basophil and comparing it to a lymphocyte and an eosinophil.

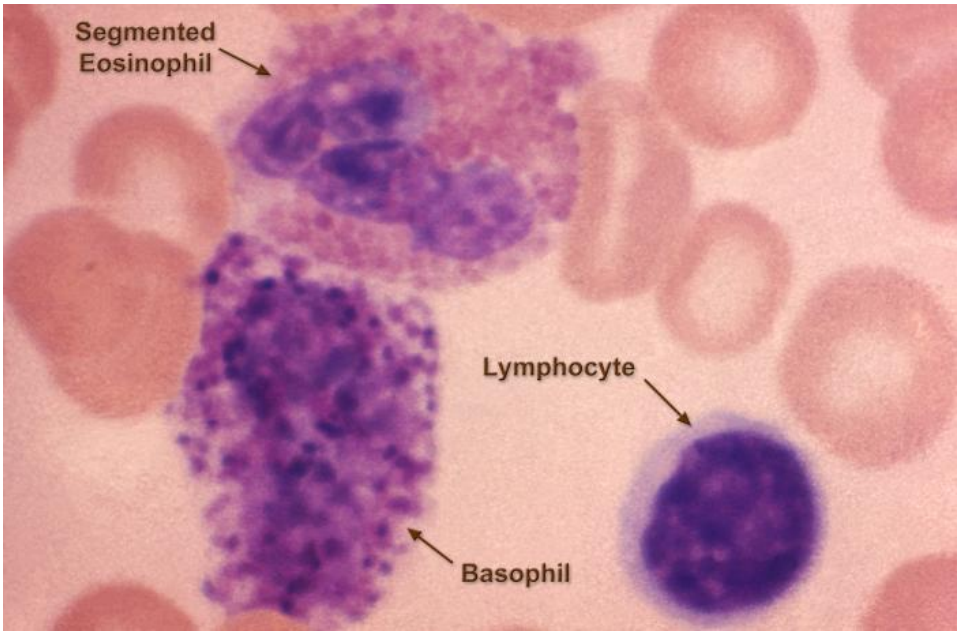

Figure 1.3: A photomicrograph of three types of white blood cells: basophil, eosinophil, and lymphocyte. Taken from [62].

1.2.3 Allergy detection and confirmation

There are multiple well-established methods for allergy detection and confirmation. All diagnoses, however, start with a patient history. This is the most powerful tool in diagnosis as it is often hard to replicate the condition under which the allergic reaction originally occurred. Usually the first test performed is a skin-prick test, or in case of sensitive skin (like in children), a sIgE level blood test. If the results are not conclusive a provocation test might be performed where the patient is exposed to a suspected allergen and monitored for a reaction. Even in the case of the provocation test, the current gold standard, the result might end up being a false negative, hence the reliance of doctors on patient history to establish a diagnosis. Currently, there isn't a single 100 % accurate method of detecting allergies. New tests, like basophil activation test (BAT) promise higher accuracy with minimum patient discomfort (something highly present in the provocation test), but rely on highly experienced staff to perform.

1.3 Biofilm prevention therapy

1.3.1 Biofilm growth

Throughout most of the history bacteria were viewed as planktonic cells floating freely in their environments. Only recently, starting in mid 20^{th} century, has attention been given to the another, more dangerous and frequent, form that bacteria can take: biofilms [63, 64]. Biofilms are described as a congregation of microorganisms (usually, but not exclusively, bacteria) linked together by a matrix of extracellular polymeric substances (EPS), and usually attached to a surface [65].

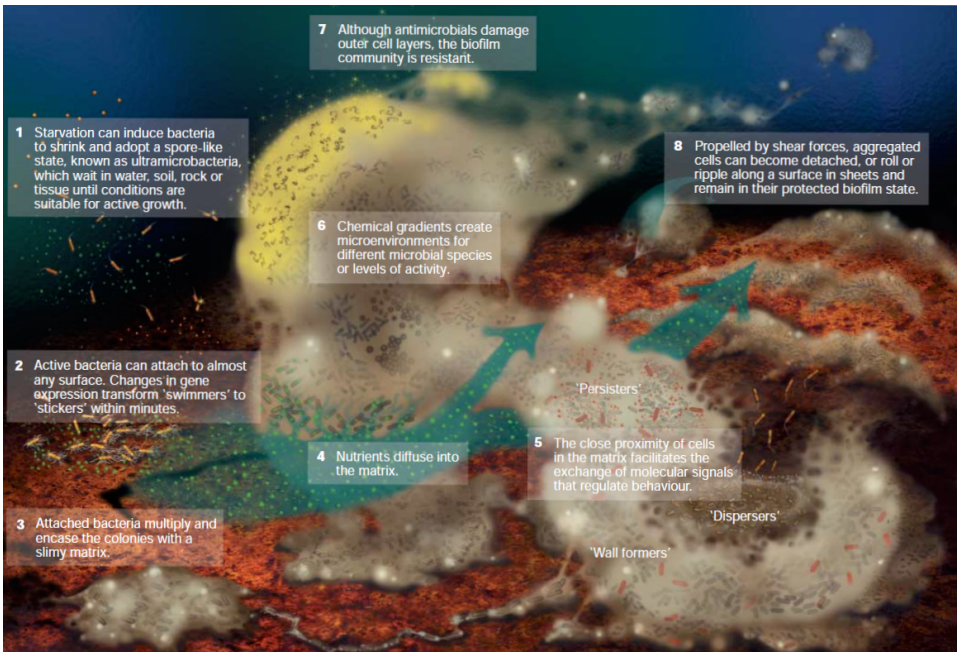

Figure 1.4: Conceptualisation of biofilm development and dyanmic behaviours. The authors have compiled the image from laboratory and natural observations of biofilms. Taken from [63].

The way a biofilm develops is different for each organism, and can be different depending on the environment (for e.g., the EPS constituents can change depending on both species and environment [66]). Based on work done on *Pseudomonas Aeruginosa* five stages of biofilm development have been proposed [63]. Figure 1.4 represents these 5 stages visually. Initially, planktonic cells attach themselves to a surface. If the adhesion is permanent the site starts to aggregate more cells and proliferate. Simultaneously, they begin to produce and excrete EPS, which mostly consists of proteins, carbohydrates, lipids, DNA, RNA and water [67], although the exact ratios differ between biofilms [68]. Micro-colonies will then start to form, and the process of maturation, in which the biofilm creates its 3D shape, will begin. Facilitating the maturation is the ability of cells to communicate with each other, called

quorum sensing [69], which ensures the "construction" of an encapsulating extracellular matrix which includes water-filled channels who's purpose is to transport nutrients within the biofilm [70]. The last stage of biofilm growth is cell dispersal. A biofilm can disperse cells in multiple ways: by releasing newly formed cells, by detachment of peripheral aggregates [71], or by unintentional dispersal of the peripheral cells due to shear or mechanical stress' on the biofilm [72]. These dispersed aggregates are highly virulent and they can form new sites for biofilm colonisation and growth [73].

1.3.2 Drug resistance and tolerance

Biofilms provide to microbial cells a means to survival in inhospitable environments [74]. It is no surprise then, that when part of a biofilm bacteria react differently to antibiotics. There are two important factors that a bacteria inside a biofilm can rely on: tolerance - the ability to survive despite the presence of antibiotics; and resistance - the ability to impede the antibiotic from working [75].

The extracellular matrix of the biofilm plays a significant role in its tolerance. *P. Aeruginosa* bacteria produce exopolysaccharide alginate, a carbohydrate that binds to certain antibiotics and renders them ineffective [76, 77]. Furthermore, the extracellular DNA found in the matrix offers extra stability but also slows down the penetration of antibiotics into biofilms [78]. At the core of the biofilm (the oldest part) the lack of oxygen and nutrients induces a state that resembles a stationary phase culture. This means that the bacteria inside the core will not uptake the available antibiotics thus increasing their tolerance [79]. All of these mechanisms contribute to an increased tolerance of the bacteria compared to their planktonic counterparts [80].

A bacteria can acquire antibiotic resistance through passing on of the resistant genes, genetic mutation, or by receiving the trait from another bacteria. The most common traits include efflux pumps, which stop the antibiotic from building up in the biofilm, and never reaching a lethal dose, and enzymes that degrade antibiotics like beta-lactemase [81].

1.3.3 Effects of biofilms on humans, and diabetic foot ulcers

While a normal part of the ecosystem biofilms can have a potentially deadly effects on humans. Infective endocarditis is an infection of the inner surface of the heart. In more than 75 % of the cases the cause is either a *streptococci* or a *staphylococci* bacteria [82]. The bacterial build-up usually starts from some small damage inside the heart, in areas where the turbulent flow is perturbed. This creates the conditions that allow the biofilm to grow. This leads to infections and clotting [63].

Cystic fibrosis (CF) is characterised by airway inflammation and chronic endobronchial bacterial infection, both of which lead to airway obstruction and, through progressive destruction of the airway epithelium, respiratory failure [63]. An important factor in CF is the colonisation of the lung by *P. Aeruginosa* which is present in its biofilm form [83].

Insertion of medical implants, like catheters, prostetic heart valves, hip replacements, pacemakers, and others, presents an invasive and traumatic medical intervention. While all of these implants have saved countless lives, due to the nature of their placement they present an opportunity for bacteria to latch on and grow into a biofilm (most common being *S. aureus*, *S. epidermidis*, and *P. Aeruginosa*). A common trait of these biofilms is the production of slime which can have negative effects on the surrounding tissue and cause, or prolong the infection present.

Chronic wound ulcers are wounds that do not heal in a timely manner. As opposed to an acute wound, chronic wounds fail to progress between the initial inflammatory phase [84], take between 12 to 13 months to heal, and return in up to 60 to 70 % of patients [85]. Diabetic foot ulcers (DFUs) are a subtype of chronic wound ulcers. Arising from a minor trauma to the foot, they are a source of major healthcare costs dedicated to their treatment and management [85, 86], are associated with substancial morbidity and mortality [87], and are a cause of over 50 % of all lower leg amputations [88]. There is strong evidence that biofilms are responsible for the prevention of normal wound healing [89], as chronic wounds were found to be poorly susceptible to antimicrobial agents [88]. Current methods of treating the biofilm in the wound bed are not adequate enough to provide a comprehensive treatment. There is room for improvement by novel methods, including those including ultrasound and microbubbles [75].

1.4 Thesis structure

Chapter 2 introduces acoustofluidics and common types of devices. Next, an overview of existing procedures, starting with water quality and anthrax detection; allergy diagnosis, both established and novel; and biofilm eradication, including the established traditional techniques, but with a focus on more novel techniques using ultrasound and microbubbles. Finally, a brief overview of the ultrasound theory is presented in section 2.3.

In Chapter 3 the modelling, design, and characterisation of the main device used in the thesis are described (although it was subsequently found that an alternative arrangement was required for Chapter 6). Analysis includes optimisation with respect to flow speeds, lateral modes, vertical forces, plate modes, streaming, etc. The chapter finishes with a description of the previous device design iterations that led to the final design.

The first of the three areas that are tackled is pathogen detection. Chapter 4 looks at the ability of the device described in the previous chapter to cap-

ture *Bacillus globigii* (BG) spores. The chapter focuses on the spore capture, leaving detection of the captured spores as future work.

Allergy diagnosis is the main theme of Chapter 5. The same device used in the previous two chapters was now applied to capturing and detecting basophils from blood samples. The use of fluorescent activated cell sorting (FACS) allowed for a more in-depth look at the capture rate inside the device. The chapter explores what the ideal flow rate is for basophil capture (as their size is an order of magnitude larger than beads or spores), as well as the basophil capture against two types of controls (no ultrasound, and no antibody) for five different patients using purified basophils. The final experiments, done on lysed blood, looked at direct detection method for samples from three different patients by using a microscope and a stain to see if basophils captured on the functionalised device slide could be used for further allergy testing.

The use of ultrasonically actuated microbubbles at a surface to aid the eradication of surface biofilms is presented in Chapter 3. Initial experiments showed that the layered device was not suitable, and a new device designed to produce more accurately controlled fields, producing both travelling and standing wave fields. Experiments consisted of a variety of methods, all involving ultrasound, microbubbles, and antibiotics. In the end, a statistical analysis was performed to evaluate which methods performed the best and which have the potential for further development into a novel surface biofilm eradiation method.

Chapter 7 offers a summary of all the conclusions drawn from the thesis and includes the possible future developments and outcomes.

1.5 Aims and objectives

The goal of this thesis was to create a device that was cheap, quick and easy to use that would be used for a variety of applications including detection, diagnosis, and eradication. Specifically, an ultrasonic transducer setting up a thin-reflector standing wave field, and a cell specific antibody coating were to be used to provide a novel and competitive method of cell manipulation and capture. It would then be tested for an application in each of the three fields to see how well it performs.

For anthrax spore detection, the aim was to be able to use the device to detect as few as 100 spores/ml, a threshold that is hard to achieve with the quick biosensor methods.

The same device was used to create a tool to assist allergy diagnosis by capturing basophils. The objective was to find the optimal conditions for quick basophil capture that would be useful in a hospital setting (i.e. fast blood processing, quick assay times, simple methods).

Very early in the biofilm eradication project it was established that the device used for other two applications was not good enough and did not meet the required specifications. With that in mind the goal first became to design

a new proof-of-concept device that would enable the interaction of ultrasound, microbubbles, and antibiotics with biofilms, that could also be easily manufactured, assembled, used, and sterilised, without the use of large amounts of water ($> 5\ l$). Once the device was designed, made, and calibrated, it would be used to test an array of different methods that combine various aspects of the approach to biofilm eradication, including: continuous vs. pulsed ultrasound, changes in microbubble concentration, adding rest periods between ultrasound exposures, and changing the duration of the rest period. Finally, two types of materials were examined as both served as a replacement for two types of tissues expected to be found behind surface biofilms: bone, and soft tissue.

Chapter 2

Literature Review

2.1 Introduction

There is a common thread for all three areas of exploration mentioned in chapter 1: detection, diagnostics, and therapy. The use of ultrasound radiation force is present in all of the cases and is the vital component of the respective methods and devices. Each, however, have their own special considerations that need to be looked at first.

Spore detection is not a new field. The oldest of the well-established methods, cell culturing, is over a century old, while polymerase chain reaction (PCR) and immunoassays, like enzyme-linked immunosorbent assay (ELISA), have been around for decades. These methods are robust and reliable, so to understand where our method offers improvement they have to be understood and quantified first. The method presented here is based on acoustic concentration and capture so comparisons have to be made with other capture methods, like magnetophoresis and dielectrophoresis, as well as other types of acoustophoresis.

The principle of the basophil capture chapter is similar to the spore capture work - an acoustic field combined with an antibody coating is used to capture basophils for further testing. There are three well-established and regularly used methods for allergy testing - skin prick test, blood analysis, and exposure test. These methods all have high accuracy, but still contain trade-offs. The background presented here helps illuminate how the trade-offs taken here compare to those of other methods.

Biofilm eradication is an ever present problem. Many methods have been developed with the most used being antibiotic treatment, or physical removal, where possible. In most cases these methods are not good enough and do not completely remove the biofilms. New methods are constantly being developed with varying success. One avenue of exploration is using ultrasound, with or without bubbles, to hinder biofilm growth and reduce its size eventually eradicating it. This is the niche in which our therapeutic area of investigation falls into.

This chapter serves as a literature review for the three connected, but disparate applications of the basic idea presented in the thesis. Section 2.2 explores the basics of acoustofluidics, including the historical development and its staples. The following three sections (2.4 - 2.6) look at the relevant history and methods used in the three areas of interest mentioned above. Finally, section 2.3 examines the theory behind the acoustic phenomena utilised by the methods developed in this thesis.

2.2 Basics of acoustofluidics

There are many types of acoustic manipulation devices, but this section will focus on layered device. As seen in fig. 2.1, there are four basic layers to this type of device: transducer, carrier (sometimes called matching) layer, fluid layer, and reflecting layer.

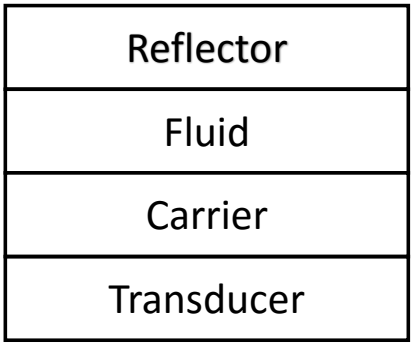

Figure 2.1: A diagram showing the four layers of a layered acoustic resonator

The transducer is the emitter of the ultrasound waves which set up the standing wave field inside the fluid layer. While ultrasound is defined as any frequency above the hearing threshold (usually taken as 20 kHz), workable frequencies for these devices are typically in the MHz range. At these high frequencies effects such as cavitation, which are generally undesirable, are avoided as they need higher energy than at lower frequencies [90]. The wavelength is also on a useful scale, being of order 1.5 mm in water at 1 MHz.

A piezoelectric material is the most common method of transduction used. It converts mechanical motion into a change in electrical current, and vice versa - when a voltage is applied the material exhibits strain. Usually, the material used is lead zirconate titanate (PZT). This is a ceramic material with ferroelectric properties, which means that it has dipoles which can be expanded and contracted based on the input voltage, thus allowing versatility in the geometry of the transducer [90].

The transducer is attached to the carrier layer either permanently or temporarily. To attach it permanently a layer of glue is placed between the two. Care has to be taken to make the layer as thin as possible, and to include it in the model of the device, as it does affect performance [91]. An alternative would be to use coupling gels as a non-permanent attachment solution [92]. Their downside however, is that care has to be taken in order to achieve good coupling and it is not easy to tell when this is the case. Repeatability can also a problem in the early prototyping stage, but is aleviated with some clever design choices (good impedance matching between transducer and carrier layer, constant volume of glue applied, etc).

The carrier layer serves three functions - firstly, it provides a boundary for the fluid layer, confining it to a space of known geometry and dimensions; secondly it serves as a protective boundary between the transducer and the fluid layer, although this is sometimes circumvented by placing the transducer as the partial boundary to the fluid layer; and thirdly it provides, to a degree, impedance matching between the transducer and the fluid layer, in order to maximise the amount of energy going into the fluid [92].

The reflective layer is placed on top of the fluid layer and, apart from constraining the fluid from the top side, it provides a hard impedance boundary for the sound wave to bounce off of, in order to create a standing wave field (perfectly rigid in theory for some device types, like a half-wave, as such a boundary creates the strongest standing wave field).

The fluid is constrained by the carrier and reflective layers on top and bottom sides, and with walls on the side. These walls can be a hard boundary or a more impedance matched boundary (gaskets). Their position on the environment - how they enclose the fluid, as well as the material they are made of, highly influences the lateral modes.

All of these layers have to be held together, and usually they are either clamped, or screws are used in order to secure them. Glue can be used as well for a permanent seal. This, however, may not be desirable as with a non-permanent seal parts can be replaced or repairs can be made [92].

2.2.1 Layered acoustic resonator types

After the sound enters the fluid layer it bounces of the reflector layer and the incident and reflected waves create a standing wave field. Typically, particles (be it cells, spores, beads or bacteria) enter the device through an inlet. They then pass through the fluid channel and are exposed to acoustic radiation forces. Typically, flow is guided out of the device towards a number of outlets, as seen in figure 2.2. The structure of the acoustic field in the active region is what differentiates the types of devices.

Acoustofluidic devices have many uses [93, 94] and as such can come in a variety of sizes depending on their function. Changing the transducer frequency and the thickness of the layers has different effects on the ultrasound

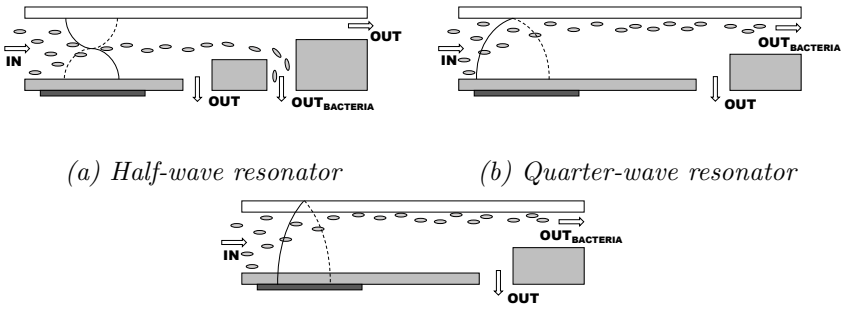

(a) Half-wave resonator *(b) Quarter-wave resonator*

(c) Thin-reflector resonator

Figure 2.2: Schematics of the sound fields and particle paths for the three types of acoustic concentrator device. The transducer is shown in dark grey, the carrier layer in light grey, and the reflective layer is white. The fluid layer is transparent

standing wave (USW) field and its use. With the right parameters the field can focus particles in the middle, and by choosing harmonics of that frequency, particles can be focused on multiple planes rather than just one. Furthermore, the parameters can be tuned in such a way that the standing wave node lies on the boundary between the reflector and fluid layer or even beyond to provide a unilateral force towards the reflector.

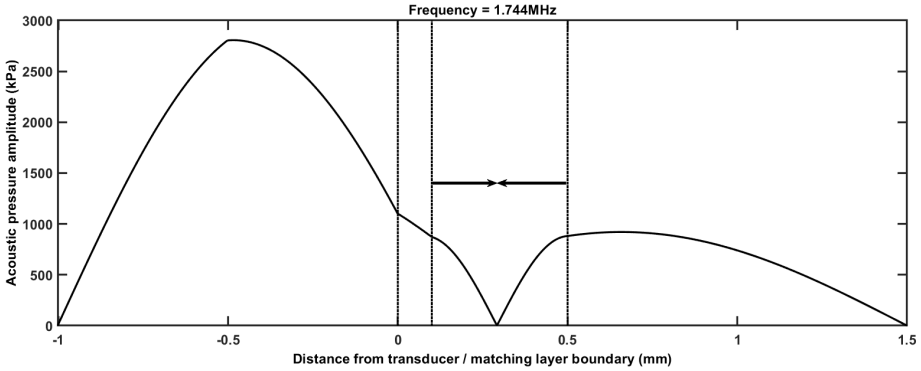

Figure 2.3: Pressure amplitude through an assembled HW resonator. The layers divided by dotted lines are: transducer, carrier, fluid and reflector. The arrows in the fluid layer show the direction of the forces.

In the first type of device, the half wave (HW) resonator (as seen in fig. 2.2a), the pressure node is at the centre of the layer. This type of device was first described in 1990 by Mandralis et al, and then by Yasuda et al. in 1992 (reviewed in Lenshof et al [92]). The particles that enter the channel are focused towards the centre (towards the pressure node) leaving the top and bottom parts of the fluid particle deficient. In typical applications, there are

three outlets, the first and the last one being for the supernatant fluid, while the middle one is for the particle rich fluid. While this type of device is robust some care has to be taken in order to align the central outlet with the pressure node, otherwise some of the concentrated fluid will escape into other outlets. Fig. 2.3 shows a pressure amplitude graph from the 1D impedance model for a HW resonator with layer thicknesses of: transducer - 1000 μm, carrier - 100 μm, fluid - 400 μm, and reflector - 1000 μm.

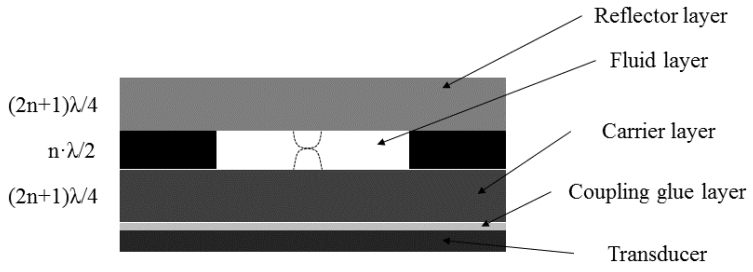

Figure 2.4: Structure of a half-wave layered resonator where, for optimal performance, all of the layers need to be tuned to specific thickness'

If the frequency is increased to find harmonics then more nodes may appear in the fluid channel so there are more focal points for the particles to go to. While this device is no longer a half-wave device, as more than half a wavelength fits into the channel, it exhibits similar behaviour.

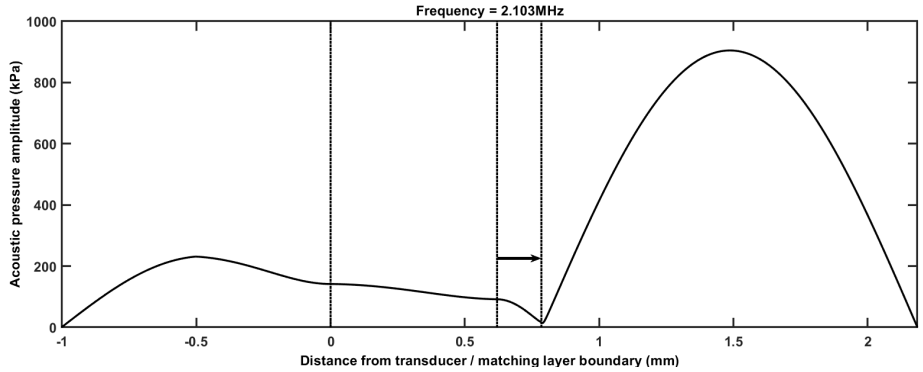

Figure 2.5: Pressure amplitude through an assembled QW resonator. The layers divided by dotted lines are: transducer, carrier, fluid and reflector. The arrow in the fluid layer shows the direction of the force.

If, for some reason, it is desirable to push particles against the reflector (or even carrier) layer, a quarter wave (QW) resonator device may be used (fig. 2.2b). First built by Hawkes [95], this device fits a quarter of a wave inside the fluid layer, most commonly with the pressure antinode at the carrier layer and the pressure node at the reflector layer. This forces the particles to move towards the reflective layer. The problem this type of device has is that it needs

high manufacturing precision. If the node is fractionally below the boundary between the two layers particles will not reach the surface, and if the node is too far inside the reflector layer some particles will start going towards the carrier layer and some towards the reflector layer. Due to the required resonance withing the reflector layer this device is highly sensitive to the thickness of the reflector layer [96]. A pressure amplitude graph from the impedance model for a QW resonator is seen in fig. 2.5, with layer thickness' of: transducer - 1000 μm, carrier - 620 μm, fluid - 165 μm, and reflector - 1400 μm.

It is not just the fluid layer that has to be tuned to the specific frequency at which the standing wave is to be set up. All of the layers have to be made a certain width in order to achieve the pressure maxima and minima at the desired point. The thin-reflector (TR) resonator, first described in a study by Glynne-Jones *et al.* [97]. and seen in fig. 2.2c, relies on the first structural resonance of the layered structure. This leads to a pressure node located at the solid-air boundaries. This means that the device is more robust than the QW resonator, and also that it has a positive force towards the reflector layer at all points in the fluid. It is also more robust to changes in thickness than the QW resonator. Fig 2.6 shows the pressure amplitude graph from the impedance model for a TR resonator, and from this it is visible how in the TR resonator the mode is of a system, rather than each layer having their own mode. The layer thickness' are: transducer - 1000 μm, carrier - 100 μm, fluid - 100 μm, and reflector - 100 μm.

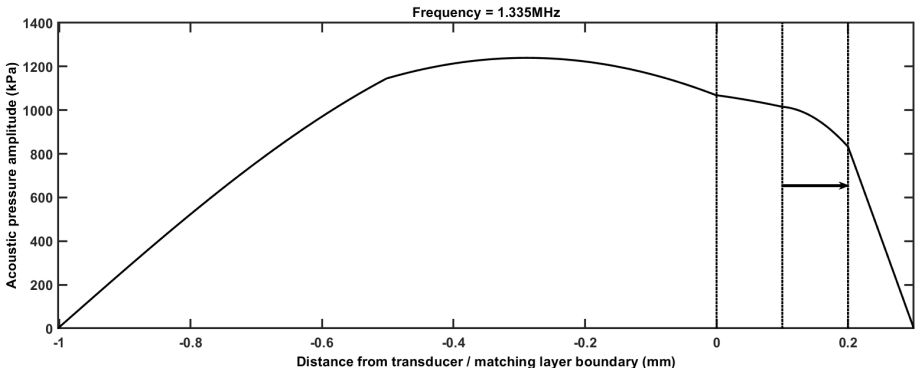

Figure 2.6: Pressure amplitude through an assembled TR resonator. The layers divided by dotted lines are: transducer, carrier, fluid and reflector. The arrow in the fluid layer shows the direction of the force.

For the purposes of making bacteria stick to the antibody coated reflective layer the TR resonator device is best suited. With its robustness and unidirectional force it meets the criteria for a simple, easily altered bacterial capture device.

2.3 Ultrasound theory

The acoustofluidic device described in this report for use in detection and diagnostics uses standing waves. Once an ultrasonic standing wave field is set up inside the device the particles are pushed by the "acoustic radiation force" towards either the node or the anti-node, depending on the compressibility and density ratios between the particle and the surrounding medium [1]. It is present in all types of waves (travelling and standing), but in a travelling wave it is typically weaker [2]. The property of the travelling wave to push particles and bubbles in the direction of propagation is the basis of the device used for therapy, i.e. the treatment of surface biofilms.

2.3.1 Standing wave

A sound wave in a fluid is described as a longitudinal mechanical (pressure) wave. While it can propagate through other medium, this report will focus only on fluids, and more specifically aqueous solutions. A sound wave can be described as a fluctuation of pressure and velocity, which also relate to density and displacement fluctuations. The device from this report uses ultrasonic frequencies (around 0.8 MHz) in order to manipulate bacteria.

A standing wave can be conceptualised as two waves, heading in opposite directions, interfering. In most scenarios this is an interaction between an incident and a reflected wave. In planar geometries they can be represented as two one-dimensional plane harmonic waves with their displacement being represented by $s_1(x,t) = s_0 sin(kx - \omega t)$ for the incident wave and $s_2(x,t) = s_0 sin(kx + \omega t)$ for the reflected wave. Because of the linear nature of the waves at these amplitudes, the two can be added to get the total displacement of the standing wave field:

$$s_{tot}(x,t) = 2s_0 cos(\omega t) sin(kx). \tag{2.1}$$

The amplitude of the standing wave is given by s_0, and in (2.1), because the two waves add up, the maximum amplitude is twice that of any of the two initial waves. The wavenumber is given by $k = 2\pi/\lambda$, while the angular frequency is $\omega = 2\pi f$, where λ is the wavelength, and f is the frequency of the standing wave. From this equation it is evident that the wave is stationary, with a temporal oscillation from the $cos(\omega t)$ term. To find the minima and maxima we set the $sin(kx)$ term to zero and the maximum, respectively. When $x = \frac{n\lambda}{2}, n = 0, 1, 2...$ the amplitude is zero - these are called nodes; while at $x = \frac{n\lambda}{4}, n = 1, 3, 5...$ the amplitude is at maximum - the antinodes.

[1] In most cases for living organisms like bacteria, spores, and cells, they are pushed to the node

[2] Given equal pressure at the source and ideal conditions, the standing wave would produce stronger radiation forces because it can be seen as a superposition of two travelling waves so the maximum and the minimum pressure are twice that of the travelling wave. In real life, the difference will most likely not be as strong.

To obtain the pressure a relationship with the displacement is used:

$$p(x,t) = -B\frac{\partial s(x,t)}{\partial x}. \tag{2.2}$$

This yields the following, final equation, when combined with (2.1):

$$p_{tot} = p_0 cos(\omega t) cos(kx), \tag{2.3}$$

where $p_0 = 2Bks_0 \equiv p_{max}$. The symbol B denotes the bulk modulus (sometimes expressed as K) which is a material's resistance to uniform compression. The $\partial s(x,t)/\partial x$ is positive with an increase in displacement which in turn means decreased pressure. The negative sign is placed in (2.2) to express that as $p(x,t)$ represents the total increase of pressure over ambient pressure.

2.3.2 Primary radiation force

The primary radiation force was first noticed by Kundt [98]. Later it was studied by Rayleigh [99, 100] and others, but it was not until 1934 that a full derivation was presented by King [101], who considered the incompressible particle in an acoustic field. The next advance came from Yosioka and Kawasima in 1955 when they included the compressibility of the particle [102]. Their findings were generalised by Gor'kov in his seminal 1962 article "On the forces acting on a small particle in an acoustical field in an ideal fluid" [103]. The viscosity of the fluid was later included in the theory in 1994 by Doinikov [104]. In 1997 a model for thermal dissipation was included [105], and in 2012 Settnes and Bruus added a viscous boundary layer correction factor [106].

The primary radiation force is the time-averaged force on a particle, over a period longer than a single cycle, located inside an arbitrary sound field [107–110]. An approach to obtain a generalised expression for the force would be to consider the compressible, spherical and micrometer-sized particle as a weak scatterer. The velocity potential of the incident and scattered waves can be found, and a surface integral of the time-averaged second-order pressure and momentum flux tensor calculated which gives the radiation force. The second-order pressure is what drives the radiation force and is acquired by expanding the Navier-Stokes equations to include second order terms [109]. In the non-visous, small particle approximation, the overall radiation force is then given as:

$$F_{rad} = -\nabla U, \tag{2.4}$$

where U is the force potential, and is given by the expression [109, 110], as first derived by Gor'kov [103]:

$$U = V\left(f_1 E_{pot} - \frac{3}{2} f_2 E_{kin}\right). \tag{2.5}$$

The force potential is derived from the velocity potentials, where $V = 4\pi a^3/3$ is the volume of the spherical particle with radius a, and E_{pot} and E_{kin} are the time-averaged potential and kinetic energy densities at the particle location, respectively. They are given by:

$$E_{pot} = \frac{\langle p^2 \rangle}{2\rho_0 c_0^2}, \tag{2.6a}$$

$$E_{kin} = \frac{\rho_0 \langle v^2 \rangle}{2}, \tag{2.6b}$$

where p and v are the pressure and velocity fields, respectively. The subscript "p" (seen later) denotes particle, while subscript "0" denotes surrounding fluid. The variable c_0 is the speed of the sound in the surrounding fluid. The time-average is denoted by $\langle ... \rangle$. The two dimensionless correction factors f_1 (arrising from monopole-like radiation - see Acoustofluidics 7 by Bruus [109] for more details) and f_2 (arrising from dipole-like radiation, i.e. translation of the particle [109]) are given by:

$$f_1(\tilde{\kappa}) = 1 - \tilde{\kappa}, \quad \text{where} \quad \tilde{\kappa} = \frac{\kappa_p}{\kappa_0}, \tag{2.7a}$$

$$f_2(\tilde{\rho}) = \frac{2(\tilde{\rho} - 1)}{2\tilde{\rho} + 1}, \quad \text{where} \quad \tilde{\rho} = \frac{\rho_p}{\rho_0}. \tag{2.7b}$$

Here, $\tilde{\kappa}$ is the compressibility ratio between particle and suspension fluid, where the compressibility for a fluid is calculated using $\kappa = 1/\rho c^2$ (isentropic), and for the solids it is the inverse of the bulk modulus $\kappa = 1/B$. It should be noted that c represents the phase speed of the sound field. The density ratio between the particle and the fluid is represented by $\tilde{\rho}$.

By combining equations (2.4) - (2.6) we get the final expression for the primary radiation force, as a gradient of the Gor'kov force potential:

$$\mathbf{F}_{PRF} = -\frac{4\pi a^3}{3} \left(f_1 \frac{1}{2\rho_0 c_0^2} \nabla \langle p^2 \rangle - f_2 \frac{3\rho_0}{4} \nabla \langle v^2 \rangle \right). \tag{2.8}$$

From these equations it can surmised that the particles in a standing wave field are attracted to the minimum of the force potential. Furthermore, the two properties of the particle, compressibility and density, and their relation to the surrounding fluid are what determine whether the particle will travel towards the node or the anti-node of the standing wave. Fig. 2.7 shows at what values of the compressibility and density ratios does a particle move towards the pressure minimum or maximum.

Equation (2.8) shows a generalised form of the primary radiation force. This equation, when constricted to a single dimension, may be solved analytically (examples may be seen in Bruus [109] and Ohlin [110]). However, when using this equation to model real life devices, not only does the solution have

to be in three dimensions, but it also has to include additional forces such as acoustic streaming and Bjerknes forces, as well as lateral acoustic forces, and forces resulting from fluid dynamics. Acoustic streaming is the bulk fluid motion induced by losses within a fluid or in fluid boundary layers. The secondary radiation force (also known as Bjerknes force) appears when two particles are in proximity to each other and start experiencing an attractive (or in some cases repelling) force, resulting from sound scattered from one impinging on the other [111]. Lateral forces are lateral components of the primary radiation force acting in lateral directions, resulting from variations in the standing wave field which can be created by the reduction of energy towards the edges of the axial field, some near field effects, enclosure modes, structural modes from the boundaries, or inhomogeneities [90]. The hydrodynamic flow itself does not have a uniform velocity profile - due to viscous drag forces it has a curved profile, meaning the particles in the centre travel faster than the particles at the edges [110].

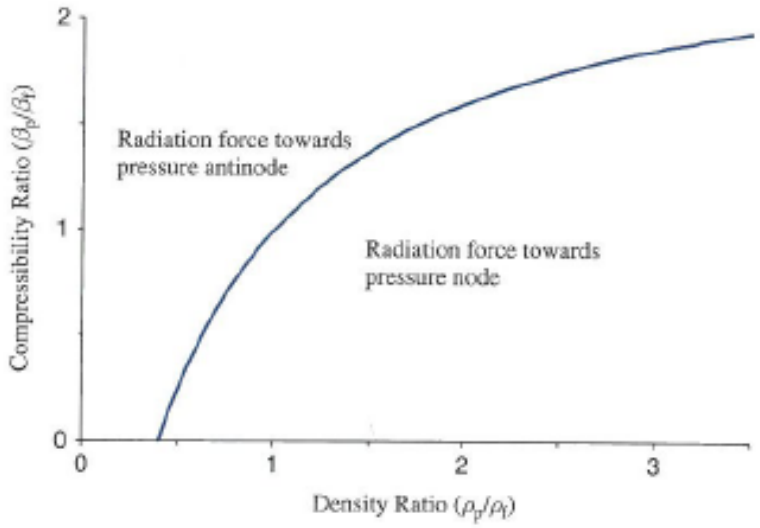

Figure 2.7: Density ratio plotted against the compressibility ratio, where the line is a solution to $U = 0$. On the left-hand side the force is towards a pressure antinode, while on the right-hand side it is towards the node. From Principles of bacterial detection, chapter on Ultrasonic Microsystems for Bacterial Cell Manipulation by Hill and Harris [90]

2.4 Pathogen detection

There are over 30 well known pathogens that reside in water and form potential threats to human health [7]. With just over 3 % of all worldwide deaths attributed to water-borne diseases [1], timely detection is of utmost importance,

especially in far-removed places where state-of-the-art labs are not easily accessible. There have been advances in the well established methods which now provide faster than ever detection, but it is in the field of novel biosensors where the biggest advances have been made [6, 112–114].

Ever since 2001 and the anthrax terrorist attacks in the United States first responders have desired a quick and reliable method for detecting anthrax [115]. Currently, commercial devices exist which provide results in less than an hour but their detection thresholds are usually high and they are prone to false negatives [31]. Anthrax detection as a whole is still to overcome certain problems that are present with any detection method. The *B. anthracis* spore has very similar properties to the non-virulent *Bacillus* species *B. cereus* [27, 28]. The two species have been documented to coexist in many environments making easy detection impossible with the current technology [29, 30, 116, 117].

2.4.1 Biosensors and bacterial detection devices

The "traditional", well-established methods, some of which have been present for over a century, are known to be robust methods that can provide very good accuracy of up to 2.5 colony forming unit (CFU)/ml [6, 15, 16]. However, there is a need for improvement with regards to speed, eventually moving to real-time detection. Fast detection is very important when using any method to ensure public safety, or even when trying to reduce costs [6].

The oldest of the traditional methods are the culture techniques. While they vary in the details, the basic principle is that a sample is put on an agar gel that is made to provide the best growing conditions for the pathogen that is being analysed. After a certain amount of time, by counting the number of colonies that are present a negative (takes between 4-9 days) or positive result (14-16 days) can be given [6]. Like all of the well-established methods that are going to be given here, this one has an amplification stage - a stage during which the identifiable object (be it bacteria, DNA, etc.) is replicated in order to make detection easier, or even possible. The culturing itself being the amplification stage, in this case. This makes the culture method a very robust one, as it could detect a a very small number of pathogens ($2.5 - 994$ CFU/ml in case of *Legionella pneumophilla*) [6, 15], after it has formed a colony that can be detected, but because of the time it takes to get a result, scientists are moving towards other, faster methods. Newer studies have shown that not all pathogens form colonies questioning this method as the gold standard to which all others are compared [118]. From this point a move towards counting individual cells was made.

For *B. anthracis* using cell culturing is straightforward. It takes 1-2 days to get a colony developing [119]. However, there are many problems that present themselves with this method. Just culturing isn't enough as its physical properties have to be tested, and since a lot of the properties are shared between

the various *Bacillus* species, and the variation within the *B. anthracis* itself mean an increased number of tests [30, 120]. The similarity to *B. cereus* and their presence in similar environments means anthrax detection in environment samples is considerably harder than with lab-grown samples and currently cell culturing and all of the following tests require a lab environment and cannot be done *in situ* [27, 28, 30].

The second method that is being widely used is immunoassay capture and detection. The first and most widely used of these is ELISA. It was first proposed in 1971 [121], and has become an established method for finding pathogens (although, some manuals still insist on confirmation of results with culture-based techniques [122]). Before starting the assay various enrichment steps should be taken. The pathogen needs to be secured to the walls of the containing vessel, usually a microtiter plate, either by absorption to the vessel walls, or by using a layer of antibodies (as in the "sandwich" ELISA). The pathogens then attach another layer of antibodies containing specific enzymes. Finally the enzyme's substrate is added. It binds only to the enzymes bonded with the antibodies as the others are washed away. This enzyme-substrate reaction usually induces a colour change which can then be monitored and compared to reference curves [15]. Fig. 2.8 shows the schematic for the procedure. ELISA is a very popular method as it is much faster than the culture technique (exact time depends on type of ELISA used, but it varies around a day) [6, 16]. It is also very good at detecting small quantities ($10^0 - 10^4$, depending on type of method) and can distinguish one type of pathogen from a very heterogeneous sample. It, however, still needs a day to perform the assay [6]. Plenty of modern biosensors are based on the immunoassay method as they use ligands (antibodies, peptides or aptamers) to capture specific pathogens, which are then later analysed [30].

In case of anthrax, affinity-based immunoassay method are the cornerstone of field testing. There are well over 8 different methods for detecting *B. anthracis* spores [30], including ELISA [123] and magnetic particle fluorogenic immunoassay [124]. Currently, the only commercially available field tests are affinity-based and use antibodies as ligands. These are used as an easy-to-handle and quick *in situ* test, giving out results within 15 minutes. They are usually a part of a platform designed for air monitoring [125, 126]. The companies claim a detection threshold between $10^2 - 10^5$ but in a study done by King *et al.* they showed that the real world detection thresholds are between $10^5 - 10^6$, a considerably worse result than what the companies reported [31]. This is especially problematic since a false negative may relax the responders and give them a false sense of confidence. Currently the biggest hurdle for the affinity-based methods is the specificity of antibodies used. As it stands they cannot fully distinguish between *B. anthracis* and *B. cereus* which raises the detection threshold [127]. If new antibodies are developed the threshold may be dropped to levels useful for detecting low concentration *B. anthracis* spores in an environmental sample.

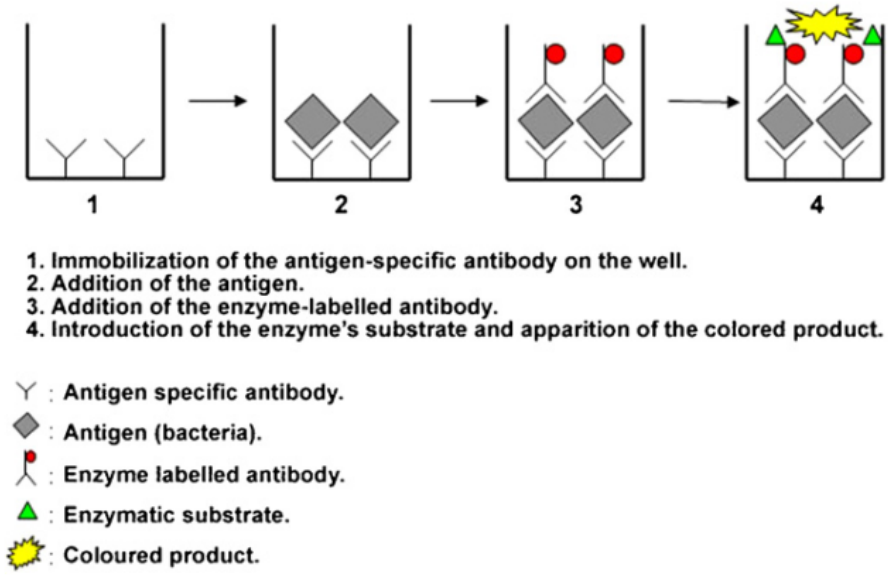

Figure 2.8: Schematic of the "sandwich" ELISA procedure. Taken from Lazcka et al. [6]

PCR was developed in the mid 80s [128] and in the current form it takes anywhere between 5 to 24 hours to get a result [6]. PCR relies on isolating, amplifying and quantifying short DNA sequences. Sequences of heating and cooling are used to replicate the target DNA using DNA polymerase. Heat denatures the DNA into two strands which allows the primers (DNA polymerase) to replicate the full DNA from the two strands (as seen in fig. 2.9). The repetition of this process increases the number of target DNA molecules exponentially [6]. Electrophoresis is then used to sequence the DNA and compare it to a bank of known DNA samples [15]. PCR has become a staple in pathogen detection because of its speed [129] and accuracy ($10^0 - 10^6$, depending on type of method) [6], but it does come with its own problems: the target DNA cannot be contaminated with other DNA as that may introduce noise; some (faster) method variants cannot tell between viable and non-viable cells, etc [130]. In practice, PCR can fail for many reasons, and getting a detection limit below 100 CFU/ml is usually not possible [129, 131], which is why good optimisation is key.

Nucleic acid-based detection are becoming a cornerstone in *in situ* anthrax testing. The hardest challenge with these methods is finding specific nucleic acid sequences that are unique to *B. anthracis*, and not shared with *B. cereus* [132–134]. One of the first PCR sequences to work used the pXO-1 and pXO-2 proteins and they managed to get a detection threshold of 10 spores/ml, which was obtained from soil samples that had as low as 10^4 spores/g soil, by using real-time PCR. The assay took 3 hours [135]. There is a wide spread of other DNA-based targets for anthrax spores, that are still unique to them

[136, 137]. Another promising DNA-based method is called loop-mediated isothermal amplification (LAMP) [138]. The DNA amplification is carried out at a constant temperature range of 60 - 65 °C for 1 h, and only requires a heat element. The method has even been used with a portable pocket hand warmer, which eliminated the need for a power supply. In this test they managed a detection limit of 1000 copies of genomes of BA [139].

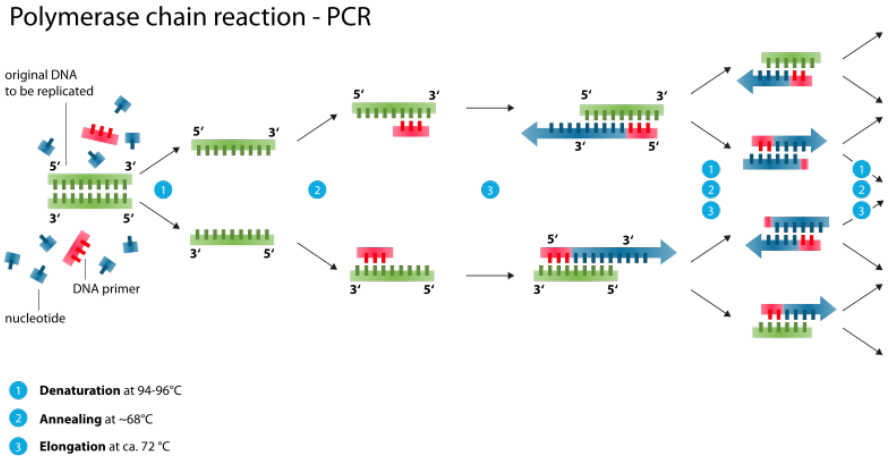

Figure 2.9: Schematic of the PCR procedure. Taken from Wikipedia.org and licensed by Creative Commons [140]

All of the methods mentioned so far (with the exception of real-time PCR) trade speed for accuracy. This mostly arises from the fact that they need to amplify the signal first before they can detect it. Biosensors, on the other hand, use various biological material (like proteins, enzymes, antibodies, etc.) in order to capture the pathogen [6, 15]. After the capture they use various detection methods to tell if there are any pathogens present, the method being a source of classification. Biosensors promise to deliver on the real-time detection speed that was lacking so far, while retaining the same accuracy. While this goal still has not been reached it is feasible that in the foreseeable future biosensors will be able to perform such detection [15].

The most popular detection technique in biosensors could arguably be optical detection. Using fluorescent compounds, such as fluorescein isothiocyanate (FITC), attached to antibodies (similar to ELISA technique of producing colour change) pathogens could be counted by observing the amount of fluorescent light entering the microscope and comparing it to a control curve [6, 141]. Surface plasmon resonance (SPR) sensors measure the reflectivity of polarised light shined form a laser bouncing back from a thin film metal surface. This gives them the additional benefit of not only being able to detect pathogens, but also the ability to monitor antigen-antibody reaction kinetics. These devices are quite big and require trained staff to use meaning they

are not readily available to use at any situation, despite their high accuracy ($10^2 - 10^9$ CFU/ml) [6, 142]. Surface-enhanced Raman spectroscopy (SERS) is a method in which a surface is exposed to a light source and is monitored for specific Raman scattering. This gives information on vibrational properties of systems and objects on the surface, which can then be matched to bacteria. Wang *et al.* developed a low-cost device that utilised Raman scattering to detect bacteria. They managed to detect very low concentrations of 10^2 CFU/ml of both *E. coli* and *S. aureus*, with an assay of only 25 minutes [131]. Anthrax bacteria can be detected by using SERS as well. Zhang *et al.* developed a low-cost, battery-operated, and portable Raman spectrometer which is capable of detecting spores with a concentration as low as $2.6 \cdot 10^3$, with an assay that lasts 11 minutes [143].

Electrochemical biosensors use current or potential changes in order to measure the number of pathogens captured. The most common of these are amperometric methods which are based on the linear relationship between analyte concentration and current. As current, voltage, or resistance are interchangeable linearly using ohm's law any of them can be used to measure the current changes [141]. If a direct exchange of electrons between electrode and analyte is not possible, redox mediators are introduced to facilitate the exchange. Using this method a result can be obtained between 3-4 hours with an accuracy of $10^3 - 10^4$ CFU/ml [6]. Piezoelectric biosensors observe the changes in the resonance frequency on a quartz crystal microbalance (QCM) using a frequency sweep. As the pathogens are deposited on the microbalance, the resonance changes and this shift allows the user to determine the mass of the pathogens on the quartz crystal. This method offers an assay time of around 3 hours with an accuracy of $10^3 - 10^8$ CFU/ml but is not suitable for automation which renders it useless in some areas [144]. Like the QCM method, electrochemical impedance spectroscopy (EIS) uses a frequency sweep to deterimine the number of pathogens in an analyte. However it determines the impedance of the analyte from the resultant current of the transducer. Depending on the route the user wants to take, they can either solve a system of partial differential equations or go with a more simple method of equivalent circuits. The user must be careful, though, as they have to make sure that the equivalent circuit makes physical sense. This route may even give erroneous results as different circuits can fit the same data [6, 145]. The main advantage of EIS is that labels are not necessary, hence preparation time is reduced. Unfortunately, the accuracy is worse than in traditional methods with an average of 10^5 CFU/ml, below which the signal decreases, but the authors have quoted a detection threshold of 83 CFU/ml [6, 146].

2.4.2 Methods of pathogen concentration and delivery

So far the focus has been on the methods of detection of pathogens. The capture is performed using either antibodies or enzymes or other types of biological

material - the most popular of which are antibodies. They are most commonly applied to the surface in three ways: through absorption, with a thin gold film on which the antibody will be placed; using the Avidin-Biotin interaction between an avidin coated surface and biotinylated antibodies; and using self-assembled monolayer (SAM) formation on which antibodies are immobilised [6].

The actual methods of delivering the pathogen to the biosensor's active area vary. One way would be to use gravity after placing a droplet of the analyte on the biosensor. The smaller the droplet the less there is to travel for the pathogen. A more useful technique, and one capable of better automation, is using flow to bring new pathogens into the device and let them get captured on the active area, but unless this area is directly in the way of the flow chances of capture are low as only the pathogens next to the active area of the device will be captured. Several methods were developed to improve this efficiency, few of which are: acoustophoresis, electrophoresis, and magnetophoresis.

Magnetic beads can be controlled by varying the magnetic field in the electromagnets on either side of the device. Because the magnetic field is so strong it is hard to precisely control the beads so they are limited to simple motion. After being covered with antibodies they become the active area. They are either suspended in the middle of the flow or made to move perpendicular to the flow to maximise the capture rate [147]. The use of magnetic beads has many functions outside of antibody capturing as they can be used for drug delivery, protein purification, etc. [148]. Gu *et al.* have developed a device that uses magnetic nanoparticles functionalised with pathogen specific antibodies to capture the pathogens to have them analysed by ELISA. They have managed to obtain a limit of detection of only 10 CFU/ml, in a 1 h assay [112]. Figure 2.10 shows a graphic of the interaction between the magnetic nanoparticles and the pathogens, as well as a microscope image of a cell interacting with the nanobeads. The beads can also be paired with different detection techniques, like in the case of the work done by Gatto-Menking *et al.* with *B. anthracis* spores. The have combined the beads with electrochemiluminescence (ECL). This immunomagnetic ECL (IM-ECL) method was reported to detect as low as 100 spores in 40 minutes, although the volume of detection was not specified. It could imply that no matter the volume, after the magnetic beads were run through the sample if there is at least 100 spores captured they will be detected [149].

Electrophoresis is a technique in which an electric field is applied to a volume, in which the particles become temporary dipoles, thus inducing motion in one direction or another, depending on the field strength and direction. The speed at which they move also depends on the size of the particles. This technique can be used to make pathogens go towards an antibody coated surface, amongst others. After the right pathogens are attached the rest are washed away with the flow. Suehero *et al.* showed that by using dielectrophoretic impedance measurement (DEPIM) and electropermeabilisation-assisted DE-

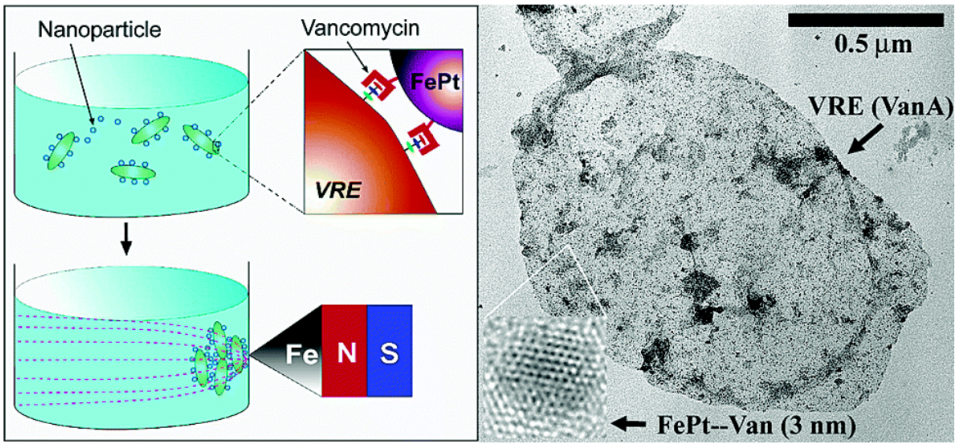

Figure 2.10: Schematic of the interaction between pathogen cells and the nanoparticles on the left, with a microscope image of the interaction on the right. VRE stands for vancomycin-resistant enterococci, while FePt is the chemical composition of the magnetic particle (iron-platinum). Taken from Gu et al.*[112].*

PIM (EPA-DEPIM), a biosensor using antibody capturing methods can reach a sensitivity of 10^4 and 10^2 CFU/ml, respectively, and all in a flow of speeds up to 12 ml/min [113]. They do this in 3 h, and require bacteria specific optimisation. If the cells are mixed with single-wall carbon nanotubes (SWNT) their response to the electric field is increased so a detection threshold of 10^4 can be achieved [150].

Acoustic radiation forces have been used for decades as a method of manipulating particles [153]. It has the ability to move particles in bulk [94], but without damaging them and keeping their viability preserved [90, 154]. There are many uses for this technique, such as filtration (both at the boundary between two fluids and by using a porous mesh) [155], concentration (pushing pathogens in a single or multiple planes [156], a derivative of which may be pushing the pathogens towards an antibody coated surface) [96], cell washing [151], and others [90]. An important aspect of an acoustofluidic device is the ability to focus, separate or concentrate cells. USW can be used to filter small, micron-sized bacteria with a filtration efficacy of over 99 % in case of *Saccharomyces cerevisiae* and just over 80 % in case of *E. coli* [155]. The filtration device can be see in figure 2.11. Instead of filtration, separation can be used, and in case of *E. coli* 95.65 % of them can be separated from peripheral blood mononuclear cells, by using surface acoustic waves (SAWs) [157]. If two orthogonal USW fields are used $>$ 95 % of *E. coli* cells can be focused to the centre of the channel, a feat not easily achieved due to streaming issues associated with high pressure USW fields [158]. In high flow scenarios, a device made by Carugo *et al.* managed to increase the concentration of particles 60 fold [156]. This device insipired the device designed in later chapters. If latex

Table 2.1: Summary table of the detection methods mentioned in this section including the limit of detection and the assay duration, and including any important remarks about the method.

Method	Capture limit (CFU/ml)	Time	Reference	Note
Cell culture	2.5	4-6 days	[6]	Not all cells culture
ELISA	$10^0 - 10^4$	$<$ 1 day	[6]	
Anthrax test kit	$10^5 - 10^6$	15 min	[31]	Commercially available, not cheap
PCR	$10^0 - 10^6$ *	1-24 h	[6]	Very powerful, requires databases
pXO-1 PCR	10	3 h	[135]	Protein chain not unique to *B. anthracis*
LAMP	N/A	1 h	[139]	Detects up to 1000 copies of BA genome
SPR	$10^2 - 10^9$	Not quoted	[142]	Bulky and requires experienced user
SERS	$10^2 - 2.6 \cdot 10^3$	15 min	[131]	Low-cost, can be battery operated
Amperometric	$10^3 - 10^4$	3-4 h	[6]	
QCM	$10^3 - 10^8$	3 h	[144]	Not suitable for automation
EIS	10^5 †	10 min	[146]	Hard to match a model to real-life scenario
Mag. nanoparticles	10	1 h	[112]	Potentially costly
IM-ECL	N/A	40 min	[149]	Detection up to 100 spores in unspecified volume
EPA-DEPIM	10^2	3 h	[113]	Flow up to 720 ml/hr, requires optimisation
SWNT-DEP	10^4	10 min	[150]	Requires additional 30 min of preparation
real-time (RT)-USW	$1.6 \cdot 10^4$	N/A	[114]	Real-time detection
USW-PCR	10^3	2 h	[151]	
USW-metal-clad leaky waveguide (MCLW)	10^3	5-25 min	[152]	
QW Immunosensor	10^4	N/A ‡	[96]	QW is very sensitive to changes in device

* In most cases the detection threshold is up to 100 CFU/ml. Lower thresholds require a lot of expertise and specific conditions [129]

† The authors have quoted a detection threshold of 79 CFU/ml, but have said it requires further statistical analysis. [146].

‡ The assay time in the device is only 2 min, but the detection is done through post-assay imaging and counting which takes further, unspecified time.

particles are used in conjuction with *E. coli*, up to 95 % again, can be captured, using the secondary acoustic radiation forces between the seed particle and bacteria to assist capture. With this method even sub-micron particles down to 110 nm can be focused [114, 159–162], and can exhibit an increase in detection up to 128 fold [161]. Ultrasound is incorporated in some *in situ* systems where rapid detection is necessary: Ohlsson *et al.* demonstrated a device that uses ultrasound to separate, trap, and wash red blood cells, and deliver them to a PCR chip for analysis. They managed to attain a limit of detection of 10^3 *Pseudomonas* bacteria/ml in 2 h [151]. Real-time detection is a long sought-after goal for a lot of field tests, and Bavli *et al.* have managed to create a real-time monitoring device that uses USW combined with latex-beads to achieve a limit of detection of $1.6 \cdot 10^4$ CFU/ml for *E. coli*, and $4 \cdot 10^4$ CFU/ml for *Salmonella enterica*, both in water [114]. This is a signifi-

cant improvement over the tests that do not use ultrasound. *Bacillus globigii* (BG) spores often are used as a safe substitute for anthrax and a few groups have worked with them to find methods for anthrax detections. By utilising ultrasound with an optical MCLW sensor Zourob *et al.* have managed to get a detection limit of 10^3 spores/ml, which is a 100 fold upgrade over MCLW alone [152]. Another device seminal to the development of the device in chapter 3 is the one developed by Martin *et al.*. By combining a quarter wave device with an immunosensor surface they managed increase the capture of BG spores 70 times, and get a detection limit of 10^4 CFU/ml [96].

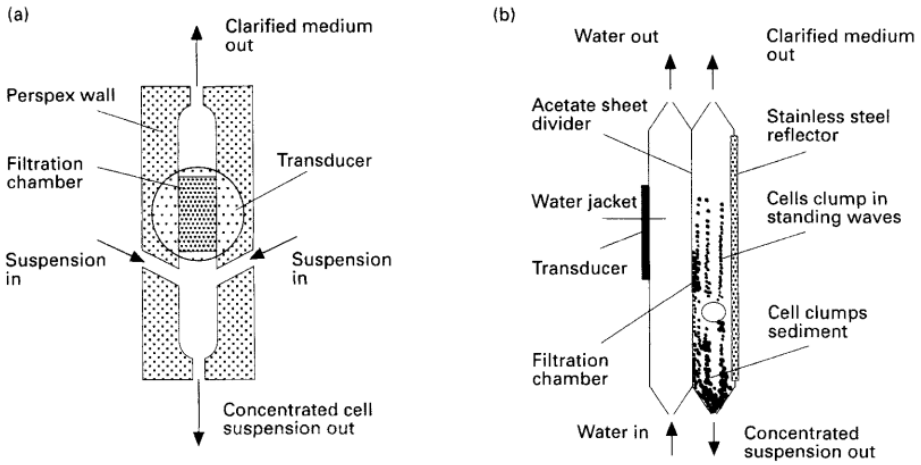

Figure 2.11: (a) Front view through the filtration chamber. The dark gray rectangular region represents the 1.0 x 1.5 cm electrode area on the back face of the circular transducer. (b) Side view through the filtration chamber. The acoustic path length through the cooling water section is 1.45 cm and the additional path length through the suspension to the reflector is 1.25 cm . Schematic taken from Hawkes et al.*[155]*

Table 2.1 shows a summary of all the methods mentioned in this section. It looks at the time it takes to complete the analysis, as well as the detection limit, and it gives any comments important to the method (low-cost, easy or hard to use, etc.). It will focus only on the devices that provide a number for the detection limit.

2.5 Allergy diagnostics

Testing for allergic reactions is not a straightforward process. No method can reliably check a patient's response in all conditions and for all allergens [3] [163]. As such a few methods are used regularly to provide double positives and confirmation of reaction, each with their own trade-offs.

[3]for instance skin testing is not a good method for detecting inhalant allergies

Before any tests are performed the patient history should be taken. This is usually the best indication of whether or not a reaction is an allergy, and it is the best tool a clinician can have during diagnosis [164–166].

One such method is the skin prick test (SPT), sometimes followed by intradermal test (IDT). For a skin prick test, a small prick needle is inserted into the skin percutaneously through an allergen solution, usually on the forearm. This is repeated for every allergen that is to be tested. It is also accompanied by a positive control, most often achieved by a histamine solution (10 mg/ml), and a negative control in the form of saline (0.9 %) [166]. After 15-20 minutes the prick site is checked for a wheal and flare response on the skin. The size determines the strength of the reaction. This tests offers moderate sensitivity and is well suited for testing drug allergies. However, if the patient is susceptible to rashes a false positive may occur, and if the allergen is unstable no reaction may occur [167].

If a negative reaction occurs when performing a SPT the next step is to do an IDT. A volume of allergen between 0.02 - 0.05 ml is injected intradermally, creating a small "blip" around 3 mm in diameter. For each allergen there is a series of tests starting off from the smallest concentration and then increasing with each new test. It allows for a more sensitive and precise measurement of the reaction. Intradermal testing is more sensitive than skin pricks but it is less safe and reliable as it can often lead to false positives (an even higher susceptibility to rashes [168]). In extreme cases it can lead to anaphylaxis [167]. Furthermore, if a patient is taking antihistamines the test won't reveal an accurate picture [168].

The current recommendation both in literature [166] and government guidelines [169] is that alongside the SPT specific serum immunoglobulin E (sIgE) levels are taken from blood samples. By using an fluorescent immunoabsorbant assay an sIgE response to an allergen can be measured. By themselves these *in vitro* tests are not accurate enough as they depend on the initial sIgE concentration - the higher the initial concentration the poorer the diagnosis, as levels of sIgE drop over time suggesting desensitisation [170]. A positive result indicates that the patient is sensitised to the allergen tested, although this in itself is not enough to determine clinical allergy in some cases [169]. Errors do occur when the allergen specific IgE level is wrongfully correlated with the probability/severity of the patient reacting to the allergen [171]. This leads to serum IgE immunoassays being considered less predictive than SPT [172]. Neither the skin prick test, nor the serum IgE tests are enough by themselves to determine allergy as they might point to different causes of allergic reaction - SPT shows a mast cell reaction, while sIgE points to an antibody IgE mediated reaction [169].

In extreme cases, where the usual SPT, IDT, and sIgE test do not provide a conclusive result on the existence and severity of an allergy, doctors can resort to a provocation test (PT), also known as a drug challenge test, or oral challenge test. It is the current gold standard for testing for drug allergies

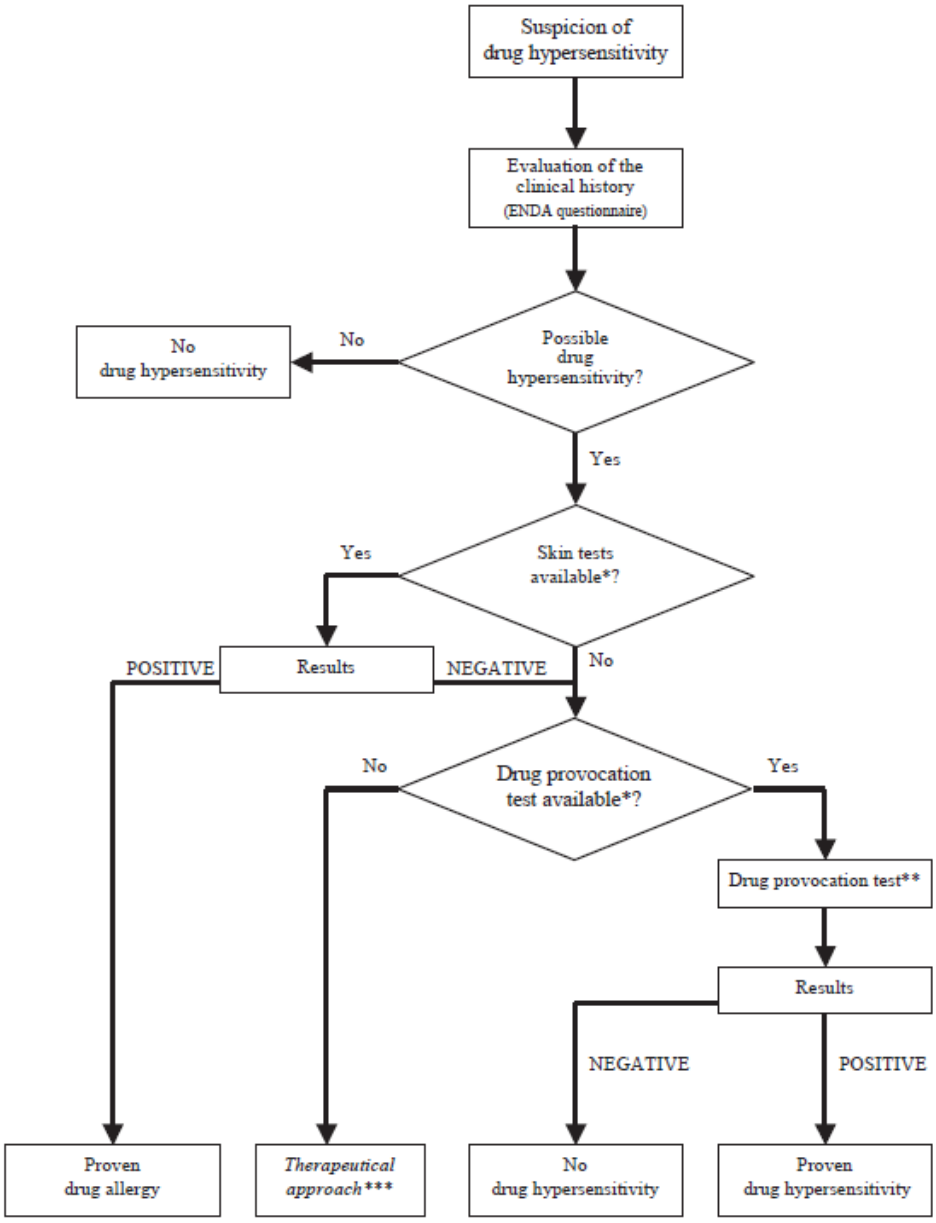

*Figure 2.12: Flow chart when assessing drug allergies (adapted from [173]). * Currently available biological tests to diagnose drug allergy lack sensitivity. **In the absence of contraindications. ***If no alternative is available (e.g., NMBA, chemotherapeuticadrugs), readministration of the drug is allowed under close surveillance, considering premedication and/or desensitization.*

[165]. While never the first test implementation, its dangerous nature means that under different guidelines it has different uses: it is used as a method of confirming a negative reaction [174]; a mostly exclusionary method with a

potential to confirm drug allergies in less severe cases [175]; or as a gold standard used to confirm drug allergies, but with some limitations on the use [176]. Figure 2.12 shows the flow chart of assessing drug allergy. The test itself uses the same type of exposure that caused the reaction in the first case: usually this consists of oral ingestion of the drug [165] or food [166] in question. For drug allergies the initial dose ranges from 1:10000 to 1:10 of the therapeutic value, depending on the drug in question and the patient's possible reaction. It is then slowly increased in intervals of at least 30 minutes, depending on various factors, until either an adequate reaction is observed or the upper dose limit is reached [176]. For most common food allergies, the mass of the substance ranges usually from 3 mg to 3 g and is increased in half-logarithmic steps. For best results it is performed in a double-blind setting [166], known as a double-blind, placebo-controlled food challenge (DBPCFC). Provocation tests are inherently dangerous, with guidelines requiring that trained staff are always present in case of life-threatening emergencies, and that emergency resuscitative equipment is always available. While these types of tests usually have a very high negative predictive value (NPV) they do have further problems: patients do not want to be exposed to the drug or food that caused a reaction, and a negative test does not prove a tolerance to a drug in the future, but rather only during the time of the challenge and to the doses that were challenged [165].

The basophil activation test (BAT) is an experimental procedure that is still not implemented in hospitals and allergy centres worldwide. BAT has first gained use in testing for food allergies but this has been expanded to also include drug and pollen allergies [177]. It relies on basophil expression to enzymes such as CD63 [178] or CD203c [179], which is analysed using fluorescent activated cell sorting (FACS). The process itself is very quick, and lasts around an hour, while the patient only experiences the minimal discomfort in form of a single needle prick. In addition to running positive and negative controls, this technique can test the basophils on varying doses of the allergen providing high precision [179]. The technique has higher specificity and NPV than SPT or sIgE, without loosing specificity or positive predictive value (PPV). However, BATs require highly skilled technicians, and access to specialised and expensive equipment (FACS machines). The technical knowledge needed to successfully perform this test is quite high [166]. Furthermore, the ability of basophils to express for either CD63 or CD203c diminishes over time with some studies suggesting that even 4 hours at 4 °C is enough to reduce expression, although most sources agree it takes between 24 and 48 hours to see a considerable diminution of expression [177]. This means that the central piece of equipment is a limited, shared resource, while the samples themselves have a time limit during which the test needs to be performed resulting in very limited use and possible bottlenecks in allergy centres.

Table 2.2 shows the estimated times each of the above mentioned tests would take, both from the patient, and technician perspective as well as the

Table 2.2: Duration time (for the patient and to obtain the final results), expertise required to perform the test, as well as the accuracy of the test (presented in the form of the negative predictive value (NPV) and positive predictive value (PPV)) for all allergy test types mentioned in this section. For all test types the NPV and PPV values have a high range since the tests have varying rates of success depending on the type of allergen (drug, food, environmental) and in some cases are dependant on individual allergens.

Test	Patient time	Total time	Experience level	NPV	PPV
Skin prick test	$\sim$ 30 min *[167, 180]	$\sim$ 30 min *[167, 180]	Low [166, 167]	72-100% [180, 181]	29-99% [180, 181]
Intradermal test	30-40 min *[167]	30-40 min *[167]	Low [166, 167]	X	X
serum IgE test	5 min	24 h [6, 169]	Medium [171]	76-89% [182]	22-95% [182, 183]
Provocation test	$\sim$ 8 h †[166]	$\sim$ 8 h †[166]	High [165, 184]	94-98% [165, 185]	<50-100% ‡[186, 187]
Basophil test	5 min	60-90 min [179, 188]	High [166]	22-99% [178, 179, 189]	71-100% [179]

* If delayed reaction is to be observed the patient needs to return after 24, 48, and/or 72 hours.

† For delayed reactions constant monitoring is needed between 1-4 weeks [166]

‡ In case of food allergies the DBPCFC is considered the gold standard and therefore the most accurate way of testing for allergies [182, 186]. As such, it is almost impossible to find studies that examine the PPV of the test.

experience level required to complete them accurately. Finally it shows the range of PPV and NPV for each of them. What is clear is that there is a gap in the abilities of various allergy tests that is yet unfulfilled: a quick test that is relatively painless for the patient, has high predictive values and is easy to perform.

2.6 Biofilm reduction therapy

Preventing or reducing and eradicating biofilms in wounds is particularly challenging. Preventing attachment of bacteria to the wound tissue can be achieved with a glycoprotein lactoferrin. It is a part of the human innate immune response and can be found in tears, saliva, mucous, and milk [75]. It has a strong binding affinity to iron which reduces bacterial motility during the initial stages of biofilm formation and adhesion. It binds to components present in the cell walls of Gram-negative bacteria, ultimately causing lysis [190]. Xylitol is an artificial sweetener that can cause lysis in Gram-positive bacteria and prevent their adhesion. The two have been used separately, or together to prevent the formation of biofilms. Great efficacy has been shown in treating *Pseudomonas Aeruginosa* (*P. Aeruginosa*) biofilms *in vitro* with a combination of lactoferrin and Xylitol [191]. By combining the two in gel form and applying a silver dressing, a further achievement in term of biofilm viability reduction can be realised [192]. The treatment may however still take months to be fully successful [193].

Quorum sensing inhibition (QSI) is one of the most popular methods of biofilm prevention. Small signal molecules are secreted throughout the biofilm in order to regulate virulence, motility, metabolism and more. The bacteria sense these molecules in their surrounding and adjust their behaviour accordingly. This behaviour is known as quorum sensing (QS) and is similar to how higher organisms behave on an cellular level [194, 195]. The disruption of this mechanism can therefore be a critical therapeutic target. It however does not cause dispersal of the biofilm, nor its detachment [196], but rather it decreases the tolerance of the biofilm towards antibiotics. Substances like furanones and Manuka honey act as inhibitors by downregulating the four major quorum sensing genes [75].

The most basic and longest established method of biofilm eradication is physical removal, known as debridement [75]. It can speed up wound healing, and reduction of wound size, but complete wound healing only comes after weeks of treatment, if at all [193, 197]. The efficiency of debridement can be increased with the use of chemicals such as hydrogen peroxide or certain enzymes [198]. A big issue with this method is the presence of persister cells - bacteria left behind after most of the biofilm has been removed. These allow for the regeneration of the biofilm, which makes debridement not a permanent solution [199].

2.6.1 Ultrasound as a biofilm treatment method

Plenty of research in the past few decades has focused on finding non-invasive biofilm treatments, with a specific focus on overcoming antibiotic resistance and tolerance [75]. Despite the mechanisms not being fully elucidated, ultrasound can be used to increase antibiotic efficacy. 66 A combination of low-intensity ultrasound with aminoglycosides was shown to improve antibiotic efficacy [200, 201] and reduce the minimum inhibitory concentration (MIC) by 50 % in planktonic cultures of *P. Aeruginosa* and *S. aureus* [202]. In contrast, a study done by Pitt *et al.* on planktonic *P. Aeruginosa* and *E. coli* using a low-intensity and low-frequency ultrasound, showed an increase in growth rate of both bacteria [203]. Likewise, further studies showed no difference in the biofilm structure with and without ultrasound, when examined with confocal laser scanning microscopy [204].

A low intensity ultrasound, similar to that in previous experiments, was shown to increase the permeability of *P. Aeruginosa* to several tagged molecules [202, 205]. The most likely explanation for this behaviour was offered by Runyan *et al.*, who concluded that the increased absorption of antibiotics through the cell membrane was the cause [202]. At low intensities, the ultrasound was found not to be damaging to cell viability by itself, despite the lack of consistency in the ultrasound parameter reporting [206, 207].

If the intensity of the ultrasound is increased it can be used in a different "mode" of operation. Destructive ultrasound, as it is known, has been shown to remove biofilms from implants and wounds [204, 208]. It has been shown that by using high-intensity ultrasound it is possible to reverse the biofilm tolerance and resensitise the bacteria to antibiotics [209]. One possibility is that the ultrasound disrupts the biofilm matrix, as well as exposes the bacteria inside the biofilm to nutrients, thus stimulating growth [203].

There are however several limitations to using ultrasound. In the majority of the studies, the test period was between 1 and 2 days, which is highly impractical in a clinical setting. Even the low intensity ultrasound, when used in setting that promote a faster and higher bacteria number reduction, there is tissue damage present [201]. Finally, due to the application method of the ultrasound with the antibiotic, there is still possibility of the antibiotic affecting the the host, and not just the biofilm [210].

Despite the lack of conclusiveness, there is plenty of evidence that suggests ultrasound can be used as an effective treatment against biofilm antibiotic resistance and tolerance, either by destroying the extracellular matrix, or by altering the cell permeability.

2.6.2 Using gas microbubbles to aid ultrasound in biofilm treatment

Microbubbles, through their behaviour, allow ultrasound to combine the low-intensities that are shown not to damage tissues, with some of the properties

of "destructive" ultrasound, namely, the ability to disrupt the extracellular matrix. In a way, it is the natural progression of the ultrasonic treatment method.

Biofilm removal can be achieved by using microbubbles that are undergoing inertial cavitation due to ultrasonic stimulation. Birkin *et al.* have created a device capable of cleaning surfaces using only cold water and the microbubbles present in it by using this principle [211]. They applied this device to biofilm removal from hard surfaces like teeth [212] and glass [213]. It was effective in removing the biofilm, but so far not enough research was done to see if wound tissue damage is to be expected. Furthermore, by just removing the biofilm there is a possibility that the biofilm fragments may reattach somewhere else, as they are still alive at the time of removal.

A different approach to biofilm treatment using microbubbles is to use them to only disrupt the matrix. He *et al.* used a combination of low-intensity ultrasound with microbubbles and antibiotics to significantly reduce the number of viable cells (from 10.51 to 7.17 log_{10} CFU/ml) [214]. They showed that the microbubbles (MBs) created micro-pores in the biofilm. By altering the extracellular matrix the MBs have increased the antibiotic uptake. These micro-pores also allow an influx of nutrients to the deeper layers of the biofilm, which encourages bacterial growth and reactivation. This can result in an even increased antibiotic uptake [215].

Studies have shown that the combination of ultrasound (US) and MB can reduce the MIC of the antibiotic by 50 % [216] and by using the two with a sub-inhibitory quantity of 50 μg of Gentamicin, significant reductions in the biofilm biomass can be achieved [217]. It should be noted that the studies dealing with microbubble and biofilm interactions have focused mostly on single-species biofilms, not taking into account the more real-world variants.

Chapter 3

Device Characterisation

3.1 Introduction

In this chapter an acoustofluidic device capable of directing cells to a glass surface as they flow through the device is developed and characterised. The design is motivated by two applications, the capture of spores from aqueous samples and the isolation of basophils from blood. these are explored in chapters 4 and 5 respectively. In both applications an antibody coating on the glass surface was the key to capture.

There is a trend in medicine and biology towards devices with disposable fluidic cells, with the advantage of sterility and a lack of cross-contamination between samples. The device described here can be considered a prototype which could be further developed towards this model. This device was constructed so that most parts can be sterilised and handled, and it is planned for the assembly to be easy and intuitive. Only a few components are discarded after use, and those are easily replaceable.

This chapter will start by providing the development history of the current device by going through its previous iterations, including the Aquality device (section 3.2). It is then going to describe the device design and how it was informed by the computer models first (sections 3.3 - 3.4). Then it will go into the various aspects of the device, such as flow rates, acoustic forces in both Z- and Y-direction, streaming, and others in sections 3.5 - 3.10. The last large part of the chapter is devoted to the biological aspects of the device - pathogen tagging, and antibody coating, as seen in sections 3.11, and 3.12, respectively.

3.2 Previous iterations

This section describes previous iterations of the device design showing the steps that lead to the final design.

3.2.1 Aquality device

The first prototype tested was based on the Aquality device described in [156] and [218]. In construction it is very similar to the final device used in this thesis - it is a layered thin-reflector (TR) resonator, but instead of a stainless steel carrier layer it used Macor. The device, both disassembled and assembled is shown in fig. 3.1. The biggest difference was in the number of outlets: since the device in the paper was made for concentrating pathogens instead of capturing them it needed to have two outlets: one for the enriched medium, and one for the depleted one. When used in the capture experiments central to this thesis one of the outlets was sealed. This device was soon replaced with other prototypes primarily because of the how hard it was to machine Macor, as well as the second outlet not being needed.

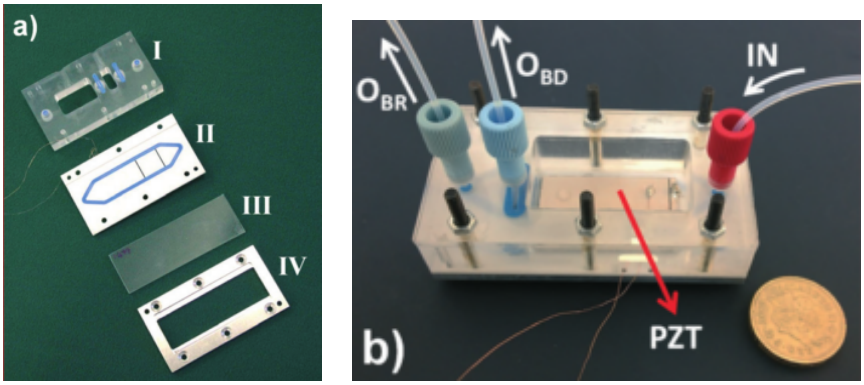

(a) Disassembled *(b) Assembled*

Figure 3.1: The Aquality layered resonator with all of the parts visible. it comprises of (I) a PMMA manifold for connection of inlet/outlet tubing, (II) a milled Macor TR layer which has a recess for the fluid to pass through, and a groove on which a PDMS gasket (blue) used to seal of the fluid layer sits. The transducer is glued underneath with a layer of EPO-TEK 301 epoxy. (III) is the glass reflector, and (IV) is a metal frame with a window for optical accessibility and struts across it for the rigidity of the glass reflector. Taken from Carugo et al. [156]

3.2.2 Glass carrier layer thin reflector resonator

The glass carrier layer thin reflector resonator (GTR) was the first device fully developed for this project. In it, the Macor carrier layer was changed for a glass one. Macor was replaced because of its unavailability and the high level of skill needed to properly machine it. It had a strong autofluorescence and could not be used as a background for fluorescent microscopy - the Auramine stained spores were too dim compared to the background.

The carrier layer was made out of a glass cover slip ($\sim$ 170 μm) on top of which a transducer was glued with epoxy. An acrylic scaffold was created to provide rigidity to the carrier layer by attaching them together with polydimethylsiloxane (PDMS). The PDMS was mixed in a 10:1 ratio and after application it was cured overnight at 80 ℃. The scaffold was made so that it fits perfectly on the manifold for ease of use. The fluid channel walls were made with Parafilm M (film made out of paraffin wax, used for its elasticity), by cutting a channel shape into a thin sheet (170 μm) of Parafilm using either a scalpel or a laser cutter. When the device is firmly clamped the width of the Parafilm is $\sim$ 140 μm. The rest of the device remained the same as before.

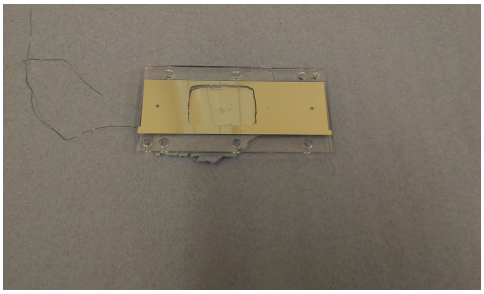

(a) Top view

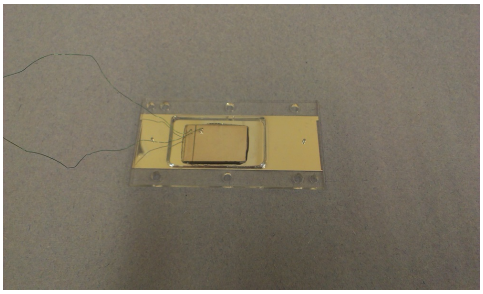

(b) Bottomw view

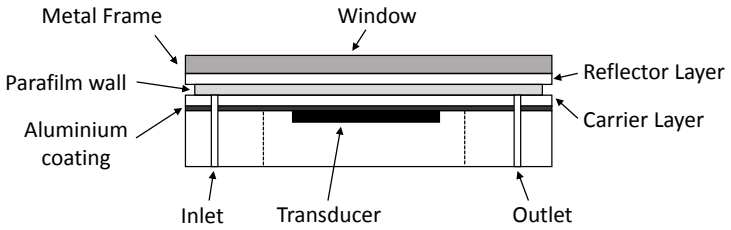

(c) Schematic

Figure 3.2: Image showing the aluminium coated TR resonator manifold with carrier layer and transducer and its schematic. The transducer is detached and had to be posed to show its original position

While the glass carrier layer did not autofloresce the spores were still very dim. The addition of an aluminium coating (200 nm layer applied through nano deposition) to the back side of the carrier layer (the side facing the transducer) provided an improved contrast when imaging the spores. Because of the aluminium coating, this device, the mirror thin reflector resonator (MTR), did not create an autofluorescent background. In construction it is the same device as GTR, except the coating of aluminium that was deposited onto the coverslip. Fig. 3.2 shows the manifold of the device with the attached carrier layer. The transducer has separated since the last use and no images exist from the time experiments were performed. While the cover slip did not provide any major benefits to the strength of the ultrasound standing wave (USW),

the aluminium coating did make counting and viewing spores a lot easier. The limit of detection for this device was too high to meet the goals set for this project.

3.2.3 2 stage Half-wave/Thin-reflector resonator (HW/TR)

In the previous iterations there was only one TR transducer in the latter half of the channel doing all the focusing. The purpose of this iteration was to add a pre-focusing stage in the initial half of the channel that would bring all of the spores to the centre of the fluid layer by using a half wave (HW) transducer. The pre-focused spores would enter the TR field at the same height, which would reduce the capture area, as all are affected by an equal force. The device features an extended channel (length-wise), but made thinner (width-wise). There are two sections in the channel: first, following the flow, is

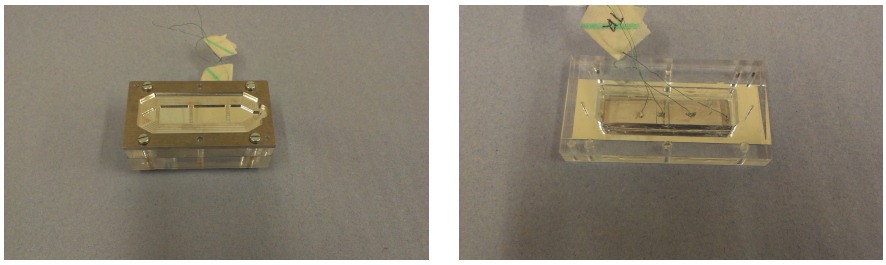

(a) Top view *(b) Bottom view*

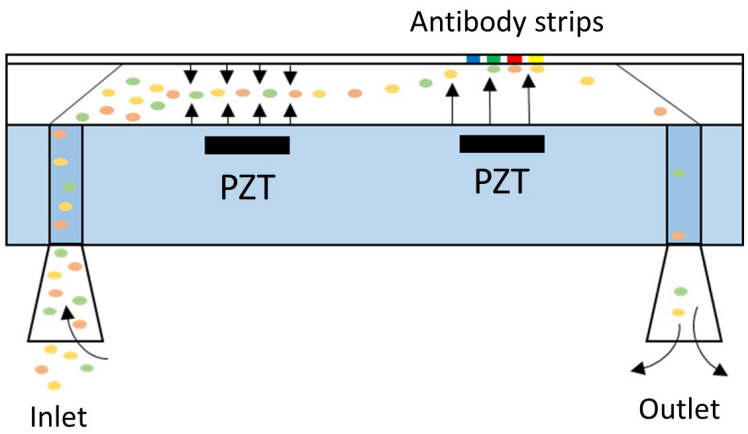

(c) Schematic

Figure 3.3: Image showing the HW/TR resonator device and its schematic

the half-wave section, where the transducer is emitting a half-wave resonance frequency in order to focus the spores to the centre of the channel, and all in one plane. The second half is the thin-reflector section which performs as in the previous devices, forcing the spores onto the antibodies attached to the

reflector layer glass slide. The planarity of the spores as they enter the TR standing wave field is intended to ensure all the spores take approximately the same time to arrive at the antibody slide and improve the chances of the spore reaching the antibody coating before exiting at the outlet. At this point some preliminary tests were made with PDMS fluid channel walls but Parafilm was still used as a main method of containing the fluid within the channel. The device and its schematic is shown in fig. 3.3.

Further changes include switching the carrier layer from a glass cover slip to a 1 mm thick glass slide. Modelling has shown that at the bottom of the fluid channel, near the carrier layer, the force is stronger with a slide rather than with a coverslip. The glass slide provides additional stability as it does not crack easily. Because it is thicker the flexural waves are less present therefore the transducer will take longer to separate from the glass.

It proved difficult to tune the HW mode on a device already tuned to a thin-reflector mode and therefore its contributions were minimal. The switch to a different carrier layer thickness showed that more modelling was needed which provided the impetus for a search for the appropriate material. Furthermore, by using thicker materials, the device is simplified considerably as it removes the need for the acrylic scaffold.

3.3 Device design

The pathogen capturing device is primarily a TR layered resonator. It consists of a lead zirconate titanate (PZT) transducer (PZT26) secured to a stainless steel carrier layer with epoxy (Epotek 301) [1]. The stainless steel sheet has a $\sim 100\ \mu m$ recess milled inside it. A gasket, cast out of PDMS, is placed inside the groove to provide the side boundaries of the fluid layer, the bottom being the carrier layer and the top the reflector layer. Just outside of the gasket a spacer made out of cut cellulose acetate and 100 μm high is placed to ensure planarity and constant hight. On top of the gasket and the spacer lies a thin, 170 μm glass coverslip reflector layer. The inside of the reflector layer is coated with an antibody designed to capture specific pathogens. All of these layers are held in place with six screws and an acrylic manifold on the bottom, and a steel frame on top. The steel frame has a window so the fluid channel can be observed with a microscope. The inlet and outlet tubing is screwed into the manifold and has access to the fluid layer through two small holes in the carrier layer. Figure 3.4 shows the disassembled and assembled images of the device, as well as a cross-section schematic (if the z-axis is defined as going along the flow, the cross-section is taken along the XY plane in the middle of the device). Figure 3.5 shows the exploded diagram of the device.

[1] The epoxy is applied to transducer which is then placed on the carrier layer. The two are then held in place for 1 hour with magnets to let the epoxy thickness reduce to, ideally, 1 μm. It is then placed in the oven at 70 °C for 2 hours.

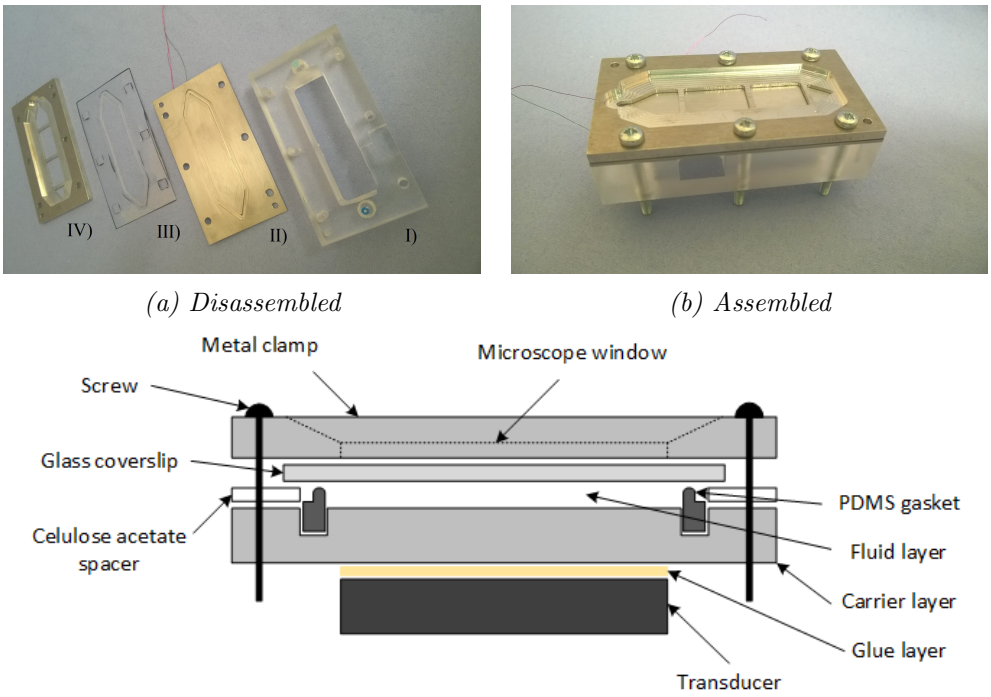

(a) Disassembled *(b) Assembled*

(c) Cross-section schematic

Figure 3.4: Images showing the pathogen capturing device. The components are: I) the acrylic manifold, II) the steel carrier layer with the groove around the fluid channel, and transducers on the back side, III) the cellulose acetate spacer, and IV) the metal frame to clamp the device securely. Not seen on the image, but a glass coverslip goes between III) and IV), and a PDMS gasket goes into the groove. The schematic is not to scale and only serves an illustrative purpose

Table 3.1: Dimensional and physical properties of the TR resonator. The thickness value is given for the active region of the device, and was normalised to the wavelength of the median resonant frequency at 922 kHz.

Layer	Thickness (μm)	Thickness/λ	Material	Density (kg/m^3)	Speed of sound (m/s^2)	Impedance ($Mrayl$)
Transducer	1000	0.182	PZ26 (Ferroperm)	7700	4530	34.9
Carrier	980	0.140	Stainless steel	7890	5790	45.7
Fluid	130	0.072 ($\ll \lambda$)	PBS	~1000	1480	1.5
Reflector	170	0.024 ($\ll \lambda$)	Glass	2500	5872	14.7

The device is held together by screws which allow for fast prototyping and testing. Planarity of the device is ensured by an even force applied from all screws, with the fluid layer thickness also determined by the torque applied. This thickness centres around 130 μm, but measurements showed that this varies by as much as $\pm 20 \mu m$. The resonant frequency of the device therefore

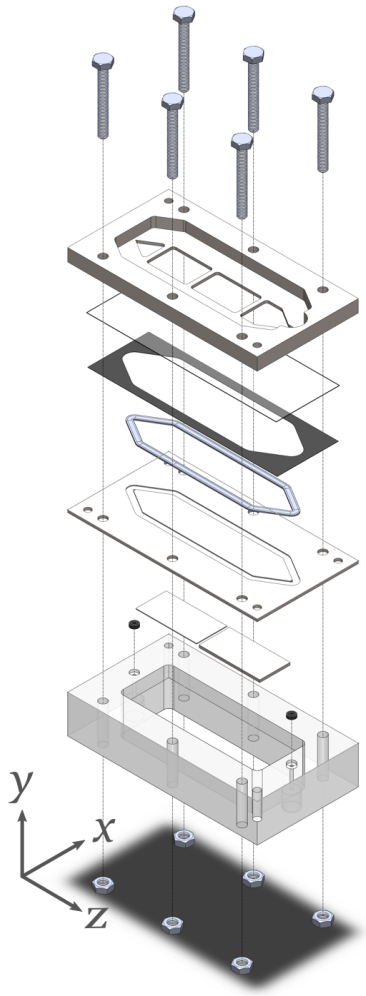

Figure 3.5: An exploded schematic of the device

lies in a range that was experimentally determined to have a mean of 927 kHz, and an standard deviation (SD) of 31 kHz (its median is 922 kHz). Table 3.1 shows the breakdown of layers and materials alongside their properties. It displays the thickness both as an absolute value in μm but also normalised to a wavelength. This wavelength was taken to be the wavelength of the median resonant frequency.

3.3.1 Construction and assembly

The transducer used in the device is a FerroPerm PZ26, 1 mm thick, PZT transducer. Figure 3.6 shows an image of the transducer with the most important aspects highlighted. It is first cut to size: 24 mm long and 12 mm wide. Along the width, some 3 mm from the edge a line is scored into the transducer using a diamond tipped scoring tool, in order to separate the small

part electrically from the rest of the surface, thus creating two terminals. The edges are smoothed out with a 1200 grit sandpaper. The transducer is then cleaned in a pH 13 basic solution to remove any oily residues. Silver paint is applied to the edge of the transducer to connect the smaller area from one side to the area of the other side. Two wires are soldered onto the transducer, one on each terminal.

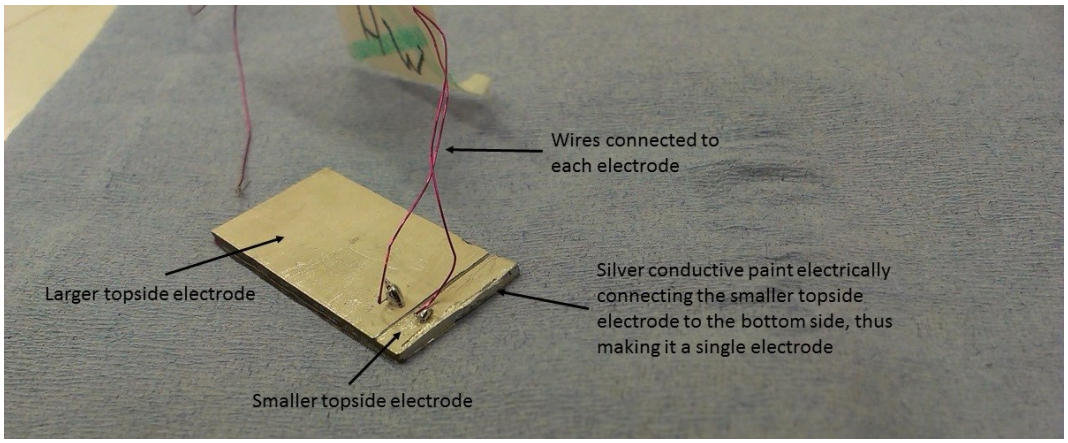

Figure 3.6: Image of transducer for the thin-reflector device with annotations of most important components

The stainless steel carrier layer, acrylic manifold, and stainless steel clamp, were all designed in computer aided design (CAD) software and cut out of metal or acrylic pieces using a computer numerical control (CNC) routing machine.

Before the transducer could be attached. the carrier layer was also cleaned in a pH 13 basic solution. Afterwards a thin layer of Epo-Tek 301 epoxy was applied onto the transducer which was then attached to the carrier layer. They were clamped together and left at room temperature for 2 hours in order to reduce the thickness of the epoxy layer. Afterwards they were placed in an oven at 70 °C for 1 hour to cure. Measurements showed that the epoxy layer before clamping had a thickness of 10 μm, while after clamping it was between 1 - 3 μm.

As mentioned above, the gaskets were cast out of PDMS inside a specially designed mould machined from acrylic. They were coated with a fine coat of talc powder to prevent them from sticking to other components during assembly and disassembly. The spacer was cut manually out of cellulose acetate with scissors.

Once all of the components were prepared they were assembled according to the schematic in figure 3.5.

3.4 Computer modelling of layer thickness'

A simulation is the quickest, cheapest, and easiest way to test which material is best suited for the carrier layer. An equivalent circuit model was developed by Hill et al [219] where an equivalent circuit [220], that was previously developed, was coupled with impedance and force transfer equations to predict most of the device behaviour. By approximating the layered resonator as a one dimensional model it can look at transmission and reflection ratios to determine how much of the wave is propagated through different layers. It does not take into account any two or three dimensional aspects of the device, like lateral modes or spatial distributions of the acoustic field.

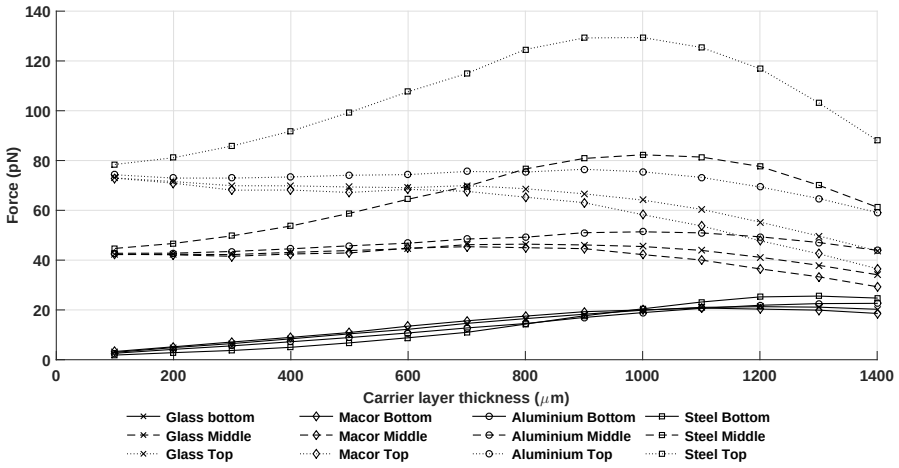

Figure 3.7: A comparison of the radiation force on a 10 μm bead as they change with varying carrier layer thickness. Four materials were explored - glass, Macor ceramic, aluminium, and stainless steel

The initial idea was to find a material that impedance matched either the PZT or the water in the fluid channel, thus reducing the energy dispersion on at least one boundary. The material properties were referenced from Onda Acoustic Properties of Solids [221] and Plastics [222] databases. Further limitations were the accessibility of the material and the ease with which it can be machined. A number of materials was quickly modelled (checked how strong the resulting resonances were), and the list was reduced to two new candidates: aluminium and steel. Metals have shown to be very good at strongly exciting resonances and the amount of energy being transferred into the fluid channel was greater than for other potential materials like some plastics (such as PDMS, acrylic, or Acrylonitrile butadiene styrene (ABS)). They were compared alongside two other materials that were used in these types of devices before: Macor [156, 218], a machinable ceramic from Corning [223], and glass[92].

The four materials were compared in MATLAB. The thickness of the

Table 3.2: Properties of the materials used for the contruction of the carrier layer

Material	Density (kg/m^3)	Speed of sound (m/s)	Impedance (Mrayl)
Glass	2500	5870	14.7
Macor	2540	5510	14.0
Aluminium	2730	6380	17,4
Stainless steel	7890	5790	45.7

carrier layer was varied and the radiation force on a 10 μm bead was calculated. The density, speed of sound and impedance values for the materials is given in table 3.2. Figure 3.7 shows the radiation forces at three points inside the fluid channel for all four materials. The best performance was found from stainless steel with a thickness of 1 mm, where the maximum radiation force was well over 100 pN, the only one to exceed that value. Furthermore throughout the channel the radiation force in the device with the steel carrier layer is bigger than that of the other materials, with aluminium coming the closest. The specific impedance of stainless steel (45.7 Mralys), which is the closes to the specific impedance of the PZT (34.9 Mrayls).This confirms the hypothesis that a material who is most closely impedance matched to the transducer may transfer more energy into the fluid channel - both aluminium and stainless steel performed better than glass or Macor, and both have closer matching impedances. The impedances can be found in tables 3.1 and 3.2.

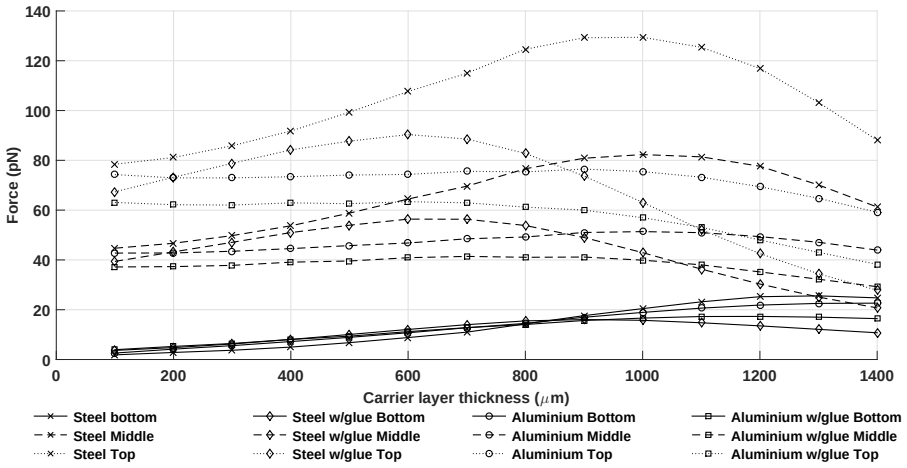

Figure 3.8: A comparison of the radiation force on a 10 μm bead as they change with varying carrier layer thickness. Two materials, aluminium and stainless steel, were explored, both with a 1 μm and a 10 μm thick glue layer. The "Bottom", "Middle', and "Top" descriptors refer to the position inside the fluid layer at which the radiation force is simulated

More importantly, there is a robustness associated with all of the carrier

layer materials. A change of a 100 μm won't make a big difference in the radiation force inside the fluid channel, as was shown in the modelling. This is important because it means the manufacture does not have to be extremely precise but rather the tolerances can be up to 10 % (a number matched by the machining tolerances given by the in-house manufacturers of the carrier layers).

The model presumes a 1 μm thick layer of glue which, in real life, may be unlikely. Values can commonly go up to 10 μm, which was the experience when trying to build the device. To test the effect of changing glue thickness two of the best materials, aluminium and steel, have been included in a new simulation, this time with a glue layer of 10 μm. Figure 3.8 shows how the strongest device resonance is found with a thinner carrier layer. For both steel and aluminium the best resonance carrier layer thickness shifted - for steel it is from 1000 μm to 600 μm and for aluminium it is from 900 μm to 400 μm.

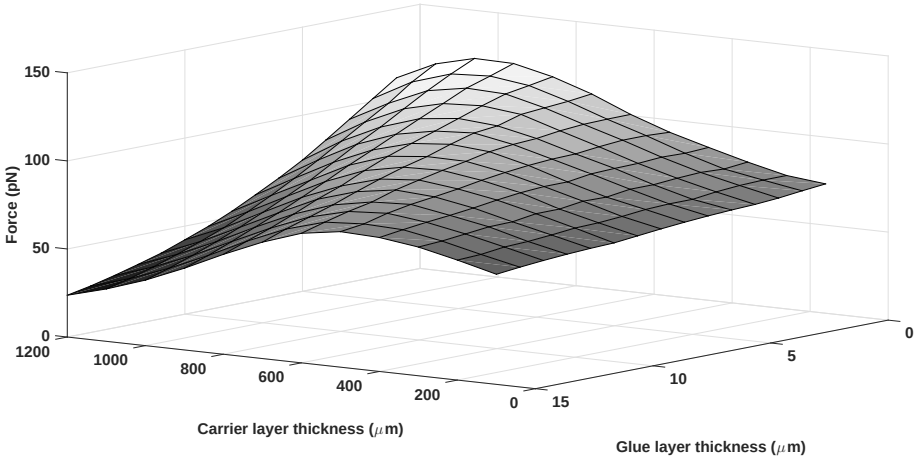

(a) Top of the fluid layer

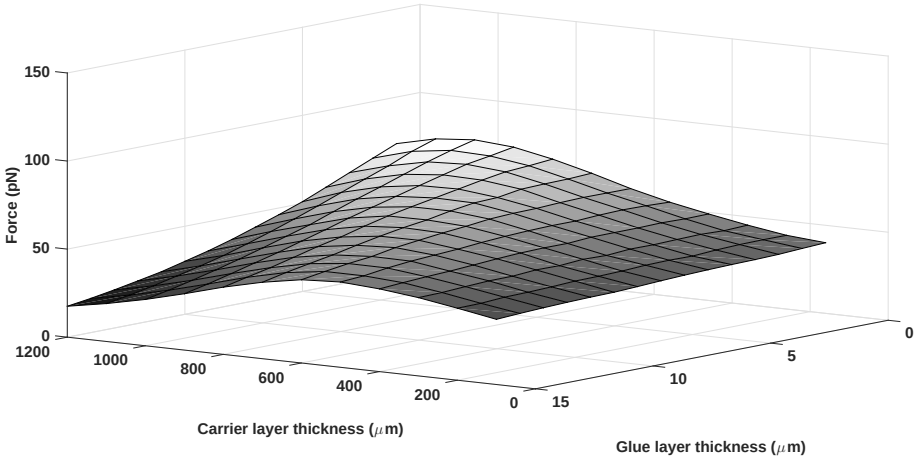

(b) Middle of the fluid layer

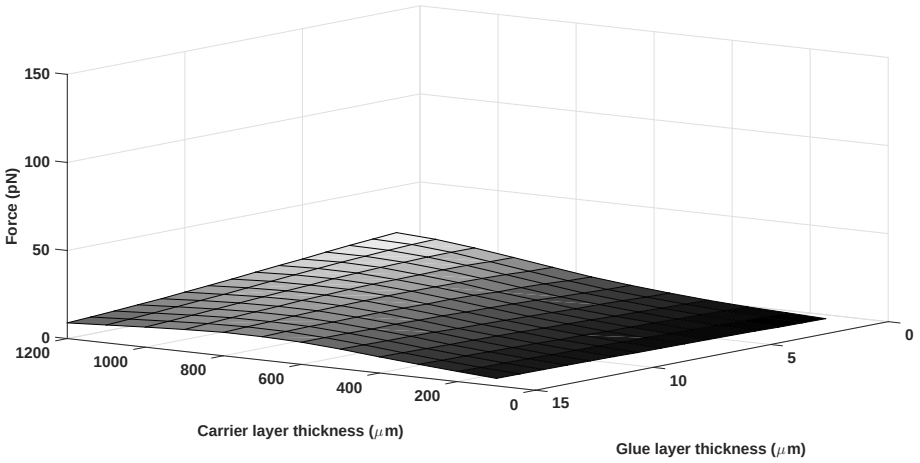

(c) Bottom of the fluid layer

Figure 3.9: Radiation force on a 10 μm bead for a combination of values for the thickness of the glue layer and the stainless steel carrier layer

This means that the thickness of the glue layer has to be taken into serious consideration.

After it was decided stainless steel was the best option some further simulation was done into the effect of the glue layer thickness. This was done to find the optimum carrier layer thickness for whatever possible glue thickness might be encountered. Using the same model as before and this time only for stainless steel, both changes in carrier layer thickness as well as glue layer thickness was explored in figure 3.9. In 3.9a the radiation force is shown for the top of the fluid layer, near the reflector layer, i.e. the glass cover slip, in 3.9b it is in the middle of the fluid layer, and, finally, in 3.9c, it is at the bottom, at the carrier layer, which is being varied as well as the thickness of the glue layer.

The three figures (3.7 - 3.9) show that the best result is obtained by matching the impedance of the carrier layer with the PZT's characteristic impedance.

Finally, fluid layer thickness modelling was performed where the glue layer and carrier layers were kept at a fixed thickness, but the fluid layer height was changed. This was performed as a final step of the layer optimising process. Three scenarios were tested: 1 mm thick stainless steel, 1 mm glass slide, and a 170 μm glass cover slip; all with a 1 μm thick glue layer. Figure 3.10 shows how the force drops rapidly as the thickness increases. The minimum thickness was settled on a 100 μm since machining anything smaller than that can be too challenging for most machines and nothing available at the University could reasonably machine thickness' lower than that [2]. Furthermore, below 100 μm

[2] As mentioned in device design (section 3.3) the fluid channel is around 130 μm thick. This is a direct consequence of the equipment not being able to reach the precision needed

the velocity at fixed flow rates was thought to be too fast for the device to work at full capacity and would require flows below 30 ml/hr which would reduce throughput. The thickness was chosen as a compromise between throughput and radiation force.

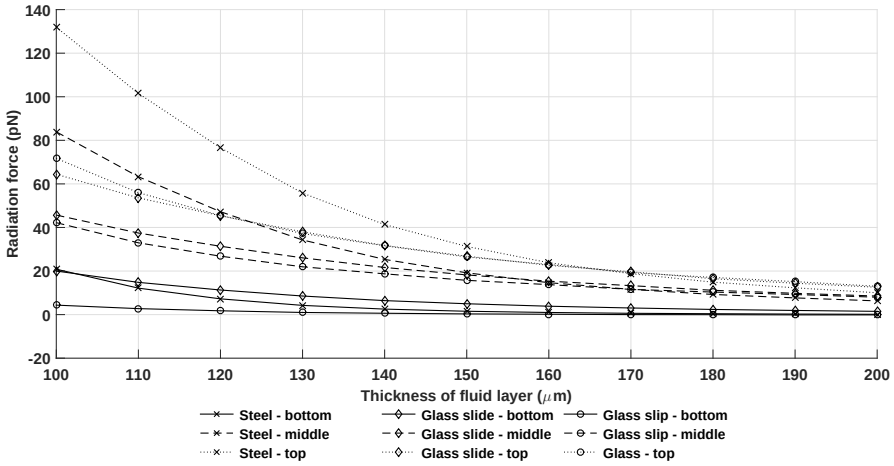

Figure 3.10: Radiation force on a 10 μm bead at the bottom, middle, and top of the fluid layer as it varies its thickness. The force is shown for a 170 μm glass coverslip, a 1 mm glass slide, and a 1 mm stainless steel sheet

Experiments to measure the glue layer thickness were carried out. They indicated that glue layer thickness was typically less than 15 μm, however a lack of precision in the micrometre used meant that the more precise figure was not obtained.

With the backing of the simulation data two stainless steel carrier layers were manufactured - one with a 600 μm thickness and one with a 1000 μm thickness. The former would be ideal for a 10 μm glue layer, and the latter for a 1 μm one.

3.5 Bead distribution across channel height

Bead (and later) spore distribution, before and after insonification with the USW field, was found by taking z-stack images inside an Aquality device, described in secton 3.2.1. These are images taken of the same position, but with the changing depth, inside the channel. In this case there were taken along 9 positions within the channel with each change corresponding to a shift of 12.5 μm towards the inlet of the device. The first position was located 6 mm from the outlet into the fluid layer. Firstly, the beads were flowed into

to get a 100 μm fluid channel.

the device and the flow was stopped. Z-stack images were then taken along 7 points on the centreline (parallel to the longest side of the device), which are: 6, 12, 18, 24, 30, 36, and 42 mm from the outlet. Next a new batch of beads is flowed in, the flow is stopped and the ultrasound is turned on for 10 s. Images are captured at the same positions. The results are shown in figure 3.11 where it can be observed that at positions 12, 18 and 24 mm there is a strong shift of the bead concentration towards the reflector layer (over 50 % of all beads conentrated in the top 20 μm of the fluid layer). These are the positions situated directly on top of the transducer. The effect is less present in positions the more further away they are from the transducer.

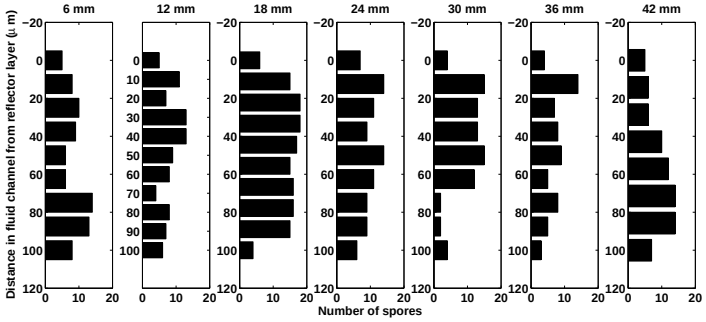

(a) Without ultrasound

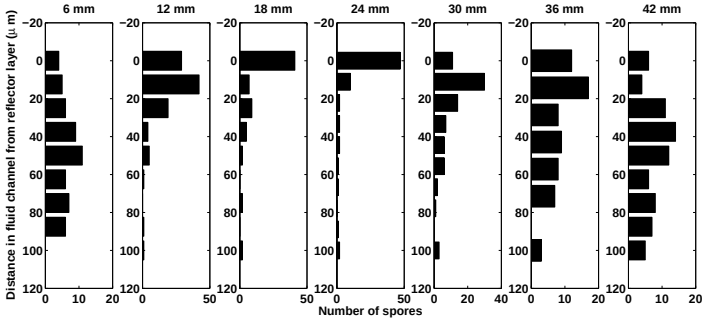

(b) With ultrasound

Figure 3.11: Distribution of beads by channel depth (starting from reflector layer) at different positions along the centreline of the device (starting from the outlet)

Because the focal plane of the objective is 10 μm it cannot be said with certainty if the beads observed at the reflector layer are truly attached as no difference can be observed in a static image between captured at reflector layer or suspended just below it.

Figure 3.12 shows the distribution of beads in the channel of the current device design (section 3.3) for flow rates between 10 and 50 ml/hr, with the PZT driven at 30 peak-to-peak voltage (V_{pp}). Again, a clear distribution difference is seen compared to no US, no flow when looking at flow values below 30 ml/hr. Successful focusing was defined as the ability of the device to cap-

ture the beads in the channel on the reflector layer, and in this figure, this was interpolated by looking at how many beads remained in the channel, as washing beads from the reflector layer became a problem. If the channel is empty of beads it means they are pushed to the reflector layer, therefore in a case of successful capture the graph should not show any beads, as opposed to the graph in figure 3.11 where there should be a concentration of beads in the top-most bar.

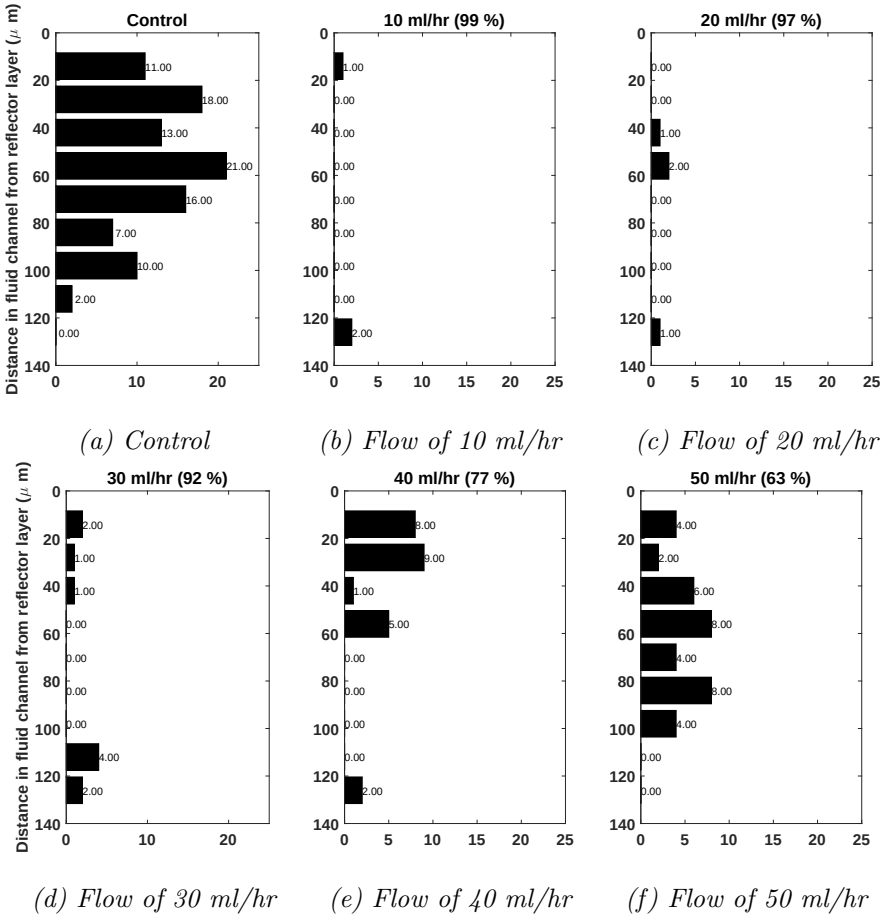

(a) Control *(b) Flow of 10 ml/hr* *(c) Flow of 20 ml/hr*

(d) Flow of 30 ml/hr *(e) Flow of 40 ml/hr* *(f) Flow of 50 ml/hr*

Figure 3.12: Bead count per image taken across the channel, height-wise. Apart from (a) all are for a 1 min assay with the specified flow and an input voltage of 30 Vpp

3.6 Lateral modes

A montage image of the fluorescent beads stuck on the glass cover slip was taken for the HW/TR devices (described in section 3.2.3) and is shown in figure 3.13. The beads were pushed to the reflector layer using ultrasound and then clear water was flowed to wash away any beads remaining in the fluid to

reduce background noise. The purpose of this was not to test the strength of the USW field, but to see the distribution of beads it forms on the reflector layer, as well as where the point of contact with the reflector layer is located.

The area above the HW transducer, spanning the left and the centre of the image and ending at the second cross-beam, does not contain many beads, as they are mainly concentrated at the anti-node at the centre of the fluid channel. Most beads come into contact with the reflector layer in the area right of the second cross-beam, where the TR transducer is active. They formed "bands" which are the result of the lateral modes inside the channel, as described in section 2.3.2. These "bands" are where the forces are strongest and having antibodies there will ensure that the spores get as big of a chance as possible for sticking. The "bands" also show the touchdown point - a point where the beads start touching and sticking to the reflector layer in bigger concentrations. At the end of the device, where the radiation force from the TR transducer is weaker the flow is dispersing the beads and they no longer come into contact with the reflector layer. This results in the "bands" breaking up.

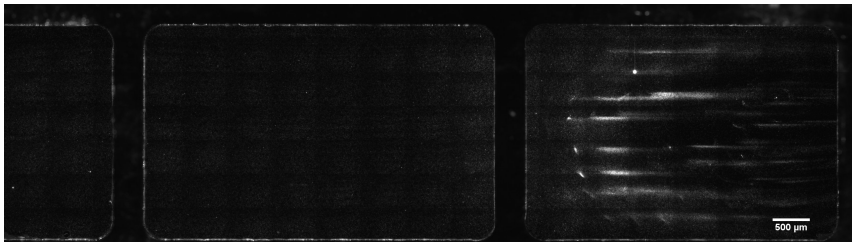

Figure 3.13: Montage of HW/TR device showing where beads attached to the reflector layer.The banded distribution is the product of lateral modes inside the device.

3.7 Optimising flow rate for capture versus throughput

Figure 3.12 was a single snapshot of a bigger experiment. The beads in the channel were counted for multiple flow rates (10 to 50 ml/hr) and input voltages (15 to 30 V_{pp}) to see how well the current device design performs. As with the figure the slices of the z-stack images at the reflector and carrier layers were discarded [3]. The beads are then summed up for each condition and compared to the control.

[3]The beads get stuck on the reflector layer and cannot be removed. If the slice was included the numbers would skew the percentages of beads in the fluid channel and would not provide an accurate overview.

Table 3.3: Number of beads found in the fluid channel with only the TR transducer for all of the combinations of flow rate and input voltage, including the control (0-0) case. The number in the parenthesis indicates the capture percentage compared to the control

		Input voltage (Vpp)			
		0	15	25	30
Flow rate (ml/hr)	0	98			
	10		34 (65)	6 (94)	1 (99)
	20		56 (48)	11 (89)	3 (97)
	30		63 (36)	26 (73)	8 (92)
	40			54 (45)	23 (77)
	50			54 (45)	36 (63)

Table 3.3 shows the total number of beads left in the fluid channel after the USW + flow assay (beads that touch the channel walls are not counted). The smaller the number in the channel the bigger the capture rate as more beads are now on the reflector layer. The number in the brackets shows the percentage of beads captured compared to the control, and is given by the equation:

$$Percentage\ captured = \frac{Control - Current\ no.\ of\ beads}{Control} * 100\% \qquad (3.1)$$

where the control is the number of beads inside the fluid channel for the (0,0) case, and amounts to 98 beads. It is seen that the TR transducer has a very high capture rate up to 30 ml/hr. Above this flow rate the percentage captured drops but the result is comparable to the results from the Aquality project device, described in section 3.2.1. The data present in the table is visualised in figure 3.14 where the number of beads present inside the channel is plotted for each flow rate and each input voltage. The control was left out so the rest can be distinguished more easily.

3.8 Plate modes, cavitation, and streaming

During the experiments a clicking sound was noticed that seemed periodical in nature. It was only present at high driving voltages and during frequency sweeps when using the current design featuring the stainless steel carrier layer (section 3.3). Further examination showed that the period of these clicks was the same as the sweep period. Figure 3.15 shows the conductance response (who's measurement method was described in section **??**) of the device with air and with water inside the fluid channel. It shows a resonance frequency at 884 kHz, but a lot of other peaks that are present in the device.

A phenomenon that was noticed was that, at high input voltages, the beads (and spores) were dislodged from the reflector layer in a periodic fashion. The

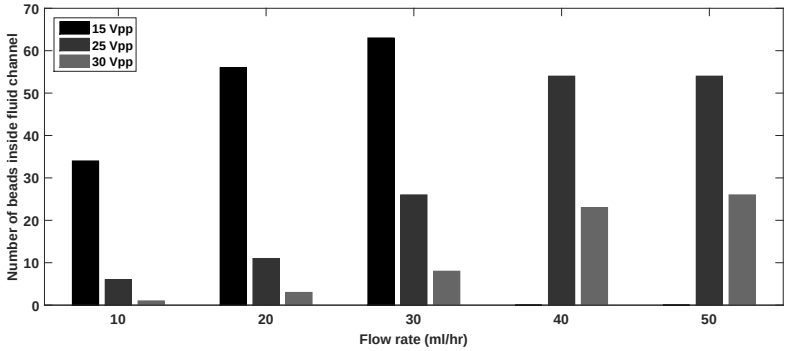

Figure 3.14: Number of beads found in the fluid channel with only the TR transducer for all of the combinations of flow rate and input voltage, excluding the control (0-0) case.

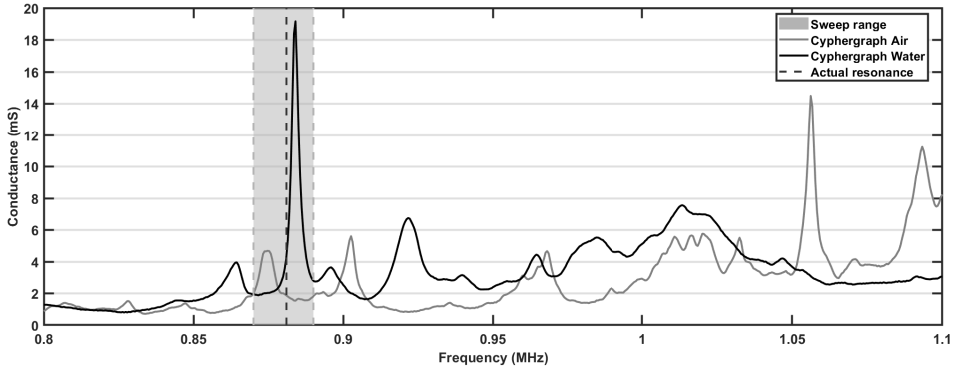

Figure 3.15: Conductance response of the device with PVDF sensor, with air and water inside the fluid channel. The resonance frequency is 884 kHz and the conductance value of the resonance is 18 mS.

dislodging process was correlated with the timing of the clicking that was heard. Figure 3.16 shows a selection of frames from a video taken of 1 μm and 10 μm beads. They demonstrate the plate vibrations of the glass cover slip and provide the reasoning behind the hypothesis that the clicking is triggering the plate modes of the coverslip who's vibration is then dislodging the beads.

If the input voltage is reduced below a certain threshold no clicking can be heard and no bead dislodging can be seen. This threshold depends on the strength (conductance) of the resonance but is below 5 V_{pp} for a good resonance. All of the experiments were just below the threshold and conducted with strong resonances.

Streaming was also present in the device at higher input voltages. Figure 3.17 shows frames from a movie that demonstrate streaming. However, it did not play a major role in the distribution of beads/spores/cells as it occured only at voltages higher than those that excited the plate modes so the input voltage was kept lower than both.

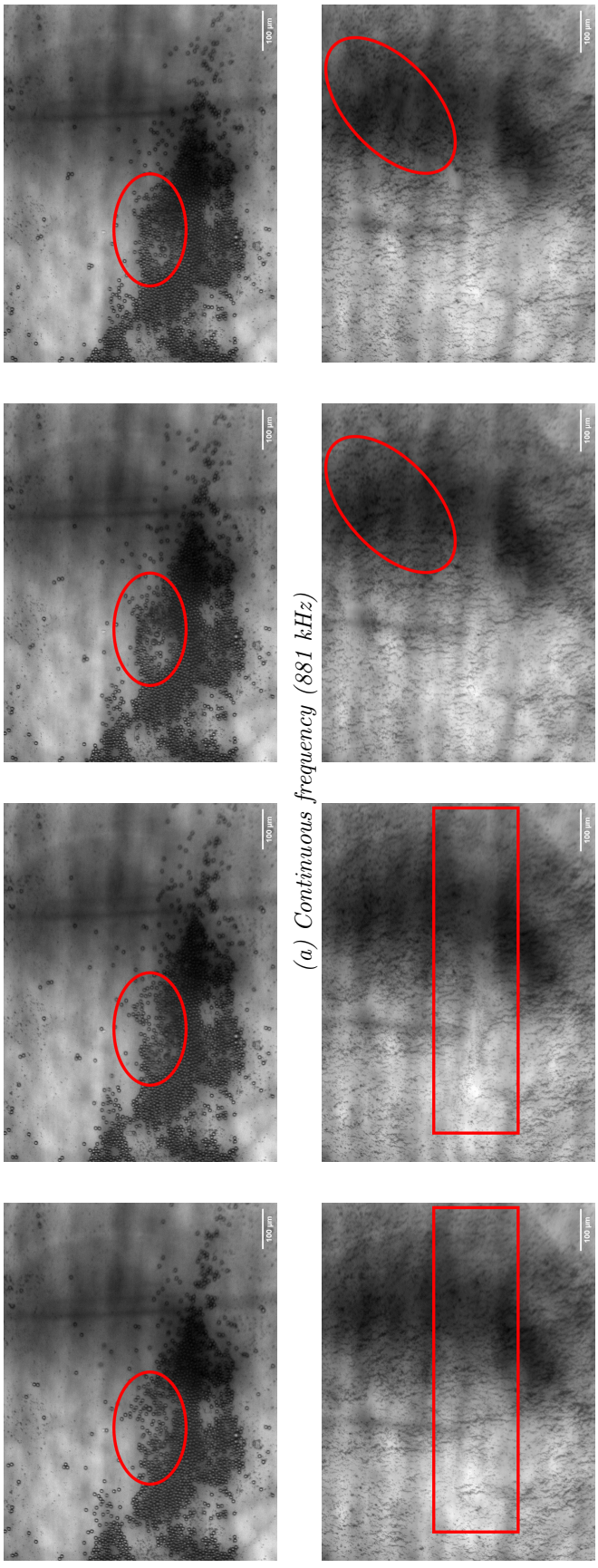

(a) Continuous frequency (881 kHz)

(b) Continuous frequency (881 kHz)

Figure 3.16: Image stills of beads being dislodged by plate modes of the glass coverslip. The areas of interested are marked in red.

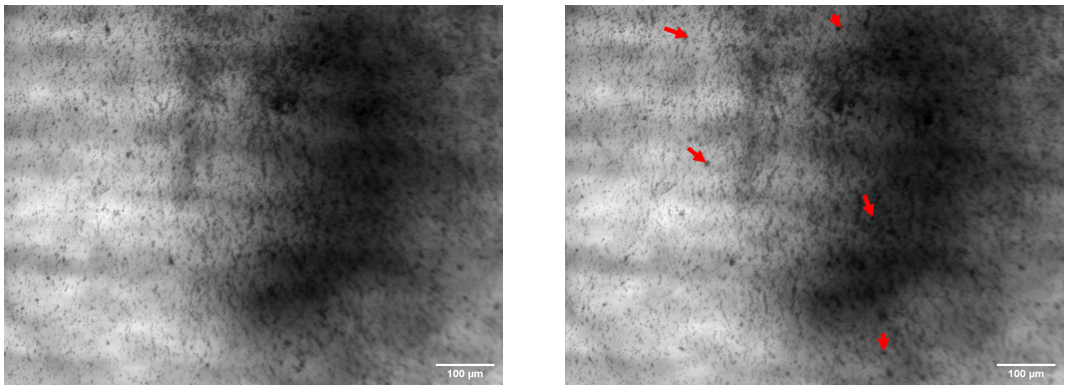

Figure 3.17: Image stills of beads being moved by streaming forces. The red arrows show the movement of some key particles inside the chamber. There is no flow present in the experiment during which this image was taken.

3.9 Ensuring planarity in the device

A big factor in how effective the device can be is the planarity between the carrier and reflector layers. If they are not parallel (or at least very close) the reflections of the ultrasound coming from the transducer are going to start moving in a direction creating a weaker, or even non-existent, standing wave field (figure 3.18 shows how an angle between the two surfaces changes the field) [4].

To prevent this a 100 μm cellulose acetate spacer is inserted around the large gasket to promote planarity by virtue of its uniform thickness. Because it does not expand or stretch with the forces applied to it [224], and its thickness has only small changes throughout, it is a great material for providing a defined length between the two layers.

For further control of the planarity the six screws are tightened manually to all apply the same torque (roughly) to the device (as this was done by hand no quantifiable numbers on the torque can be given). If they are tightened too tightly the strength of the device at resonance can suffer (it reaches the compressibility strength of the spacer material and it begins to deform too much), as well as when they are too loose or have different torques applied. Once assembled the conductance plot can be examined and if a weak resonance is observed then the tightening process can be repeated. Figure 3.19 shows

[4] In this simulation model a section of the bottom plane acts as a plane wave source. The top plane is a rigid reflector. The material inside the boundaries was modelled as water. In the first simulation the two planes are parallel, while in the second one the planes are at a 0.6 ˚angle to each other. When the planes are parallel the absolute pressure inside the model is stronger than when there is an angle between the two planes. Furthermore there is no "bleeding" effect present when the planes are parallel, i.e. the node and antinode regions are more well defined. For better performance inside the device parallel planes are wanted.

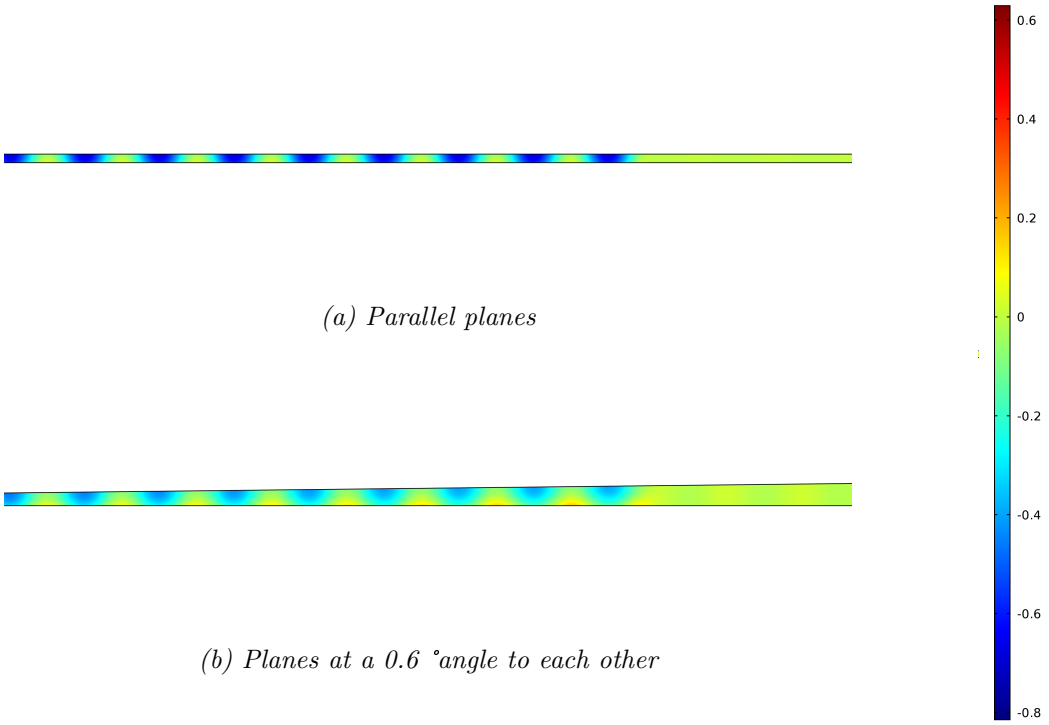

(a) Parallel planes

(b) Planes at a 0.6 ˚angle to each other

Figure 3.18: Changes in the strength of the standing wave field when the two planes are parallel and at an angle to each other. The colourmap on the right represents acoustic pressure in Pa. The values themselves are not important, but rather their relative differences

how small changes in the tightness of the screws can change the strength of the resonant frequency.

3.10 Reliability and robustness

The final design of both the device and assembly method must be robust and reliable enough to withstand not only many uses, but variations introduced by changes in temperature, humidity, density of the fluid inside the channel, and the bowing of the glass reflector layer at higher flow rates.

In its current design only some of these criteria are met. The devices themselves have withstood over a hundred tests without any effects on the strength of the resonance, noticeable change in resonance frequency, or the capture rate of the device.

To accommodate for the slight variations mentioned above a frequency sweep is used during experiments. Generally, the smaller the frequency bandwidth the more energy goes into exciting the system at the resonant frequency, but the smaller the frequency shift it can cover. The steel carrier layer gives a high Q factor to the resonances allowing the sweep bandwidth to be small.

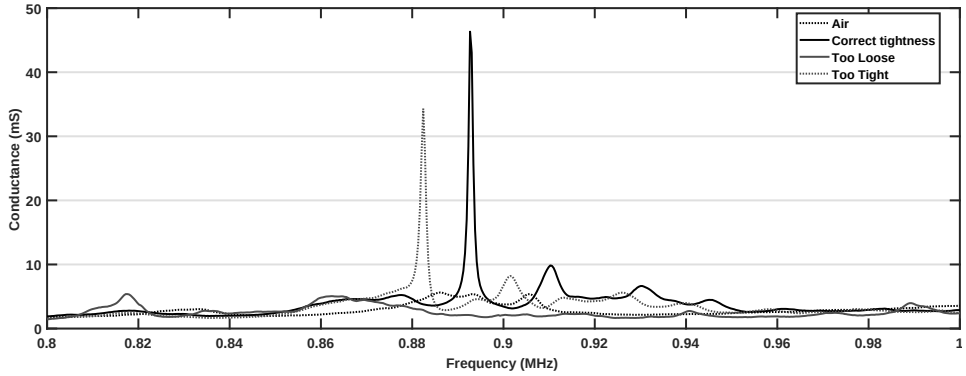

Figure 3.19: Conductance response of the device around the resonant frequency when the screws are too tight, too lose, just right, and have had different torques applied to them. The changes can be drastic compared to the just right case (up to 4.5 times lower conductance peak) showing that there is an optimal tightness to aim for and that too tight can cause problems as well as too loose.

The shifts themselves are also in the order of kHz so the bandwidth does not need to be large. In the end, a bandwidth of 20 kHz was chosen around the resonant frequency.

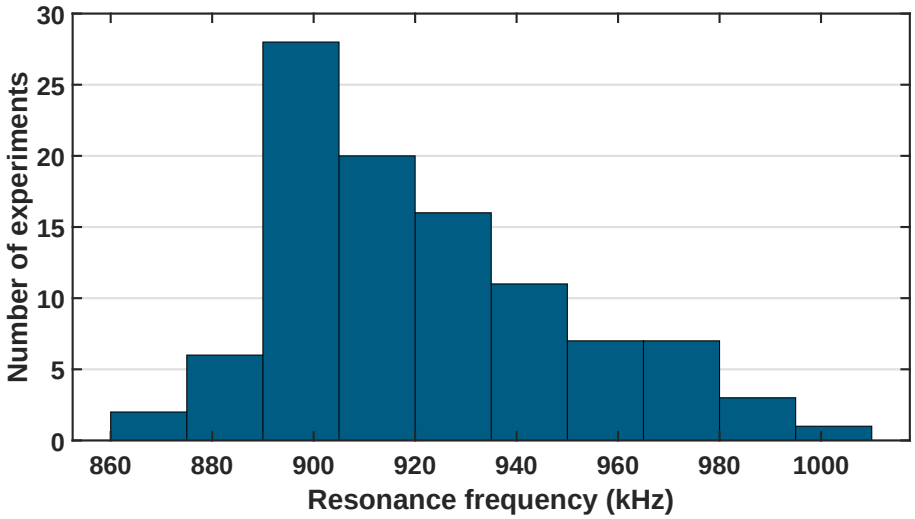

Figure 3.20: Resonant frequencies from all experiments sorted in ascending order. The straight line represents the mean value of the frequencies, while the shaded area represents the standard deviation from the mean.

The second function of the frequency sweep would be to cover all the possible variations in the resonant frequency due to reassembly. Future work is needed to focus on designs that are less variable or to develop electronic driving circuits that can respond to small changes in the resonant frequency. Resonant frequency data was gathered from all of the tests done for the work in chapters

4 and 5. The mean resonant frequency across all of the tests used [5] was 921 kHz, with the median being 914 kHz, while the standard deviation was 29 kHz. Figure 3.20 shows all of the resonant frequencies in a histogram. This range is too big for the frequency sweep to cover while also delivering enough energy into the resonance itself to push the pathogens towards the surface. Therefore it was decided that for each experiment the sweep would focus around the resonance. Ideally, however, a single sweep would be set and this would suffice for multiple device uses. Section 4.4.1 talks about the possible solutions to this problem when it discusses different clamping techniques.

3.11 Pathogen tagging

The two pathogens used with the device in its two functionalities are BG spores and basophils. Due to the design of the device (no clear transluminescence path) some form of staining had to be used in conjunction with filter cubes.

3.11.1 Spore tagging

Spores have a hard cell wall which doesn't allow for nucleic dyes to penetrate [225–228], thus a dye which stained the cell wall was used. Initial experiments were performed with AuramineO and fluorescein isothiocyanate (FITC), the latter of which performed better but caused the spores to clump together into clusters, however it was found that dies were not particularly bright and that the proportion of spores fluoresced below the noise threshold of the camera system used.

A much superior dye was found in AlexaFluor 555, an orange surface stain that provided a stable and consistent coating on the spores that was bright enough that individual spores could be picked out. Figure 3.21 shows images of spores stained with the initial two dyes taken under visible light and under fluorescent light. What can be seen is that both AuramineO and FITC have their problems (low intensity and clustering, respectively). Comparatively, AlexaFluor 555 manages to stain the spores individually (not seen here) so that the vast majority is clearly visible under fluorescent light and they are still individually separated, without any clustering appearing.

Table 3.4 shows the excitation and emission frequencies of the dyes used.

3.12 Antibody coating

The glass slides used for the antibody functionalisation have been purchased (Under the brand name Schott Nexterion Slide H) with a crosslinked PEG network that coats the glass surface. The strands of this crosslinked PEG

[5] the difference between means of different devices is within 10 kHz so I felt justified to pool all of the raw data together

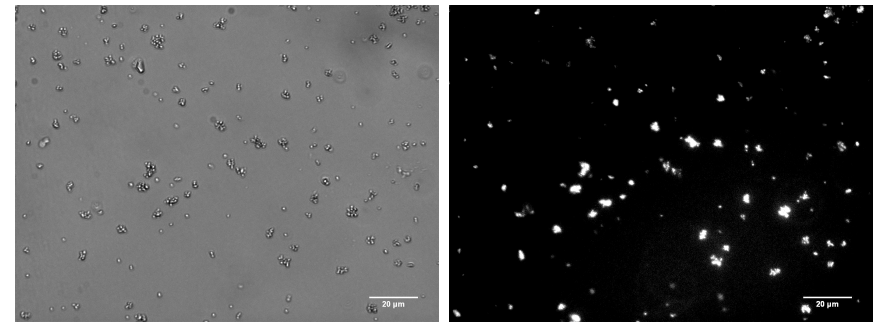

(a) FITC, under visible light *(b) FITC, under fluorescent light*

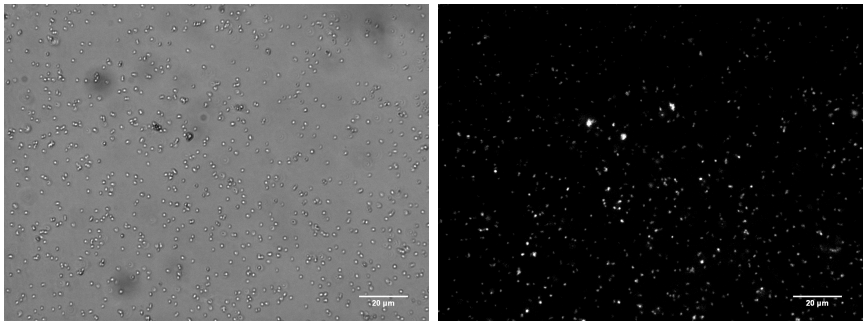

(c) AuramineO, under visible light *(d) AuramineO, under fluorescent light*

Figure 3.21: Spores stained with FITC and AuramineO, under visible and fluorescent light

Table 3.4: Excitation and emission frequencies (nm) of the dyes used in staining the spores, as well as the filter cubes that were used for imaging. The filter cubes were selected from the pool of available ones, and may not represent the best choice.

	Frequency (nm)		
Dye	Excitation	Emission	Filter cube
FITC [229]	490	525	FITC
AuramineO [230]	438	505	FITC
AlexaFluor 555 [231]	555	580	TXRED

network are terminated by N-hydroxysuccinimide carboxylic acid which can be activated. The PEG network provides non-specific binding that can be made cell-specific by applying the correct antibodies. The rest of the network can be "blocked", i.e. prevented from binding with anything.

Functionalising a glass slide or cover slip is a process that is hard to get right. To that end, in order to create an antibody coating on the reflector layer prefunctionalised cover slips were purchased. The two types that were used were Schott Nexterion Slide E, which is functionalised with an epoxysilane layer which binds most kinds of bio-molecules[232], and Schott Nexterion Slide H,

which is functionalised with a 3-D hydrogel coating which binds to the amino group found on most bio-molecules including antibodies [233]. Figure 3.22 shows the binding process for both slides.

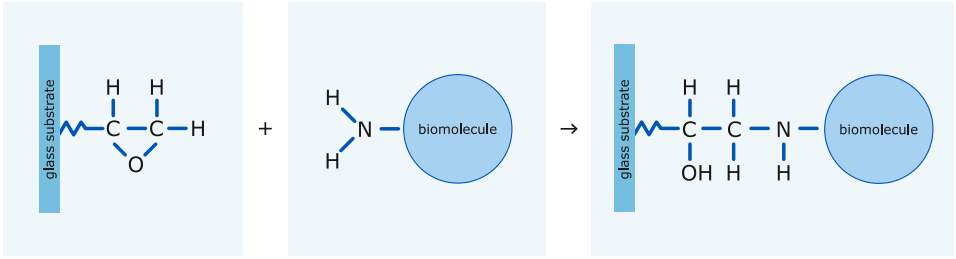

(a) Slide E (taken from [232])

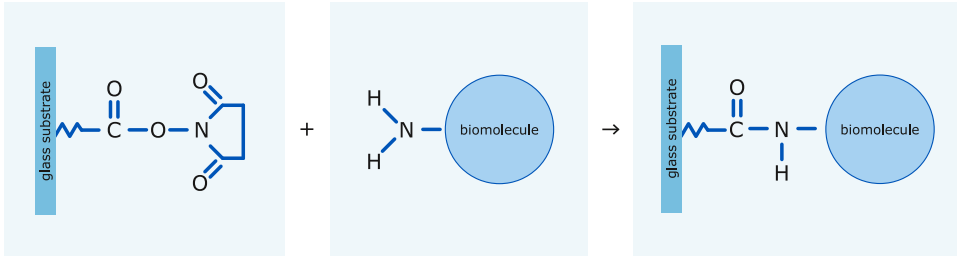

(b) Slide H (taken from [233])

Figure 3.22: Bio-molecule binding process with the functionalised regions of the slides

3.12.1 BG Spore specific antibodies

The antibody used to bind to spores is the Rabbit Anti-*B.globigii* IgG (Tetracore Inc., Rockville, USA) [234]. They are *Bacillus globigii* (BG) spore specific antibodies and to ensure capture that is specific to BG spores. Figure 3.23 shows the effect the antibody coating has on spore capture. An area of a slide was coated in antibodies and then spores in suspension at a concentration of 10^5 spores/ml were placed on top of that and allowed to sediment. Afterwards it was washed and stained with FITC so the spores could be seen under microscope. The number of spores captured on the coating, compared to the number captured on the non-coated part of the slide, is orders of magnitude greater.

Untreated glass can also capture spores but in a non-specific way. The capture of untreated glass was also tested on a HW/TR device by having one side coated with the antibody (as seen in figure 3.24) in the active area of the TR transducer. The test conditions were set such that the flow was low (3 ml/hr), the spore count was high ($3 * 10^5$ CFU/ml), and the input voltage was kept low, while the assay time was kept at 10 minutes.

Figure 3.25 shows the montage image of the device as captured by microscope with a FITC cube. The image shows an overview of the reflector layer

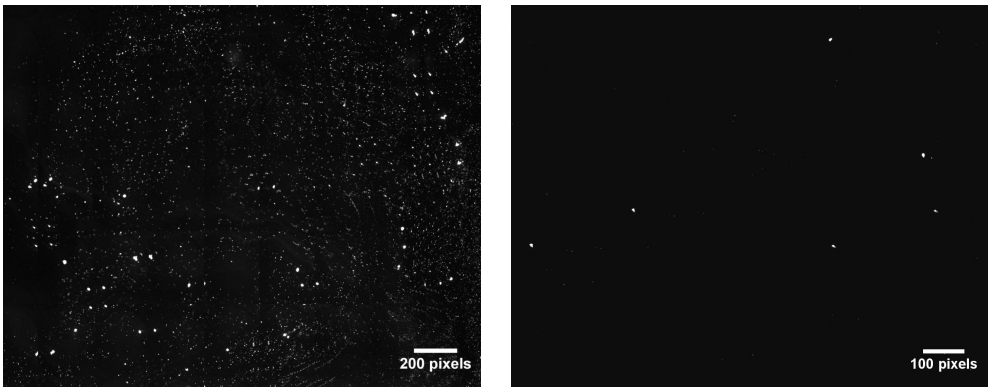

(a) Antibody coat *(b) No coating*

Figure 3.23: Images of two areas of a drip test. After the drip was left to sediment it was additionally stained so the spores are visible under fluorescent light.

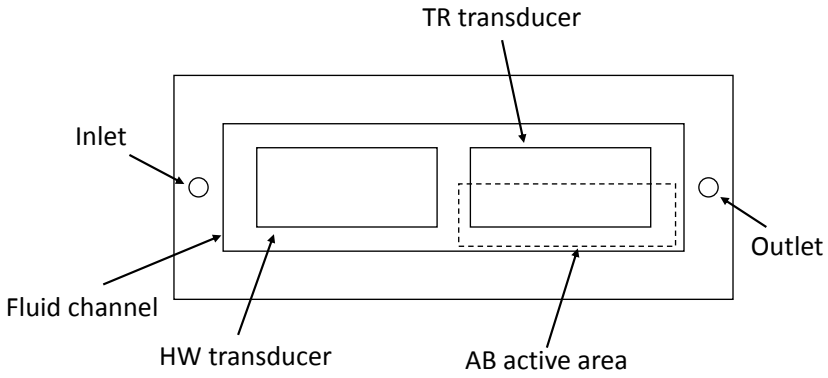

Figure 3.24: Diagram of the placement of the antibody region in a HW/TR device. The active area only covers half of the TR sonified area in order to provide a way of testing the effectiveness of the antibodies

but the spore are too small to be seen clearly in this figure. Part (b) of the figure shows the colourmap of spore capture on the imaged area. Each image had the spores on it counted and represented on a grid with a single number. The active area starts around column 11, while the steel cross-beam that obscures the light path covers columns 20-24. What is visible is that most of the capture happened on the coated side of the slide. There is also some evidence of the antibody solution spreading into the other side of the slide and covering more than 50 %.[6]

Capture of the spores was achieved despite the staining that took place

[6]A way to deal with this problem is to make sure that when coating a certain area is always coated so when imaging everything else is discarded while only this area, which is guaranteed to be coated, is imaged.

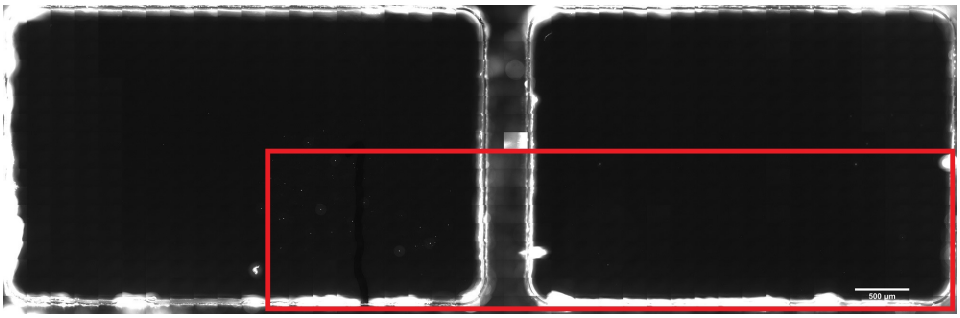

(a) Image taken with inverted optical microscope under fluorescent light

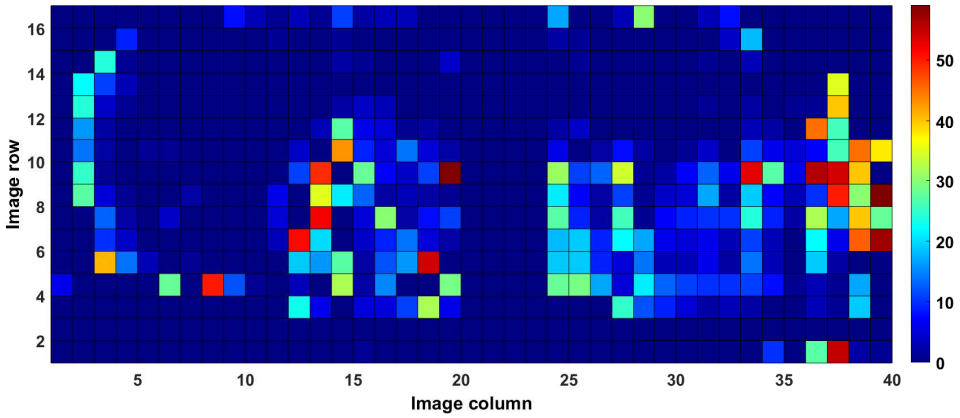

(b) As analysed and visualised in MATLAB

Figure 3.25: Spore attachment on the surface of a slide partially coated with antibodies. The top image is a composite consisting of many smaller microscope images of the device. The bottom image is a graphical representation where every block represents the number of spores counted in the associated image. The antibody coated area is highlighted with the red rectangle. The external boundaries were removed when analysing the data as it interferes with the spore count. The Cross-beam is still present and is represented in rows 20-24.

beforehand. It was not known before this experiment if staining the spores would reduce the number of available binding sites below a certain threshold after which they could not be immobilised by the antibodies.

3.13 Summary

The device described in this chapter is a simple, layered resonator, designed to capture particles on the antibody treated surface. It serves two purposes: one is to capture BG spores or any airborne or waterborne pathogen and detect it as part of a process of identifying safe-to-breathe air, and safe-to-drink water; and the other is to immobilise basophils, a type of white blood cell responsible for allergic reaction, so that they can be analysed further and

with more precision than what current tests offer.

The device materials, especially the carrier layer, were chosen with the help of modelling to produce a strong acoustic field for a small input voltage. The Z-direction scans showed that, even under flow, the USW field pushes a large proportion of the small 1 μm beads and spores to the antibody coating. While lateral modes are present they do not pose a problem to the capture of pathogens. The spores had no problems with staining and could be seen easily under the microscope.

The device described here is used subsequently in chapters 4 and 5, for which it's performance proved satisfactory. However, further work could be done in the future to enhance performance such as ensuring the device is fully planar, re-introducing a second transducer that would pre-focus the spores, and optimising the input parameters.

Chapter 4

BG spore capture for detection purposes using a thin-reflector device

4.1 Introduction

Water quality testing has had the same standard tests for decades [7], the oldest of which, cell culturing, has existed since the latter 19^{th} century. All of them are well established, but typically trade speed for accuracy. Recent developments in biosensors have made vast improvements in both fields [6], but to date have not been sufficiently mature to be adopted as a new standard.

Testing for anthrax in the field areas has to be done with speed and without the need of big and expensive lab equipment, which necessitate either whole specialised testing rooms or vans, or sending the samples to an off-site lab [115]. There is a need for quick on-site sample testing that can provide either continuous or near continuous monitoring [30, 31].

The purpose of the system described in this chapter is to provide a system that can respond quickly to the presence of anthrax spores in a portable device with a detection limit as low as 100 spores/ml [1]. The next section covers the methods used in preparation of the spores and slides, through the experiments themselves, and in post-processing. Some of the methods used were already described in chapter 3. Section 4.3 shows the results. The results are then discussed and compared to other devices from the literature review in 4.4 and the future possibilities in 4.4.1. Finally, the chapter is summarised in section 4.5.

[1] This detection limit was set by DSTL as a reasonable goal to aim for given the current state of the detection field [235].

4.2 Methods

4.2.1 Spore staining

The pathogen chosen for the experiments is a spore form of *Bacillus globigii* (BG) [2] (DSTL, Porton Down, UK). When received, the spores were washed by being centrifuged (Eppendorf, Centrifuge 5702 R, Hamburg, Germany), at 3000 rpm for 3 minutes, the suspension liquid pipetted out and replaced with new sterilised, pure water. The spores were then resuspended. This process was repeated 4-6 times in order to ensure any smaller particles are removed.

To stain the spores AlexaFluor 555 dye (ThermoFisher, UK) was used. To a single 100 μg vial of the dye, 10 μl of dimethyl sulfoxide (DMSO) was added. The spores, which had a concentration of 10^9 CFU/ml, were resuspended in 500 μl of phosphate-buffered saline (PBS), after which 10 μl of the dye/DMSO solution was added. The spores were incubated in a fridge, at 4 °C, overnight. After incubation, the spores were again washed in pure water with centrifuge and stored in a fridge, in the dark to prevent germination and photo-bleaching respectively. When used in an experiment the spores were resuspended with a shaker and diluted to the required concentration in PBS.

4.2.2 Slide preparation

The slides (Nexterion, Slide E, Schott, Germany) were functionalised with *B. globigii* specific antibodies (Rabbit anti-B globigii IgG antibody, Tetracore, Rockville, MD, USA). The antibodies were diluted in PBS to a concentration of 0.25 mg/ml. An aliquot of 0.25 ml was pipetted onto the slide into the correct region. An acrylic spacer was placed on top of the antibodies to ensure they were spread out over the entire active area and to prevent vaporisation. The height of the spacer was $\sim 80\mu m$. The slides were then placed in a humidity chamber that had a 1 inch deep layer of sodium chloride at the bottom, and was filled with pure water. Above the water was a plastic grate on which the slides were placed. Once the chamber was closed it was further sealed with Parafilm. The slides were left in the chamber overnight, at room temperature. The next day the slides were removed from the chamber and placed in a slide holder filled with a 1% bovine serum albumin (BSA) solution for at least 1 h. This was done to block the rest of the slide from capturing any pathogens or proteins. Once removed, the slide was washed with PBS and dried using pressurised air. It was then ready to be used in the device.

4.2.3 Experimental procedure

The device itself was assembled as described in section 3.3.1. Once completed, the transducer was connected to an impedance analyser (Cypher Instruments

[2] historically also known as *B. Globigii* from where the BG monker comes from, as well as *B. subtilis var. niger*.

C-60 impedance analyser) and a conductance scan is performed on the device with air still in the fluid channel, by using the proprietary software CypherGraph. The channel was then filled with PBS and the process repeated. Figure 4.1 shows an example plot with the highlighted peak corresponding to the thin-reflector mode resonance. Once the resonance was found the device was connected to the signal generator via the custom built amplifier (the schematic of the setup can be seen in figure 4.2). The resonance was fine-tuned using the oscilloscope as a guide by looking at sudden drops in amplitude while steadily increasing the driving frequency. The investigated range is centred around the frequency found by CypherGraph. The signal generator was set to sweep the frequencies with a 50 ms interval and with a sweep bandwidth of 20 kHz, centred around resonance frequency. The peak-to-peak voltage was kept between 5 and 10 V_{pp}.

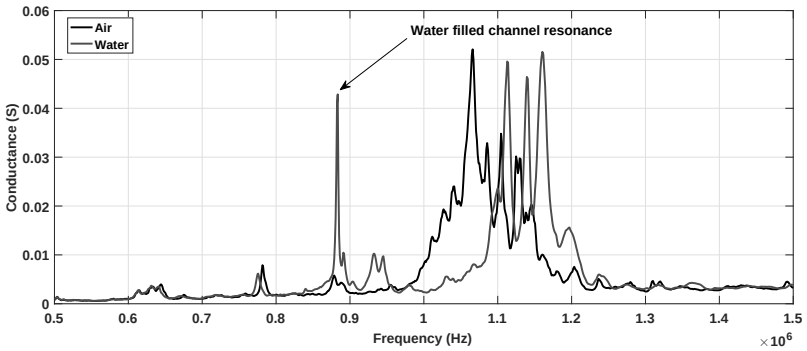

Figure 4.1: Conductance plot for a TR device for frequencies between 0.5 and 1.5 MHz. The two lines represent the air- and water-filled fluid channels. The arrow show where the water-filled fluid channel resonance frequency lies (0.78 MHz).

Once the device was setup the ultrasound (US) was turned on and spores were flowed in at the correct concentration for a 10 min assay using a syringe pump (Harvard apparatus Pump 11 Elite). Inside the syringe a small magnet was placed that would be stirred manually with another external magnet to ensure that spores do not settle on the syringe bottom during the experiment. When the assay was finished the US was turned off and PBS was flowed through the fluid channel to remove any spores that were not captured by the antibody layer. Afterwards, air was passed through the channel to remove any PBS in order to reduce the chances even further, of extra spores settling on the antibodies and attaching themselves after the experiment was concluded. The device was disassembled and the slide was washed in PBS and dried with pressurised air. The reusable components of the device were washed with pure water and dried using microscope tissues and pressurised air and the disposable components were replaced. The slides were stored in a dry and dark container at room temperature.

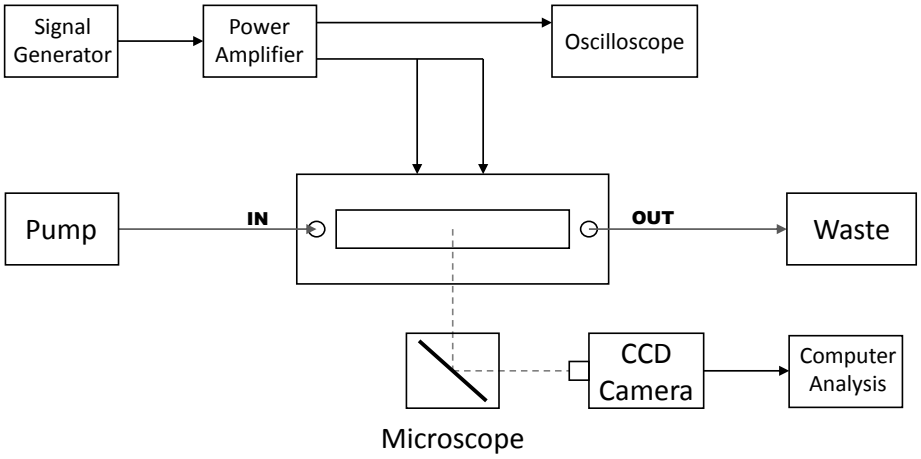

Figure 4.2: Schematic of the experimental setup for the TR resonator device, flow controls, sine-wave generation, and imaging

4.2.4 Imaging

Figure 4.3 shows the inverted microscope (Olympus IX71) and its various components that was used to image the slides. They were placed on a custom slide holder on top of an automated XY stage (Thorlabs MLS203) which was controlled by a native controller (Thorlabs apt Brushless servo controller). Two light sources were used: epi-illumination, for fluorescent imaging (Prior Lumen200), through a filter cube (Olympus FITC filter cube); and trans-illumination, for bright field imaging (Olympus TH4-200). Four types of objectives were used during the duration of the project: 4x (Olympus PLN 4x), 10x (Olympus UPLFLN 10x), 20x (Olympus PL L 20x), and 50x (Olympus LMPLFLN 50x). A Hammamatsu ORCA-ER camera was used to capture the images. Micro-manager, an open source microscopy software [236], was used to control the XY stage and camera in order to take mosaic images of the antibody coated area of the slides. An array of 10x10 images were captured totalling the imaged area to 8.8 mm x 6.7 mm, or 59.5 mm^2.

4.2.5 Post-processing

Counting the spores was done manually using ImageJ. The brightness of the image was adjusted manually so that only spores are visible, while everything else is excluded as much as possible. Separate control images of individual spores were used to find a threshold value for a binary filter which was then applied manually. The goal of the threshold was to leave only the brightest centre and the top $\sim$ 20 % of their brightness distribution. The thresholded images were then applied as a mask over the original images in order to isolate the possible spores while maintaining all of the brightness distribution details.

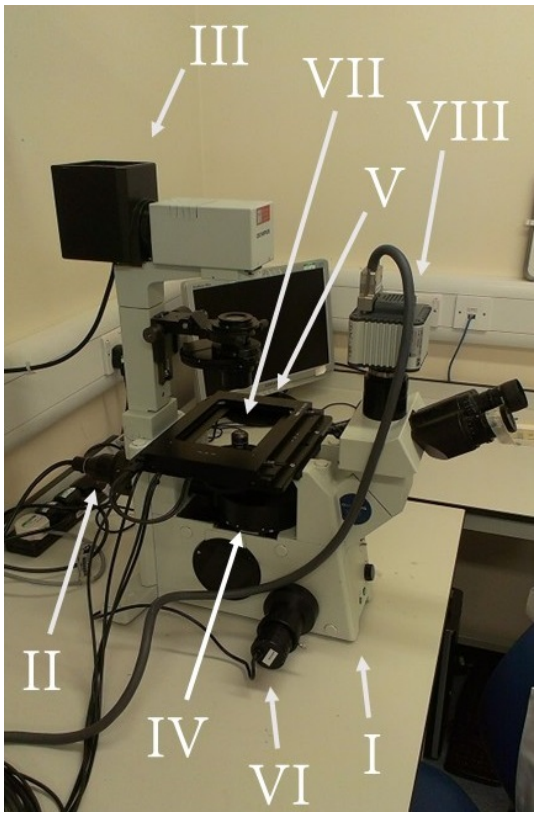

Figure 4.3: Image of the microscope setup, consisting of (I) inverted microscope, (II) Halogen light source, (III) visible light source, (IV) FITC cube, (V) automated XY stage, (VI) automated z-stage, (VII) objective turret, and (VIII) CCD camera

The spores were counted using a manual cell counter by inspecting each possible spore if it fits the criteria (very bright spot in the middle with a taper towards the edges, and a size between 2 and 15 μm^2). Each experimental condition had 3 repeats, therefore a mean was taken after the spores were counted and they were checked for statistical significance between the conditions.

4.3 Results

To highlight the advantage of using the ultrasound the rate of sedimentation by itself was assessed. A test was performed with the spores on a haemocytometer (Hausser scientific Neubauer Improved HL), which was used for its grid which provided many small areas for which spores could be counted independently and then averaged for a more robust result. Figure 4.4 shows the data of this test alongside a linear line fit. The sedimentation rate for the 0.1 mm high chamber with a cell concentration of 10^3 spores/ml, was found to be 4.4 spores/min in a single grid space (with a size of 0.05 x 0.05 mm). An

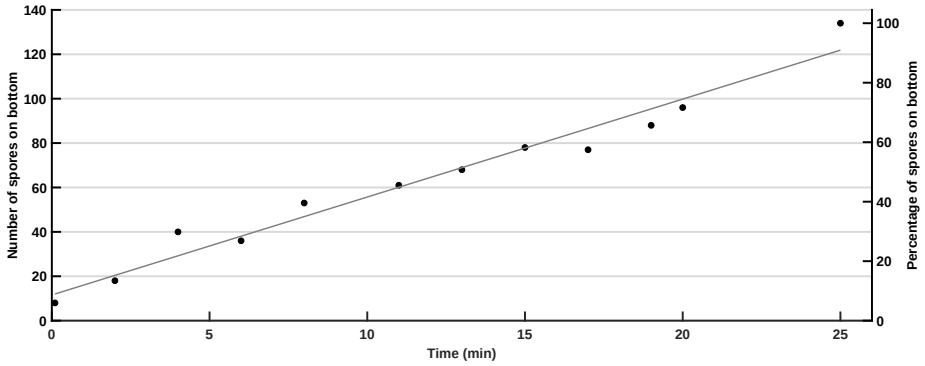

Figure 4.4: Graph depicting the sedimentation of spores on a haemocytometer with a channel height of 100 μm. The data is presented as both raw numbers and a percentage. A trendline was fitted to the data.

average over multiple grid spaces was 134 spores equally distributed though a height of a 100 μm at the beginning of the sedimentation test. That means a sedimentation rate of 3.3 % /min. The two linear fit lines have the equations of: $f(x) = 4.4x + 11.58$, and $g(x) = 3.3x + 8.6$. Here, $f(x)$ is the amount of sedimented spores after time x has passed, while $g(x)$ is the percent of the total spores that has sedimented after time x. Time is given in minutes. From

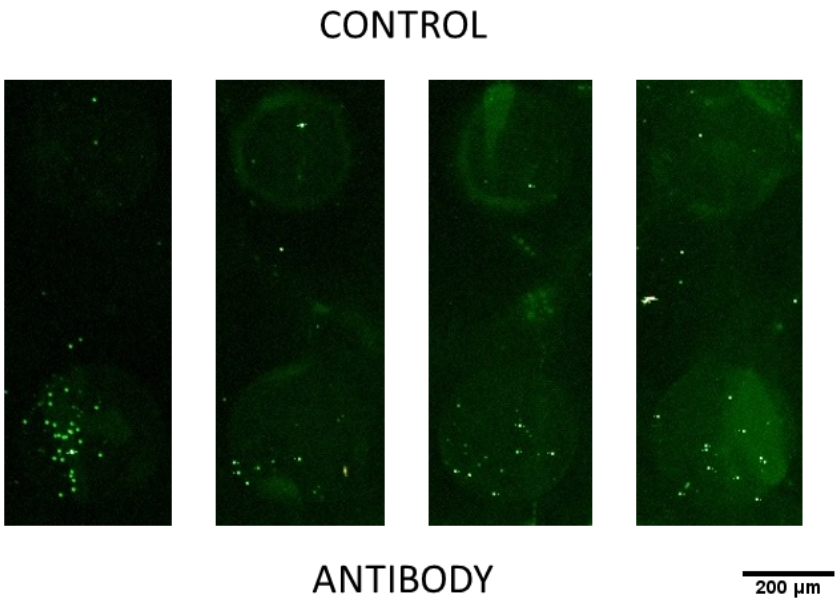

Figure 4.5: Four excerpts of an image of a spotted slide used in an experiment with a 10^4 spore/ml concentration. The bottom of the images contain spots with spore specific antibodies, while the top of the images has spots that have been blocked to prevent specific binding.

these equations a sedimentation rate of 3.6 $\mu m/min$ was calculated. After

25 minutes all spores have sedimented and the experiment was terminated.[3] However, the trendline's gradient is such that to reach 100 % sedimentation 28 minutes would be needed.

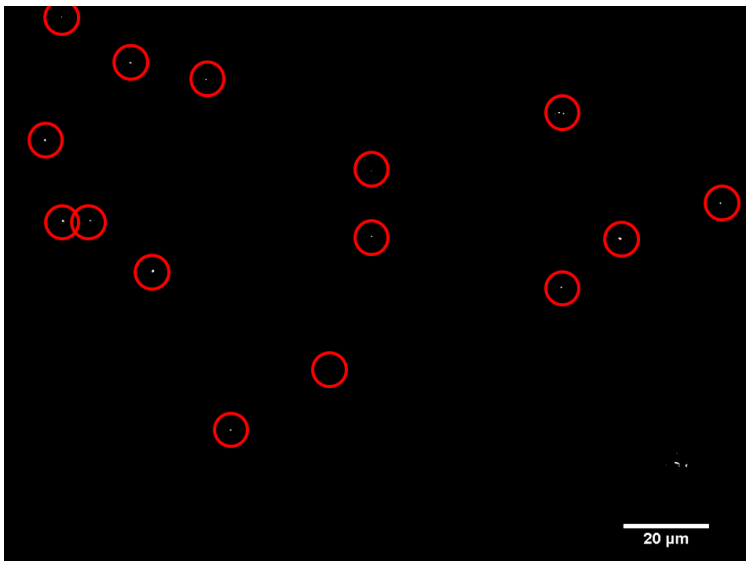

Figure 4.6: Image taken of an experiment with a concentration of 10^3 *spores/ml. The round bright dots represent spores, while the irregular shapes are fluorescent debris cought on the slide.*

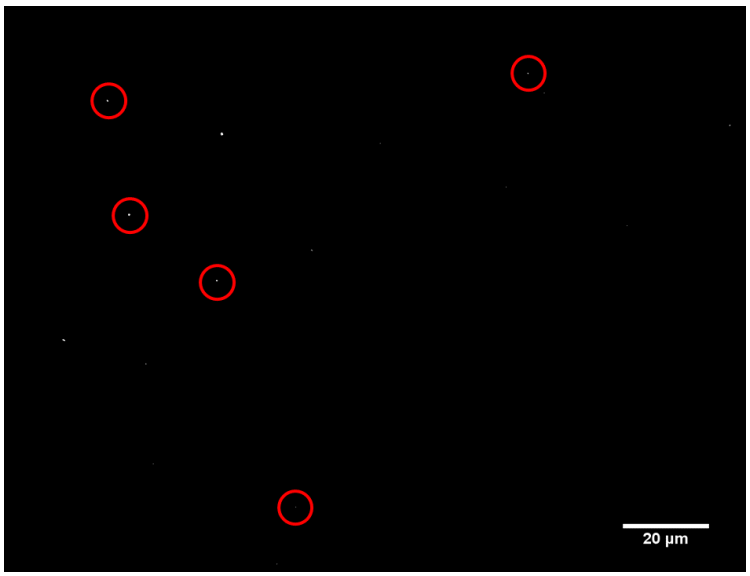

Figure 4.7: Image taken of an experiment with a concentration of 10^2 *spores/ml. Due to the small concentration of spores, only a few are visible while no debris is visible at all. The spores are circled for easier inspection.*

[3] An inspection of the entire chamber was made and no floating particles were detected.

Before quantitative experiments were done, 2 slides were spotted with antibodies. Spotting is a procedure where droplets containing antibodies are applied to the cover slip in any pattern. In the case presented here alternating rows of antibodies were created where one is coated with the specific antibody, while the other row is blocked to prevent specific binding. Figure 4.5 shows four examples of the two rows of spots: one (lower) containing the spore specific antibody, and the other (upper) being blocked in order to prevent specific binding. The examples were taken from various positions along the y-axis (the width of the slide). The figure shows the results of the initial experiment using a 10^4 spore/ml suspension. As this was part of a preliminary set of experiments, no counting was done on these slides.

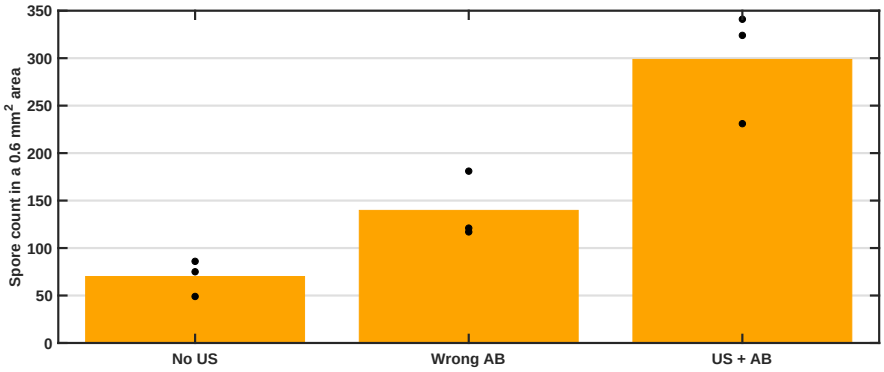

(a) Comparison of all 100 spores/ml concentration experiments

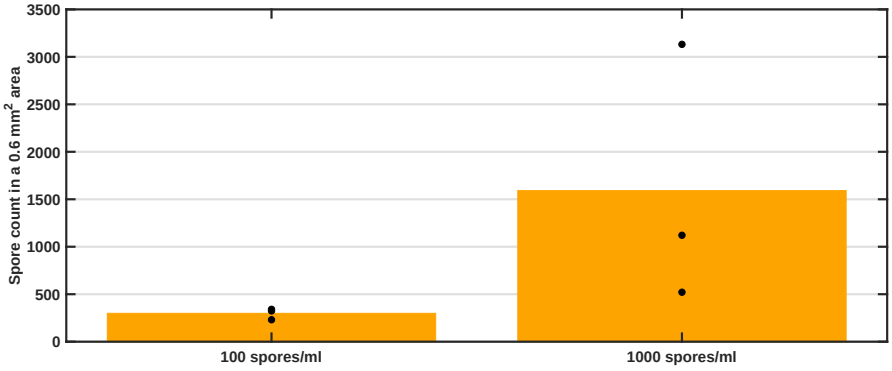

(b) Comparison of the two experiments using both the US and the antibody coating

Figure 4.8: Mean values of the spore counts for each experimental condition. Overlaid on top of the bars are the values for each individual experiment for the associated condition. In this graph AB stands for antibody.

The other experiments were performed on slides with coated areas, instead of spotting, as noted in the previous section. Figure 4.6 shows an example image from the 10^3 spores/ml experiments. The spores themselves are 1-2

μm in size, but due to their brightness their point-spread funtions (PSFs) are larger.

The final example image is shown in figure 4.7, which was taken from an experiment that had a spore concentration of 10^2 spores/ml. The slide coating was the same as it was in the prior experiment. In all three experiments there was random fluorescent debris from the staining procedure that got caught on the slide. The more obvious debris has a non-circular an irregular shape making it easy to spot and discount, but some debris is close in appearance to the spores, with the difference being in the spread of the brightness, i.e. PSF, and the maximum brightness of the object (the debris being less bright than the spores).

Table 4.1: Results from the spore experiments, including the tested variables, total number of counted spores, resonance frequency and strength of resonance as measured by an impedance analyser. The mean values for the four experimental conditions are: 70, 140, 299, and 1591 spores.

Conc. (CFU/ml)	US	Antibody	Repeat no.	Total Count	Resonance frequency (kHz)	Conductance (mS)
10^2	No	BG	1	75	/	/
			2	49	/	/
			3	86	/	/
10^2	Yes	CD203c	1	121	924	49
			2	181	962	46
			3	117	960	51
10^2	Yes	BG	1	341	977	69
			2	324	971	53
			3	231	916	27
10^3	Yes	BG	1	521	972	78
			2	3132	966	59
			3	1121	971	60

For the 10^3 spores/ml concentration 3 experiments with both ultrasound and a correct antibody coating were performed. For the lowest concentration, that of 10^2 spores/ml, alongside the full method test (consisting of ultrasound and correct antibody), two controls were done as well: no ultrasound, but with correct antibody; and ultrasound turned on, but wrong antiobdy used to test the specificity of capture (CD203c, the antibody used to capture basophils, and used for allergy tests as described in chapter 5). Figure 4.8 shows the mean values of the spore counts performed for all test conditions outlined in this paragraph, as described in section 4.2. They are represented as a bar graph. Overlaid as individual point over the corresponding bars are the values of the spore count for each experiment. The graph is separated into two to preserve the detail and give a better understanding of the difference between the values, while still keeping the linear scale. Figure 4.8a shows the results

of all experiments with the 100 spores/ml concentration, while 4.8b compares the two experiments with both US and antibody coating used. Table 4.1 gives the values for the graphed results, alongside some other conditions listed for each experiment (resonant frequency, strength of resonance). The mean spore count values for each experimental condition are:70, 140, 299, and 1591 spores. Due to there only being 3 experiments per condition, no statistical analysis was done.

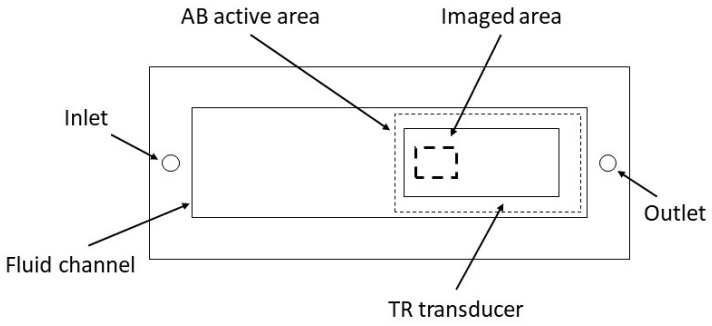

Figure 4.9: Diagram of the imaged area

The 100 images taken for each experiment can be arranged into a grid that covers an area 10 times that of a single image. This area can be seen, in figure 4.9, with respect to the antibody coating and the transducer. Figure 4.10 plots a 3D graph where each point on a 10 x 10 matrix represents the spore count of an image. This gives an overlay of the distribution of spores within the imaged area.

4.4 Discussion

The terminal velocity of a spore is determined by the following equation [237]:

$$u_{max} = \frac{d^2(\rho_s - \rho)g}{18\mu}, \tag{4.1}$$

where d is the diameter of the spore, ρ_s is the density of the spore, ρ is the density of the surrounding medium, g is the acceleration due to gravity, and μ is the dynamic viscosity of the surrounding fluid. The BG spore diameter (0.6 μm) and density (1200 kg/m^3) were found from two papers by Carrera et al [17, 238]. BG spores are elliptical in shape with an almost 2:1 ratio [17], but they were approximated to be a spore of the same volume for the terminal velocity equation since both the size and velocity are very small [237]. The value used for viscosity of water at 20 °C was 1.002 $mPa \cdot s$ [239], and the density value was taken as 1000 kg/m^2. The terminal velocity was found to be 2.5 $\mu m/min$, which is very similar to the experimental value of 3.6 $\mu m/min$. The sedimentation (figure 4.4) was performed as a baseline, albeit of limited

value, as it is sedentary. While 40 % of spores did sediment in 10 minutes, this was over a chamber height of 100 μm. For this method to be practical the total antibody surface area would need to be prohibitively large [4], and if the test chamber was taller to accommodate for real world sample sizes the experiment would take a lot longer. The results do, however, provide a worse case scenario - if nothing is done, how long will it take to capture the spores by just letting them sediment.

The experiments performed using spotted slides were a proof of principle: that the device can indeed push the spores towards the coated surface, but also that the specificity of the antibodies plays a role in the capture rate and is an important factor in the method. Figure 4.5 shows this to be true as there are barely any spores seen in the control spots, while the specific antibody spots contain streaks of spores. The high concentration of 10^4 spores/ml, allows us to see the stark difference between the two, as well as some lateral banding on the spots, since the distribution across them is not equal, but rather concentrated

[4] At chamber height of 100μm, a sample of 1 ml would require a surface area of 50000 mm^2 for sedimentation.

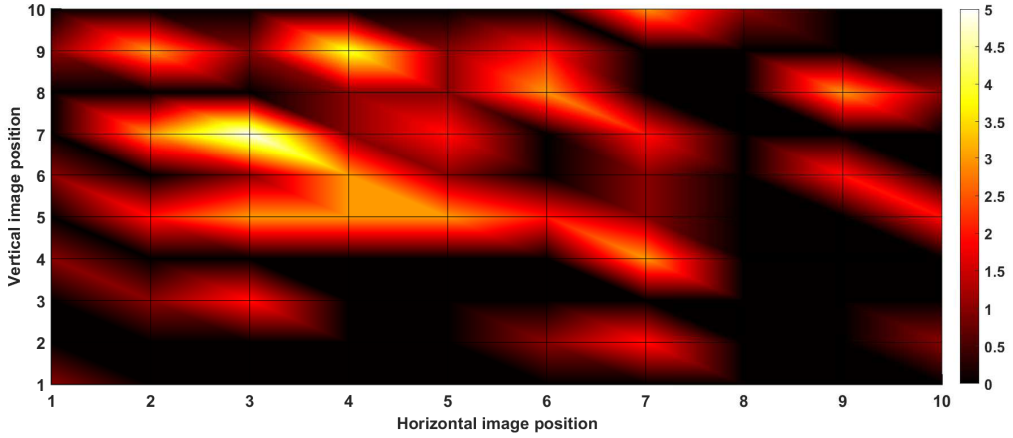

(a) No ultrasound

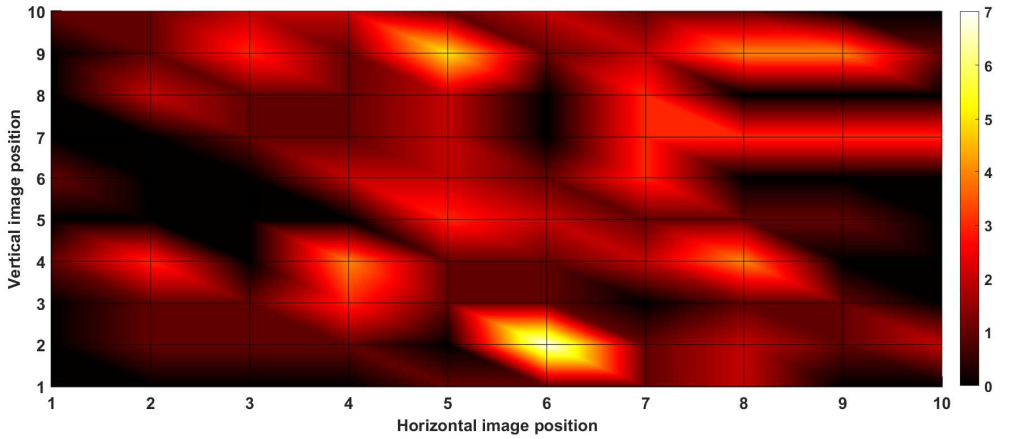

(b) Wrong antibody

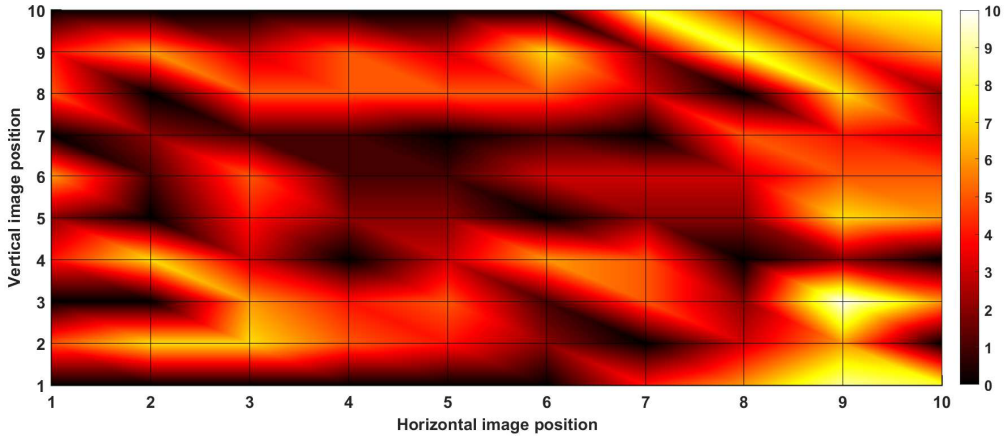

(c) Ultrasound and antibody, 100 spores/ml

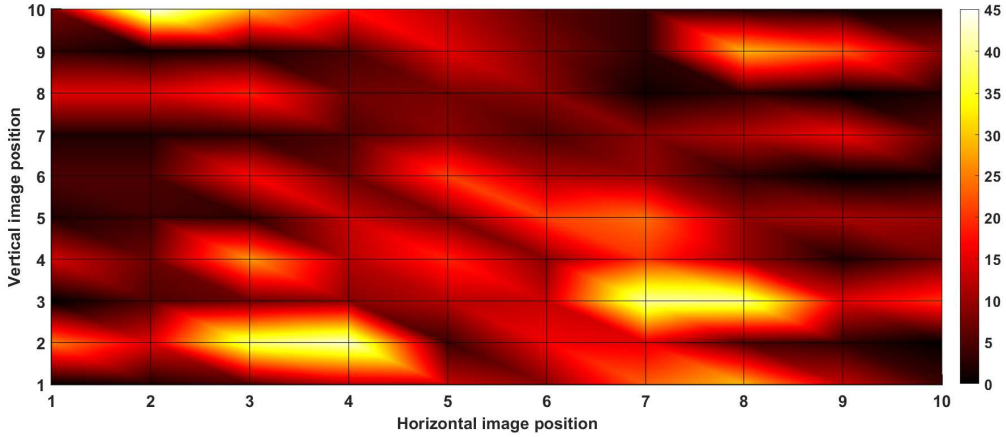

(d) Ultrasound and antibody, 1000 spores/ml

Figure 4.10: Representation of the spore distribution within the imaged area for select examples of experiments. Each point represents the spore count of the associated image in the grid. The colour between the points is interpolated from the surrounding point values.

in thin streaks.

Images in figures 4.6 and 4.7 are only examples of the images taken from the experiments of respective concentrations and are not representative of the entire spore population.

Approximately 500 spores passed through the device during the lowest concentration experiments. Without the aid of ultrasound only 70 spores were captured, on average, in the imaged area. This amounts to 14 % of the total spore number that passed through the fluid channel. With a 30 ml/hr flow, the velocity inside the fluid chamber is 6.94 mm/s (calculated by dividing the flow rate with the cross-section area of the fluid channel [240]), meaning a spore spends a total of 8.96 s inside the fluid chamber.

Figure 4.11 shows how a spore would travel through a 100 μm fluid channel with a parabolic velocity profile and a constant downward velocity. The value

for the downwards velocity was found experimentally from the sedimentation test, while the average velocity in the channel from which the velocity profile was found was calculated in the paragraph above. The velocity profile is given by the equation [240]:

$$u(r) = u_{max}\left[1 - \frac{r^2}{R^2}\right], \tag{4.2}$$

where r is the distance from the centreline, R is half the height of the channel, and u_{max} is the maximum velocity in the channel, which is also expressed as:

$$u_{max} = 2 \cdot u_{average}. \tag{4.3}$$

A sphere with the diameter of the spore was simulated for every possible height in the channel in 1 μm intervals using a *MATLAB* script supplied in appendix A. The figure shows the trajectories each of the spheres take, while the dashed line marks the end of the physical channel in the device. The number of spheres that touch down only account for 3 % of the total spheres simulated. The difference can be explained by the fact that the simulation assumes perfect laminar conditions. Because the chamber inlet is a lot smaller (a tube of 1 mm in diameter) the velocity at the inlet would be higher than in the chamber for a given volume flow rate. This means that at the inlet possible turbulence may occur which may change the equal distribution of spores assumed by the model.

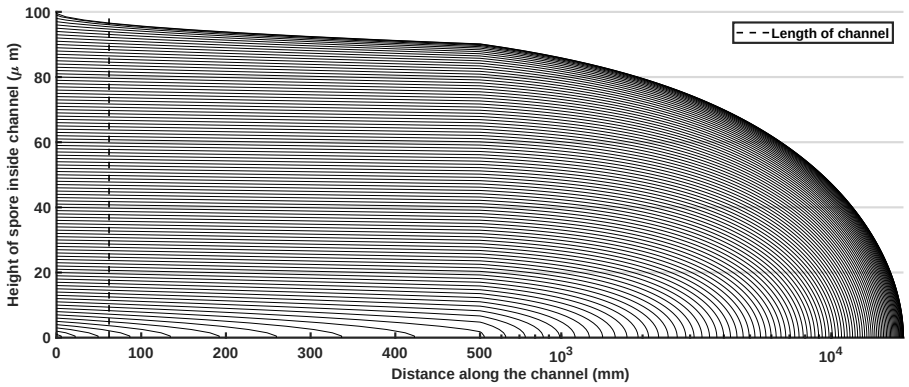

Figure 4.11: A simulation of a path a spore-sized spherical object would take inside the channel with a parabolic velocity profile and a constant downward velocity. The dotted line represents the length of the physical fluid channel. Any sphere that touches down before it can be assumed to be captured. Only 3 % of the spheres were captured this way.

Ultrasound enables more spores to reach the antibody coating, but if the coating is specific to a different receptor (as is the case with CD203c), the spore will not attach and will roll away. It is quite possible, however, that the capture rate for these experimental conditions could be even lower as the technique used to coat the slides (described in section 4.2.2) relies on imprecise methods of

controlling humidity and temperature. Perhaps with a better coating technique less spores would stick to the mismatched antibody.

When the antibody is specific to the spores, the capture rate increases from 28 % to 60 % of all the spores that pass through the device. This means that the device is capable of detecting spores at a concentration of 100 spores/ml which puts it in competition with other devices and biosensors that have some of the lowest detection thresholds.

Repeat no. 3 of the active experiments at the lowest concentration is an outlier in the series of three experiments, and it is possible that this is due to the low strength (i.e. conductance) of the resonance. Furthermore, the low resonance frequency implies that the fluid layer height is larger than normal making for a weaker ultrasound standing wave (USW) field. Section 4.4.1 discusses how this issue can be fixed.

When the concentration was increased to 1000 spores/ml, and the total number of spores in an assay to 5000, it was expected that the capture rate (all other parameters being the same) would stay the same while the numbers would increase 10 fold. The actual capture rate dropped to 31 %, while the increase in numbers was only 5.3 higher. This represents only half of the increase expected. One of the repeats did have the expected capture rate, but the others faired worse with the first repeat providing only a 12 % capture rate. One possible explanation is that the driving voltage combined with a strongly resonant peak is creating streaming effects inside the chamber, which may prevent the spores from ever attaching, as well as exciting plate modes, which may dislodge spores from the reflector layer. These effects are discussed in more detail in section 3.8.

In its current iteration, the device has shown an ability to provide a very low limit of detection (100 CFU/ml), which is only rivalled by the traditional methods (cell culture, enzyme-linked immunosorbent assay (ELISA), polymerase chain reaction (PCR)) and two of the biosensor techniques examined in this thesis: magnetic nanoparticle detection and electropermeabilisation-assisted DEPIM (EPA-DEPIM). It is significantly better than commercially available anthrax testing kits which have a limit of detection in the range of $10^5 - 10^6$ spores/ml. The advantage this device has over traditional methods is in the time it takes to complete an assay. Within 10 minutes, enough spores are captured for analysis, and paired with the right sensor the overall testing time can be kept within 30 minutes. This is better than most biosensors reviewed in this thesis (the commercial anthrax kits, alongside other varied methods like EIS, SERS, or USW-metal-clad leaky waveguide (MCLW), can show results only 15 minutes after the testing began). Overall the two parameters combined produce a device that is pushing the boundary of pathogen detection. This provides opportunities in both detection of pathogens that are present in low concentrations, both from airborne and water-borne sources, but also provides a support device that can be used in the field as a confirmation to other detection methods. The basic principle of the device (ultrasound coupled with

an antibody coating) can be used in conjunction with other sensors types to enhance their limits of detection and assay times.

The distribution of spores within the imaged area, as seen in figure 4.10, does not show any noticable pattern. Unlike the high concentration experiment on the spotted slide (figure 4.5), where the lateral banding is obvious [5], no such pattern was found at the lower concentrations. Figure 3.13 provided a reference for the distance between two lateral bands. The mosaic images of the active area for the active experiments show no evidence of lateral bands, despite being large enough to encompass multiple bands.

There was no clear correlation between the resonant frequency and the strength of the resonant peak with the number of spores captured.

4.4.1 Future work

In its current form, the device has some shortcomings that need to be addressed. By using screws to hold the device together planarity can be hard to achieve, as well as a consistent fluid layer height. By switching to a different kind of clasping mechanism, either magnetic, or lever, or otherwise, that would ensure the same height and good planarity every time the device is used, the reliability and ease-of-use would improve drastically.

Next in line for improvement is the detection method. Currently, spores are prestained and then the slide is placed under a microscope once the experiment is finished. This is effective for proving the principle of capture but is not suitable for real world application. The device would need to be combined with some form of a biosensor that could detect the appropriate spores either in real-time or within minutes, while not requiring costly or bulky equipment. There are already examples of using acoustic detection combined with PCR [151, 162], and the use of mass spectrometry or Raman spectrometry looks very promising as a detection method [131]. Coupled with an acoustic concentration and immuno-capture it could be made into a very quick, robust, low-cost and easy to use device that could be deployed on the field for both water and air safety testing.

If the device is to be used in areas with no sterilisation capabilities a disposable section of the device would need to be designed and tested. One possibility is to create an isolated fluid channel, bounded by a coated coverslip on one slide, and by a thin film of plastic on the other. This plastic film would be placed over the stainless steel carrier layer in order to couple the fluid layer to the base of the device.

In order to boost the effectiveness of the device past 10^2 spores/ml, a second transducer may be added. It could be in the half wave (HW) mode, in order to push all spores to the centre thus making it easier for them to be pushed

[5] The lateral bands are found at positions at which one would expect to find them on the slide. As the image is a selection of spot locations it cannot faithfully recreate the distance between the bands.

towards the antibodies, but also making the touchdown spot more predictable. An alternative would be as a second TR transducer which would double the length of the USW field. This would have an effect of spreading out the area of a possible touchdown site.

In order for the device to be used, easily, and cheaply, it needs to be consolidated into a single reusable unit with a disposable element. This means creating a "black box" which will contain all of the driving elements (signal generator and amplifier for the transducer and pump for the solution), a detection sensor, a very simple and intuitive interface as well as easy-to-follow instructions. In this state it would be ready to be used in any real-life application.

4.5 Conclusion

Environmental pathogens pose a threat to the health and well-being of humans [1, 3]. Even in developed nations with state-of-the-art detection facilities outbreaks can occur and terrorist attack can pose a very significant risk [115]. The methods currently in place all have their drawbacks, trading accuracy for speed, or vice versa, with newer biosensors finally breaching that trend [6].

In this chapter it was demonstrated that an acoustophoretic device was capable of detecting BG spores in a medium with a concentration as low as 100 spores/ml, within an hour. To achieve this the device used a lead zirconate titanate (PZT) transducer that established a thin-reflector mode which pushed all of the spores onto an surface coated with antibodies specific to BG spores, designed to capture them. The coated slides were then analysed under a microscope and the spores were counted.

After a 10 min assay at 30 ml/hr, with a concentration of 100 spores/ml, during which 500 spores passed through the device, 60 % of spores were captured on the coated slide. To put in perspective, controls with no ultrasound captured only 14 %, while the controls with the non-specific antibody captured 28 %.

The device is easy to manufacture using CNC routers and moulds for PDMS gaskets, and with most parts being reusable it comes to a low-cost per assay. Furthermore, with a peak voltage of 10 V_{pp}, and a power consumption of less than 5 W, the power consumption is kept very low and is very suitable for battery operation where there is no power outlets.

The device can easily be further improved to ensure even more reliability and accuracy in finding the resonance frequency, while implementing disposable aspects inside the device to ensure no contamination. Finally, the current, bulky detection method can be replaced with a faster, cheaper and smaller ones in the form of either PCR or SERS. The methods would allow for an even faster detection with possibly a lower detection threshold.

Chapter 5

Basophil capture and detection for allergy diagnosis

5.1 Introduction

Allergies are affecting around 22 % of the world [41]. Their symptoms range from mild, as is the case of rhinitis, moderate long term ailments as with asthma, and can even be deadly as is the case with anaphylactic shocks. Even in the case of mild nuisances, most people report that the symptoms can lead to insomnia, depression and irritability (as is the case with rhinitis [50]).

There are multiple, well-established methods of diagnosing allergy: from the simple skin-prick test, through blood serum IgE measurement, to the gold-standard - the provocation test [166]. All of these methods have their strengths and shortcomings, including the provocation test, which is, despite the very invasive and straightforward nature of exposing the patient to the allergen, still not 100 % accurate and can have false readings [163, 165].

Due to the prevalence of allergy waiting times at allergy centres across the UK are months, and some places even years long. A new method of diagnosing allergies is needed to resolve the two main issues presented: a test that is quick enough so that wait times can be shortened, and a test that is more accurate than the current gold standard. The basophil activation test (BAT) is an attempt at resolving the two issues, and while it can achieve high accuracy and fast turnaround it relies on expensive equipment that can still create bottlenecks [166]. An alternative solution is proposed in this chapter, where an acoustofluidic platform is used to capture basophils, the white blood cells responsible for allergic reactions, in a short amount of time without the need for any expensive equipment, while keeping them viable for further testing.

The work performed in this chapter was done with Chloe Rose and her supervisory team: Dr. Andrew Walls, Prof. Xunli Zhang, and Dr. Laurie Lau. I was responsible for device design and manufacture, slide preparation, and the performance of the experiments, as well as imaging and post-processing, while Chloe Rose was responsible for blood collection and preparation, cell staining,

slide fixing, and FACS analysis.

The next section describes the methods used in the slide and basophil preparation, and experiments. Section 5.3 shows the results from the experiments and gives a discussion on their meaning. The last section, gives the conclusion and the summary of all results.

5.2 Methods

5.2.1 Blood sample collection and preparation

Healthy subjects with self-identified grass pollen or dust mite allergies were recruited through informal contacts using the ethics application (Study No. 05/Q1702/9, Southampton Ethics Committee). From each patient 60 ml of blood was collected into 9 ml ethylenediaminetetraacetic acid (EDTA)-coated vacutainers using a winged infusion set. The coating was there to prevent the blood from coagulating. The vacutainers[1] were inverted eight times and stored in a Bio-bottle for safe trasport. Once at the lab, to ensure proper mixing, they were placed on a roller (Spiramix 5, Denley).

Blood lysis through cell density gradient centrifugation

The blood samples were diluted 1:2 with buffer 1X from a stock of 10x phosphate-buffered saline (PBS) (PBS, pH 7.4, Gibco, Life Technologies, Waltham, MA, USA), 0.05 % bovine serum albumin (BSA) (BSA, albumin fraction V from bovine serum, ProLabo VWR Chemicals, Radnor, PA, USA). A centrifuge tube containing 9 ml Lymphoprep (density 1.077 g/ml; Fresnius Kabi Norge AS, Østfold, Norway) had 9 ml of diluted blood carefully layered on top, and the two were centrifuged at 18 °C at 350 g for 45 min. The plasma layer was removed using a pipette, while the buffy coat, a layer of blood formed after density gradient centrifugation containing the white blood cells and platelets, was gathered using a syringe. It was diluted with 1:3 1X PBS dilution and centrifuged again at 18 °C at 400 g for 10 min. The pellet was re-suspended in 9 ml 1X PBS and centrifuged again at the same settings. The washing process was repeated once more. The remaining erythrocytes were removed by adding 9 ml deionised water (dH_2O) and vortexing for 6 s. Afterwards 1 ml of 10X PBS was added and the sample was centrifuged at room temperature and 350 g for 10 min. This procedure produces a solution containing only the white blood cells. Figure 5.1 shows the different layers that form after centrifugation when using Lymphoprep.

[1] A vacutainer is a a sterile glass or plastic test tube with a coloured rubber stopper creating a vacuum seal inside of the tube,used for blood collection.

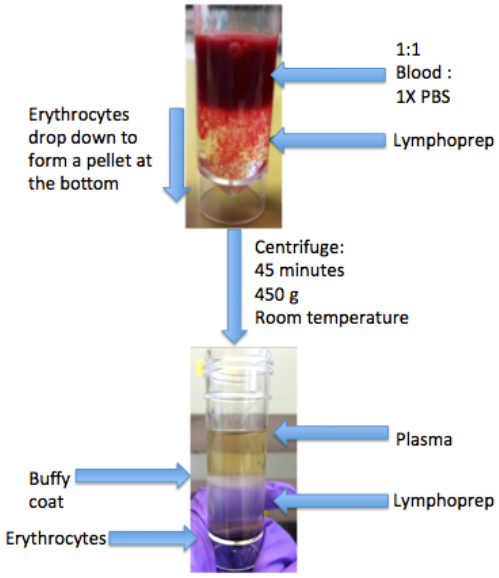

Figure 5.1: Blood separation using Lymphoprep. A 1:1 mixture of whole blood is mixed with PBS which is placed on top of Lymhoprep. The solution is centrifuged for 45 minutes to get the separation between plasma, buffy coat (containing white blood cells and leukocytes), Lymphoprep, and erythrocytes. Images taken by Chloe Rose.

Basophil purification using MACS negative selection

To further isolate the basophils into a near homogeneous solution MACS is used. This method was first described in 1999 and consists of small magnetic nanoparticles coated with specific antibodies being mixed with the solution. Depending on the type of procedure [2] the desired cells are captured and a magnet is used to remove the microparticles [241].

The lysed pellet was aspirated and supernatant resuspended with 30 μl of PBS, 0.05 % BSA buffer, 10 μl of FcR antibody cocktail (containing antibodies against CD3, CD4, CD7, CD14, CD15, CD16, CD36, CD45RA, HLA-DR, and CD 235a (glycophorin A), used to capture every cell apart from basophils, and 10 μl blocking reagent using a MACS negative selection (basophil isolation kit II, MACS, Miltenyi Biotec, Germany). After mixing, the sample was incubated in a fridge at 2-8 °C for 10 min. The cells were washed in 2 ml buffer and centrifuged at 300 g for 10 min. The pellet was aspired and re-suspended for the final time in 500 μl buffer. The MACS column amplifies the magnetic field of the magnetic separator in whcih it was placed. First, the column was washed with 500 μl of buffer, after which the cell suspension was flowed through. The magnetically tagged cells were captured inside the column while the untagged basophils passed through. Three rounds of 500 μl buffer was passed through the column to remove any stuck untagged cells. The cells were centrifuged at

[2]Negative separation procedure captures everything but what is wanted, while the positive separation only captures the wanted cells.

200 g for 10 min to form a pellet, which was then re-suspended in 500 μl of buffer.

5.2.2 Slide preparation

In-house slide coating

For basophil capture Schott Nexterion slide H was used. The slides were functionalised with anti-human CD203c basophil-specific antibody (Miltenyi Biotec, Surrey, UK), which came in a ready-to-use concentration of 0.1 mg/ml. An acrylic spacer was placed on top of the antibodies to prevent evaporation and to spread them out over the entire active area. The slides are placed in a humidity chamber described in section 4.2.2, where they are left overnight. The next day the slides are placed in a slide holder filled with a blocking buffer(76 μl ethanolamine, 1.9 g sodium borate, 50 ml water) for at least 1 h, in order to prevent adhesion to the rest of the slide. The slide was then washed with PBS and dried using pressurised air. It was then ready to use in the device.

Outsourced slide coating

The Karlsruhe Institute of Technology (KIT) in Germany has developed a new method of spotting slides called "Polymer dip pen nanolitography" whereby the tip of an atomic force microscope is manipulated to allow the surface to be "drawn" on [242, 243]. Microscope coverslips with dimensions of 75 x 25 x 0.17 mm (Logitech Ltd., Glasgow, UK) were sent to the institute and there they were spotted with the described method using anti-human CD203c (Miltenyi Biotec, Surrey, UK), in a dot-grid pattern (as shown in figure 5.2).

5.2.3 Experimental procedure

To prepare the lysed blood or the purified basophil solution for use in the device they were diluted to 50 ml with 1X PBS. The experimental setup for basophil capture was the same as the one for spore capture and was described in section 4.2.3. In the case of basophil capture the device output was not collected in a waste tube, but rather collected for further analysis later. A 1 ml sample was collected from the basophil solution before it entered the device. During the 10 minute assay 5 more 1 ml samples were collected, each for a 2 minute period. After the assay was completed the fluid layer was flushed with PBS for 30 s to remove any basophil that is not attached. The output containing these removed basophils was collected as the last sample (called a "flush" in this thesis). These basophil depleted suspensions were then taken for further analysis.

The first set of experiments performed used a purified basophil solution and it consisted of a 10 min assay with sample collection. Each experiment

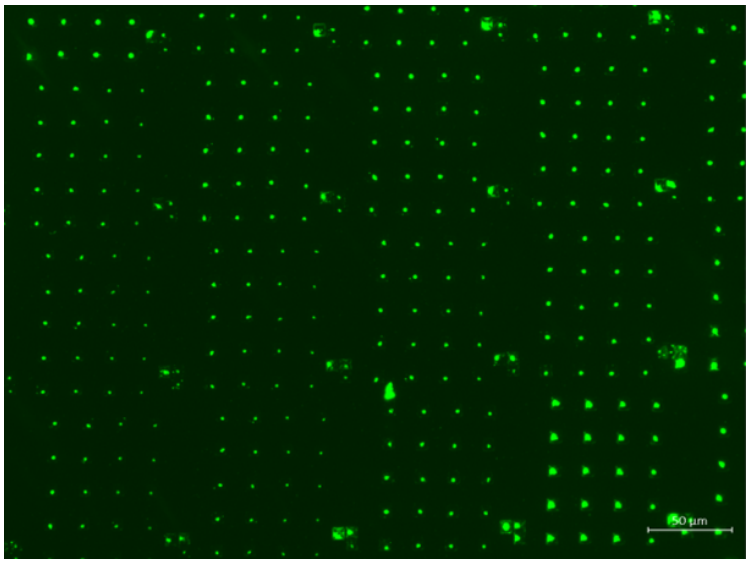

Figure 5.2: Image of fluorescently tagged antibodies spotted onto a slide using the method developed at KIT.

had a different flow rate, ranging from 10 to 50 ml/hr in 10 ml/hr increments. each flow rate consisted of two tests which were then averaged for the results.

Afterwards, when the flow rate was settled on, experiments were performed with purified basophils to find out the ideal capture rate. A total of 5 experiments were done, each with 1 no ultrasound (US), and 1 no antibody controls, alongside 3 active [3] tests.

Finally, 3 lysed blood experiments were performed, with 2 controls, as before, 2 active tests with the coated Schott slides, and 2 active tests with the spotted slides obtained from the KIT, Germany.

Slide fixing

After the device was disassembled it had to be fixed to stop the basophils from deteriorating quickly and detaching themselves from the slide due to handling. This was done by using 16 % formaldehyde ampules and leaving it on the slide for 10 minutes. Afterwards the slides were washed in 1X PBS three times.

5.2.4 Fluorescent activated cell sorting (FACS) analysis of basophil depleted suspension

To the 5 ml polystyrene round-bottomed tubes a 150 μl aliquot of stimulation buffer (BAT Flow Cytometry kit, Buhlmann, Schö nenbuch, Switzerland) was added alongside a 50 μl sample of the whole blood, density gradient lysed samples, or immunomagnetic negative separation samples and 20 μl of stain containing both CCR3-phycoerythrin (PE) (phycoerythrin) and CD63-FITC

[3] Both ultrasound turned on and antibody coating applied.

(fluorescein isothiocyanate) (Basophil Activation Test Flow Cytometry kit, Buhlmann). Avoiding direct sunlight, the tubes were incubated in a water bath at 37 ℃ for 15 minutes. Afterwards the samples wer incubated for 10 min and centrifuged at 500 g for 6 min, both at room temperature. A wash buffer (300 μl, Buhlmann basophil activation test flow cytometry kit) was added to each tube. After the re-suspension, the stained cells were processed in the FACS Calibur for analysis.

The FACS Calibur flow cytometry equipment is capable of detecting four colours (BD Biosciences). The values for FITC and PE were entered into the software as the samples contained too few basophils to carry out the compensation on the machine. The initial gating values were acquired from the negative samples. FlowJo software was used to analyse the samples and obtain a percentage of CD63 positive and CD63 negative cells within the basophil gate.

Figure 5.3 shows the scatter plots obtain from the FACS analysis. First a scatter plot (fig. 5.3a) of forward scatter (FSC) versus side scatter (SSC) is presented to ensure a separation of leukocytes into three distinct populations: granulocytes, monocytes, and lymphocytes. Then (fig. 5.3b) CCR3-PE was plotted against SSC to determine region one (R1), an area containing basophils, determined by selecting 500 events which were CCR3-positive and SSC-low. This excludes eosinophils which are SSC-high. Finally, CCR3-FITC is plotted versus CCR3-PE within R1 to determine a percentage of cells with a positive CD63 reaction. The upper right quadrant shows the activated basophils, while the lower right quadrant shows the inactivated ones. The figure shows three examples: negative control with only 0.4 % activation (fig. 5.3c); positive $\alpha - IgE$ control with 87.5 % activation (fig. 5.3d); and positive formyl-methionyl-leucyl-phenylalanine (FMLP) activated cell control with 75.8 % activation (fig. 5.3e).

5.2.5 Staining and imaging for lysed blood experiments

Once the slides were fixed, any basophil captured on the slide would be preserved up to a few months to be imaged on a microscope. A direct method for counting basophils was used for those slides from experiments with lysed blood.

The slides were stained with a general stain Alexa Fluor 647, functionalised with CD63 (Thermo Fischer Scientific, Waltham, MA, USA). After fixing, a droplet of the stain was placed on the slide and allowed to settle for 10 minutes. The slide was then washed in purified water and dried with pressurised air.

Once the slide was stained it was placed in an inverted microscope with an automated XY stage, the same as one described in 4.2.4. A grid of 10 x 10 images was taken with a 10x objective, a white light source, a Texas Red filter cube, and prepared for post-processing.

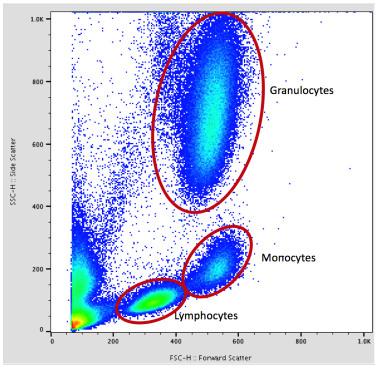

(a) FSC versus SSC

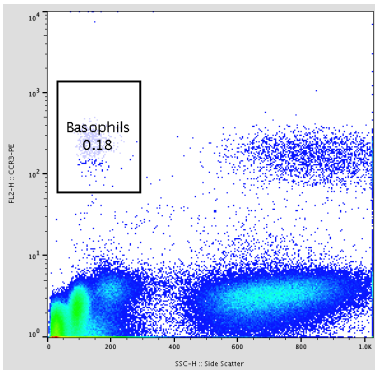

(b) CCR3-PE versus SSC

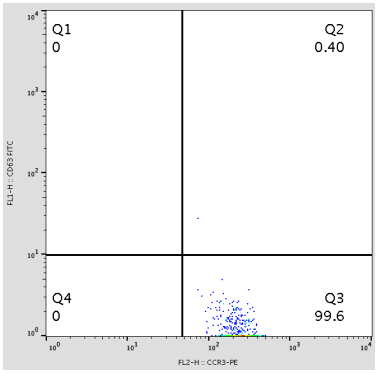

(c) Negative basophil control

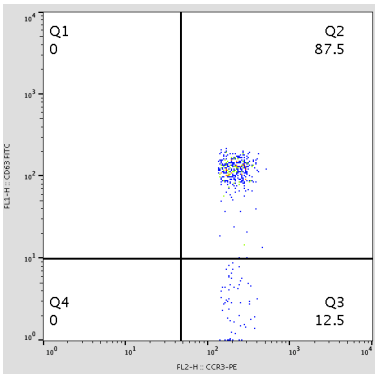

(d) Positive $\alpha - IgE$ control

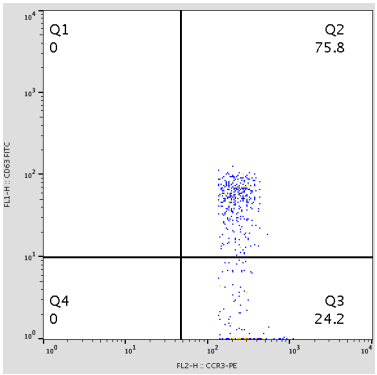

(e) Positive FMLP control

Figure 5.3: Leukocyte scatter plots obtained with FACS analysis.

5.2.6 Post-processing

For solutions containing purified basophils an indirect method was used to ascertain the possible numbers of captured basophils. A sample that was taken before the solution was run through the FACS device and set as a baseline. The 5 following samples (each collecting 2 minutes from the 10 min assay) were also run through FACS and the numbers they got was compared to the baseline to see how much of the basophils in the solution got captured in the device. Each of the 5 samples represented a maximum of 20 % of the maximum

number of basophils that could have been captured. Finally, the flush sample was run through FACS. It represents the basophils that didn't stick to the antibody coating.

To get the total number of basophils that were captured the capture for each 2 min section of the assay was determined:

$$capture_{sect.} = \frac{Baseline - Section}{Baseline}. \tag{5.1}$$

The flush was calculated using:

$$capture_{flush} = \frac{Flush}{Baseline}, \tag{5.2}$$

as we are interested in how many came out for the flush, as opposed to how many stayed, as it was for the section capture numbers. To find out what percentage of basophiles were captured, all of the individual sections are added together and the flush subtracted, and the result is then divided by the number of active measurements. Finally, the result is multiplied by 100.

$$capture_{total} = \frac{Sect_1 + Sect_2 + ... + Sect_n - Flush}{n} * 100, \tag{5.3}$$

The actual number of captured basophils was not investigated at this point, although it could have been determined. The microscope images and the basophil count from them would ultimately determine the true capture numbers.

The images of slides acquired from the inverted microscope were processed with ImageJ. An automatic threshold method that relied on the cumulative histagram of an entire image batch was used to convert each image into binary. A watershed process was then used to separate two spheroid objects that are joined so they can be counted as two. The "Analyze particles" plug-in was used to count the cells on the images.

5.3 Results

5.3.1 Flow rate testing

The flow rate experiments were done with purified basophils in order to determine the optimal flow rate for all future experiments. Figure 5.4 shows the percentage capture of the total number of basophils as it changes with 2 min sections of the total assay as well as the flush after the experiment. The final capture values for each flow rate were: 10 ml/hr (31 %), 20 ml/hr (44 %), 30 ml/hr (60 %), 40 ml/hr (-1 %), 50 ml/hr (0 %).

Initially, as the flow rate increased the capture percentage increased accordingly, most likely due to the fact that the ultrasound standing wave (USW) field was strong enough to push the basophils to the surface despite the shortened time spent in the field, as well as the larger surface of the basophil touchdown

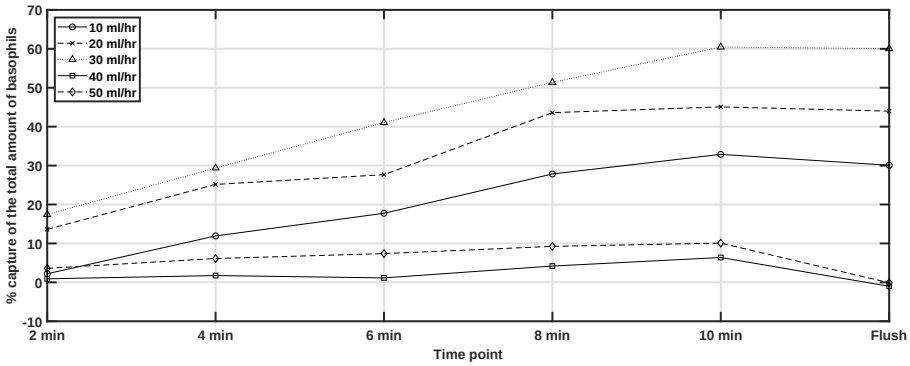

Figure 5.4: Percentage capture of the total number of basophils for the flow rate experiments.

area, meaning less basophils are blocked from sticking to the slide by other basophils. At 40 and 50 ml/hr, however, the speed of the fluid becomes to great for any basophils to reach the antibody coated area so the capture percentages drop to almost zero. In fact, in the case of 40 ml/hr, the total capture is evaluated at -1 % due to the not perfect nature of the evaluation method (described in section 5.2.4).

The figure also demonstrates why the flush is an important part of the experimental process. During the 10 min of the active assay basophils are pushed towards the antibody coated surface where they would get attached. Some basophils, alongisde other cells, get trapped either by acoustic forces or between other attached basophils, but are not attached themselves. The flush, during which PBS is run through the device without the aid of the USW for 30 s, dislodges those cells and takes them out of the device so only the basophils that are truly attached remain, as any allergy testing method will have various allergens and reagents flowing through the device after the USW is turned off. At the higher flow rates, a lot of the basophils are not properly trapped by the antibodies, rendering them useless in any real-life scenario, while at 30 ml/hr, almost all of the basophils were stuck to the antibody coating.

As a result of this experiment, the flow rate with the best capture rate, 30 ml/hr, was chosen for all further experiments.

5.3.2 Purified basophil tests

Purified basophils were used to demonstrate if the device is capable of capturing anything under favourable conditions. Figure 5.5 shows the summary graphs of the experiments performed with the blood from 5 different patients. It shows the mean of the capture rate for the active experiments - both with antibody and USW (3 done per patient), and the two controls - no ultrasound, or no antibody (one of each per patient). It also gives the standard deviation and the capture rate for each individual experiment. All of the experiments were normalised to a maximum of 100 % capture.

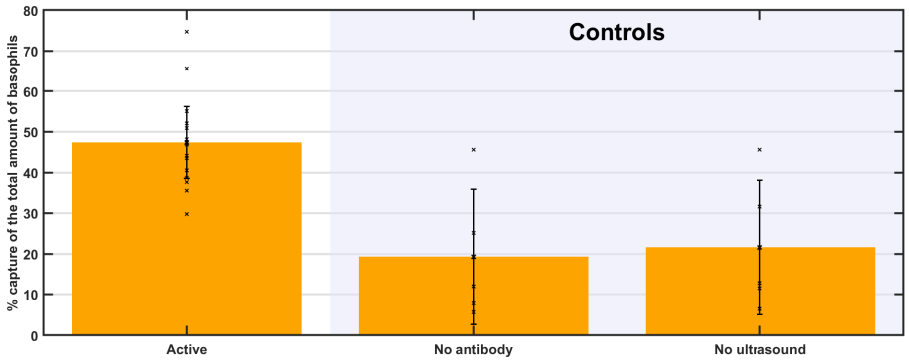

Figure 5.5: The mean average capture percentage with standard deviation of the 10 min assays containing purified basophils, alongside the two controls (no ultrasound, and no antibody). The dots represent the capture percentages of individual experiments. The data was derived from the FACS analysis.

The active experiments had an obviously better capture at a mean 47 %, while the two controls had a mean capture of 19 and 22 % respectively. After checking for normality (which all distributions passed), a paired T-test was done to see if there is statistical significance between the active experiments and the controls, and the p-value was found to be 0.06 and 0.13 compared to the no antibody and no ultrasound controls respectively. This implies that there is no statistical significance for the active experiments, at least with $\alpha = 0.05$.

After the method was improved (by using the slides obtained from KIT and by reducing the input voltage to remove streaming, cavitating, and plate modes, the active experiments were repeated two times (with blood from just one patient), but both experiments suggested a much higher capture rate of 92 and 94 %. No further validation or controls were done.

A slide containing captured basophils was put under a microscope and they were stained with both 4',6-diamidino-2-phenylindole (DAPI) and Alexa Fluor 647 CD63 stain and activated with an anti-IgE receptor to check for basophil activation on the slide after capture. Figure 5.6 shows the basophils with the DAPI stain, with the CD63 stain, and with both stains overlaid. This shows that what is under the microscope are indeed basophils and that they are successfully activated, meaning, in device activation after capture is possible. Furthermore, the activation was only present after the anti-IgE receptor was introduced which implies that the process of capturing the basophils itself does not activate them.

A further set of three 30 min assays were performed to test how the capture changes between each 2 minute interval. Figure 5.7 shows the total cumulative capture of basophils as a percentage of the total possible number in a solid black line, as well as the percentage capture of each individual 2 min section in a dashed gray line. Both of them represent an averaged experiment. Overall

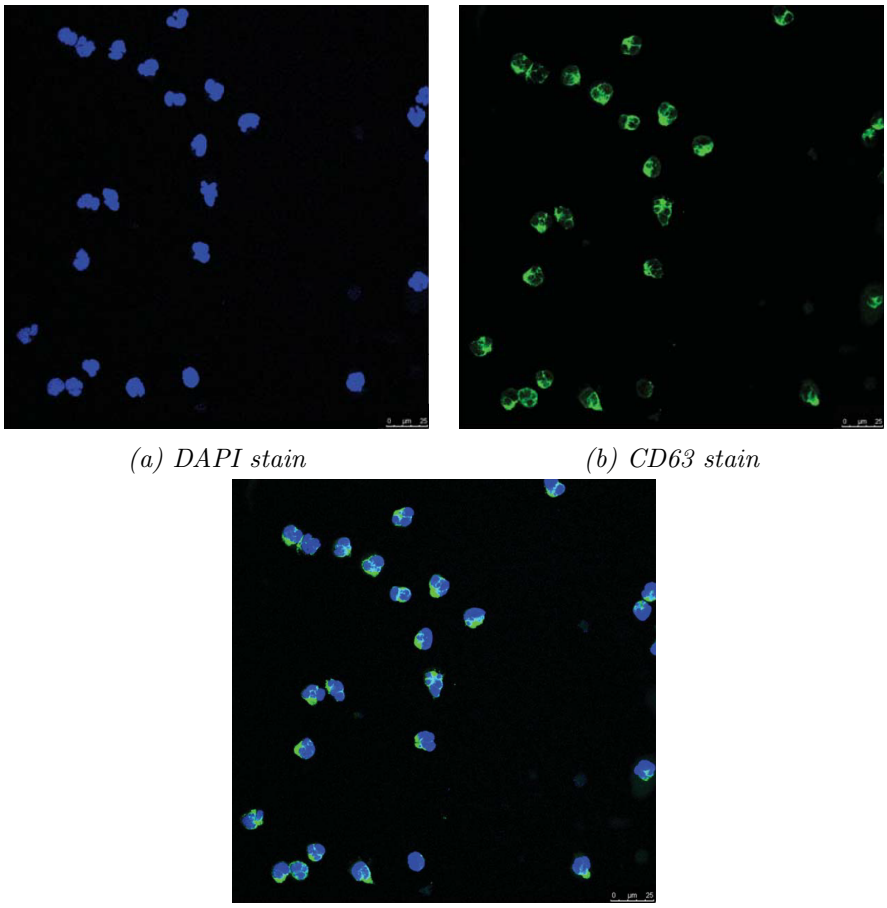

(a) DAPI stain *(b) CD63 stain*

(c) Both stains

Figure 5.6: Images of basophils under different stains with a 63x immersion objective after anti-IgE activation.

the capture seems to be fairly consistent throughout the long assay, with small variations at certain times, with the last point representing the flush, hence the drop into the negative numbers. It is also fairly consistant with the capture rates in figure 5.4. This result suggests that at 30 ml/hr, even after 30 min, there is space for more basophils to get captured.

5.3.3 Lysed blood tests

The same experiments that were done in the previous section were repeated with lysed blood. Figure 5.8 shows the mean average capture rate of the lysed blood experiments including the active ones, as well as the two controls. Because the process of lysing blood does not concentrate the basophils, only removes the red blood cells and platelets, their concentration is far lower. This means that using FACS becomes less reliable as the number of basophils counts up to 20 or so, meaning a difference of even one basophils constitutes a big percentage difference.

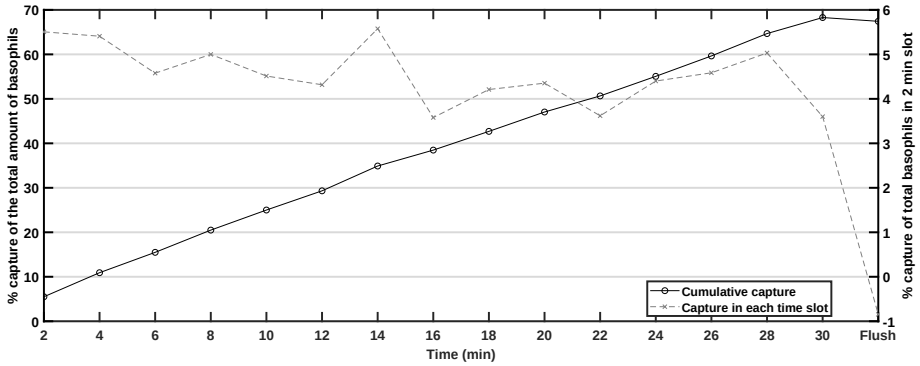

Figure 5.7: Total cumulative capture rate (——), and section capture rate (- - - -) from the 30 min assay using purified basophils.

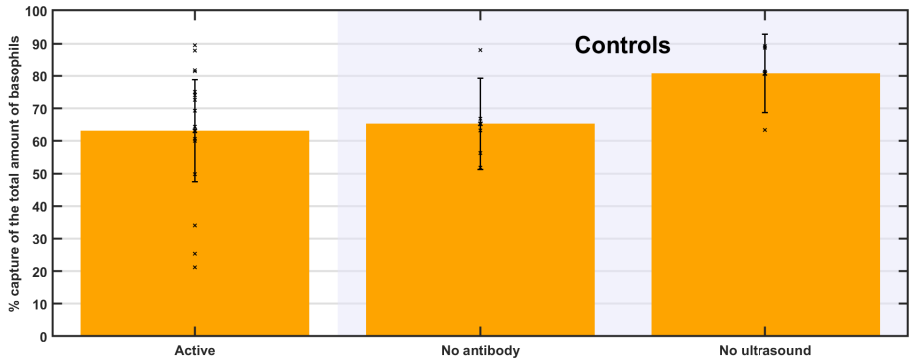

Figure 5.8: The mean average capture percentage with standard deviation of the 10 min assays containing lysed blood, alongside the two controls (no ultrasound, and no antibody). The dots represent the capture percentages of individual experiments. The data was derived from the FACS analysis.

In the figure the active means is the lowest with 63 %, while the controls are at 65 and 80 %. The high capture numbers most likely come from the problems facing the FACS analysis as it would stand to reason that without the aid of ultrasound an equal percentage of basophils would get captured on the antibody slide, which is not the case when comparing purified basophil and lysed blood experiments. Furthermore, the active experiment would be expected to perform better despite the non-ideal processing conditions suggesting that the method used in the experiments was not suited for capturing basophils in lysed blood.

After similar changes to the procedure were made as in with purified basophils (reducing the input voltage, using better coated slides, ensuring no bubbles dislodge basophils from antibodies) two active tests were performed alongside one of each control, no antibodies, and no ultrasound (only for one patient), that yielded the capture rates of 67, 60, 12, and 20 % respectively. This shows a much greater difference between active and control and, despite

the lack of accuracy present in FACS analysis, has encouraged a repeat of the original experiments with 5 patients, but with the modified procedure. Because FACS lacked the accuracy at the low basophil levels present with lysed blood [4], direct imaging would be used for further experiments to remove any uncertainty from the data.

After the experiments were performed some preliminary images were taken of four slides, one for each condition (two controls, one active with the Schott slide, and one active with the KIT slide). The slides were stained with CD63, a non specific stain, to check if anything was captured. The data was interpreted under the assumption that the stained cells are basophils as the antibody coating was specific only to them, and the flush would remove any other type of cell. The cell count for each slide is given in table 5.1. It can clearly be seen that the two active slides, regardless of slide type, have captured at least two orders of magnitude more than the controls. Figure 5.9 show sample images from each of the four slides.

Table 5.1: Basophil count from the imaged areas for four slides representing four different conditions using lysed blood

Condition	Basophil count
Control, no antibody	450
Control, no ultrasound	60
Active, Schott slide	11000
Active, KIT slide	23000

The imaging was stoped after the four slides as a specific dye was to be applied at a different laboratory to ensure only basophils are visible to remove the assumption from any further image count. Unfortunately, due to circumstances outside of our control, the staining could not be performed for three months after which the fixed basophils deteriorated and were not detectable under microscope even with the dye. Therefore it was impossible to show whether the cells seen on the images from figure 5.9 are indeed basophils or not, and it was not possible to confirm, beyond statistical doubt, that this method is a valid way of capturing basophils quickly and efficiently.

A long 30 min assay was performed with lysed blood, and the results are shown in figure 5.10 as an averaged experiment, where the solid black line represents the total cumulative capture as a percentage of the total possible number of basophils, and the dashed line is the percentage capture of each individual section. As with the purified basophil experiment, the capture rate of individual sections is fairly consistant with slight variations, although the mean capture is lower than in purified basophil experiments.

[4]With purified basophils the numbers are in the hundreds which provides enough cells to have certainty in the results.

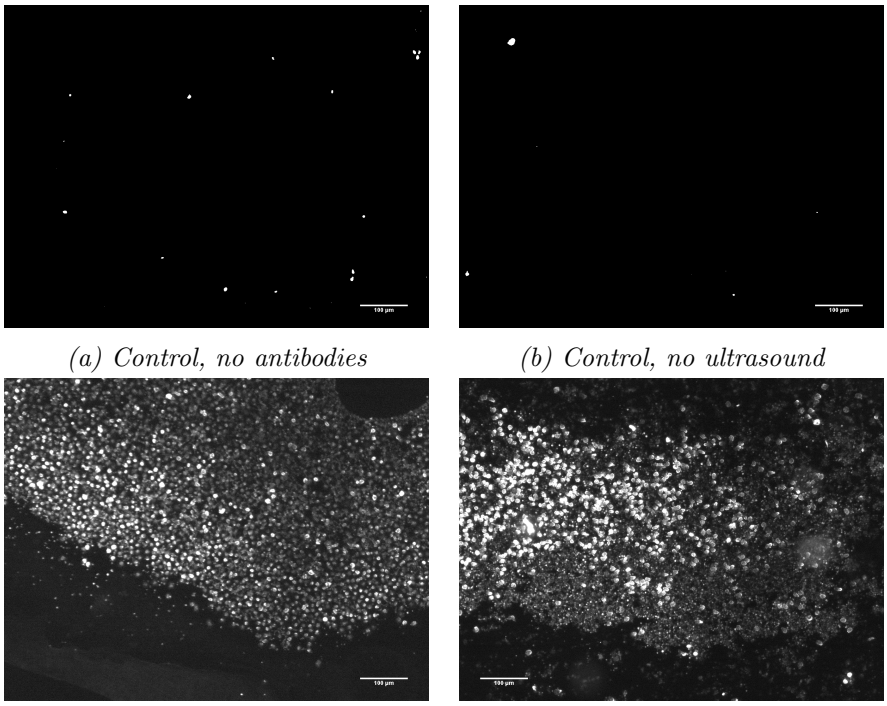

(a) Control, no antibodies *(b) Control, no ultrasound*

(c) Active, Schott slide *(d) Active, KIT slide*

Figure 5.9: Images of cells, possibly basophils, taken from various slides during the repeat lysed blood experiments.

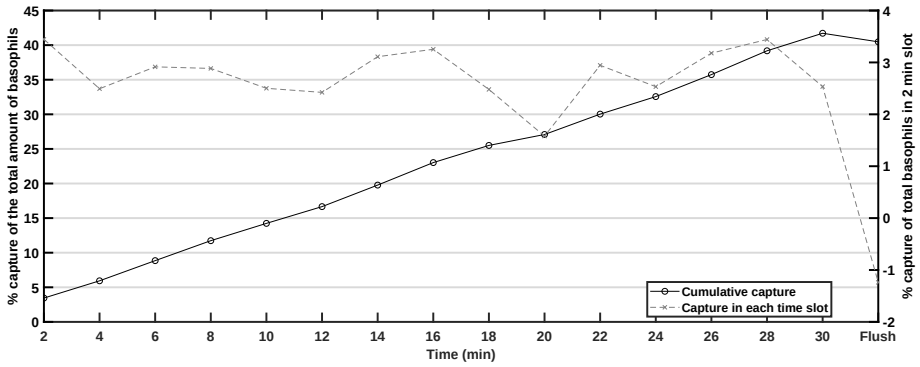

Figure 5.10: Total cumulative capture rate (——), and section capture rate (- - - -) from the 30 min assay using lysed blood.

5.4 Future work

Due to the deterioration of the basophils in the already performed experiments, the first point of order would be to repeat those experiments and image the slides with the appropriate basophil-specific stain to ensure only basophils are being counted.

The next step thereafter would be to perform a full allergy test with the device to prove the principle of the intended application. After the basophils

have been captured and the device was washed with PBS a solution containing an allergen would be flowed through the device and the basophils would be observed for any activation under the microscope.

Further integration of the procedure into the microfluidic platform is possible and would follow the allergy tests. Red blood cells can be lysed by using purified water and their debris can then easily be separated from the rest of the cells, and platelet separation methods already exist in literature and industry [244]. Pumps can be integrated into a final device and thus removing the need for any external devices outside a microscope, and by using a series of valves, both PBS and allergen solutions can be flowed into the device automatically.

5.5 Conclusion

An acoustofluidic device was constructed in order to capture the white blood cells responsible for allergic reactions, basophils, as a part of a larger method designed to replace the already existing diagnostic tools for detecting allergies. It is intended to be cheaper, faster, and easier to use than what is currently available, while maintaining the same accuracy in detecting specific allergies.

The first experiments were done with purified basophils - a solution consisting of over 95 % basophils, after all other cells were selectively removed. They consisted of 3 active tests with both USW field and specific binding, and two controls, one without ultrasound, and one without specific binding. These 5 tests were repeated for 5 patients. The results showed a ±45 % capture rate compared to the controls 20 %.

From this result, the same experiments were repeated with lysed blood - a product of removing red blood cells and platelets, containing only white blood cells and plasma. The results showed no improvement of the active assays over controls as well as high capture rates for all tests, which was most likely a product of the low number of basophils present which made FACS testing inaccurate.

After the method was refined another set of experiments was done with lysed blood, and this time direct analysis was used. The initial images made with a non-specific CD63 stain showed thousands of cells (presumed basophils) in the imaged area of the active slides, while the controls contained dozens or only hundreds of cells. Unfortunately before further imaging with specific staining could be performed the slides degraded and could not be analysed.

The latest set of experiments should be performed again in the future to see if the revised method is capable of capturing basophils at a higher rate than the controls, and at numbers which would be adequate for allergy tests. If successful, the method could then be further developed into a stand-alone device capable of performing allergy testing with minimum input in a short amount of time.

Chapter 6

Biofilm eradication using insonified microbubbles as aid to antibiotic treatment

6.1 Introduction

Anti-microbial resistance (AMR) is an ever-increasing threat, and is often associated with excessive antibiotic (AB) usage. For instance, *Escherichia coli* is reported to have 18 % resistance rate to the most common antibiotics, and multidrug resistant bacteria are becoming more frequent in post-operative infections [245]. Diabetic foot ulcers (DFUs) are a type of chronic wound with high risk of bacterial infections that are poorly susceptible to antimicrobial agents, and cause 50 % of all lower-leg amputations in the UK [246]. Thus, there is a growing need for the development of more effective therapeutic approaches.

A quick, cost-effective, and reliable method was needed to meet the demands presented by biofilms. The biofilm stimulation device presented in this chapter was made to be easy to assemble, operate and sterilise, and to be robust. By using well-placed absorbing material it was possible to make a working device in a tank of only 3ℓ in volume. Its purpose was to test if using microbubbles (MBs) insonified with an ultrasound (US) field, in conjunction with low quantities of ABs, has any added benefits in biofilm bacterial number reduction, compared to using ABs alone. Any reduction in the antibiotic minimum inhibitory concentration (MIC) means a lesser chance of the biofilm developing AMR and reduced side-effects from the antibiotic.

The specific bacteria investigated is *Pseudomonas Aeruginosa*. This biofilm forming bacteria is a major cause of bronchopneumonia in patients with cystic fibrosis, a disease which currently requires lifelong treatment [247]. It is highly susceptible to developing AMR, as it has protective layers and defences which reduce the effectiveness of antibiotics [248]. Some specific strains of *Pseudomonas* require only 40 $\mu g/ml$ of antibiotic (i.e., gentamicin) to prevent

regrowth, while a wild-type could require up to 500 $\mu g/ml$ and has a higher risk of developing AMR [76].

The work in this chapter was done in a collaboration with Public Health England and their team: Charlotte Hind and Mark Sutton. I was responsible for the designing, simulating and manufacturing of the device, production of the microbubbles, as well as performing the experiments themselves, and analysing the data gathered from them. Charlotte Hind prepared the biofilms and antibiotic solutions before the experiments, as well as processed the biofilms once the experiments were done. Gareth LuTheryn from the University of Southampton provided assistance with some control experiments. Mark Sutton and Dario Carugo formed the main supervisory team, with Peter Glynne-Jones and Martyn Hill acting in a supporting role.

In this chapter, the first section discusses the rationale and design of the device used in the experiments, in which the operating principles are explained. This is followed by a section (6.3) on the computer model of said device and how it was used to chose the right materials for the biofilm substrate. Afterwards, section 6.4 explains all of the methods, starting with MB production and biofilm growth. The experimental procedure is covered alongside all of the different parameters tested and the data analysis that followed after. The results section (6.5 looks at and discusses the data from the calibration tests, the method controls, and the experiments themselves. Finally, the conclusion provides a summary of the main research contributions discussed in the chapter.

6.2 Design rationale and device construction

In this study, it was required to expose a biofilm to gas microbubbles and antibiotic, upon stimulation by ultrasound. This was done in such a way that allows the experiments to be performed with only a small quantity of microbubbles ($\leq$ 1 ml per experiment) and antibiotic ($\leq$ 8 μg per experiment). In order to remove reflections from the sidewalls of the device and thus maintain a field structure that resembled a far-field travelling wave (a wave without any interference patterns), absorbing material was placed at the lateral and bottom inner surfaces of the device. The effectiveness of this design choice is modelled below. At 1 MHz the absorbers that were used have a transmission loss of over 400 dB per m. Simulations, explained in detail in section 6.3, have shown that the setup used removes any reflection that might interfere with the incident sound wave reaching the biofilm.

Figure 6.1a shows the cross-section of the device, while figure 6.1b shows the exploded 3D model. The final design features polyurethane acoustic absorbers (Aptflex F48, 10 mm thick, Precision Acoustics, Dorchester, UK) lining the sides. The biofilm is grown on a cylindrical disc 12.7 mm in diameter and 3 mm thick, called a coupon (see section 6.4.2). This coupon is placed inside a small container 35 mm in diameter and 10 mm high (polymer coverslip

bottom dish 35 mm, Ibidi, Martinsried, Germany) partially filled with a layer of polydimethylsiloxane (PDMS) 8 mm high, with a hole the size of the coupon at the top. This container is sealed with a PDMS lid, which effective thickness above the biofilm is 8 mm. PDMS has acoustic impedance similar to water so the ultrasound passes through it without significant distortion or reflection [249]. This small container is suspended in water 2.5 cm below the transducer (1 MHz, narrowband, 15 mm diameter active area, Camasonics, Wiltshire, UK). The small container and the transducer are both held with two 3D printed polylactic acid (PLA) pieces, all of which are held in place with 3 threaded rods spaced equally around the device circumference. The absorbers are placed beneath the transducer, container, and rods, as well as between the transducer and the container, with a hole in the middle to allow for a direct sound path.

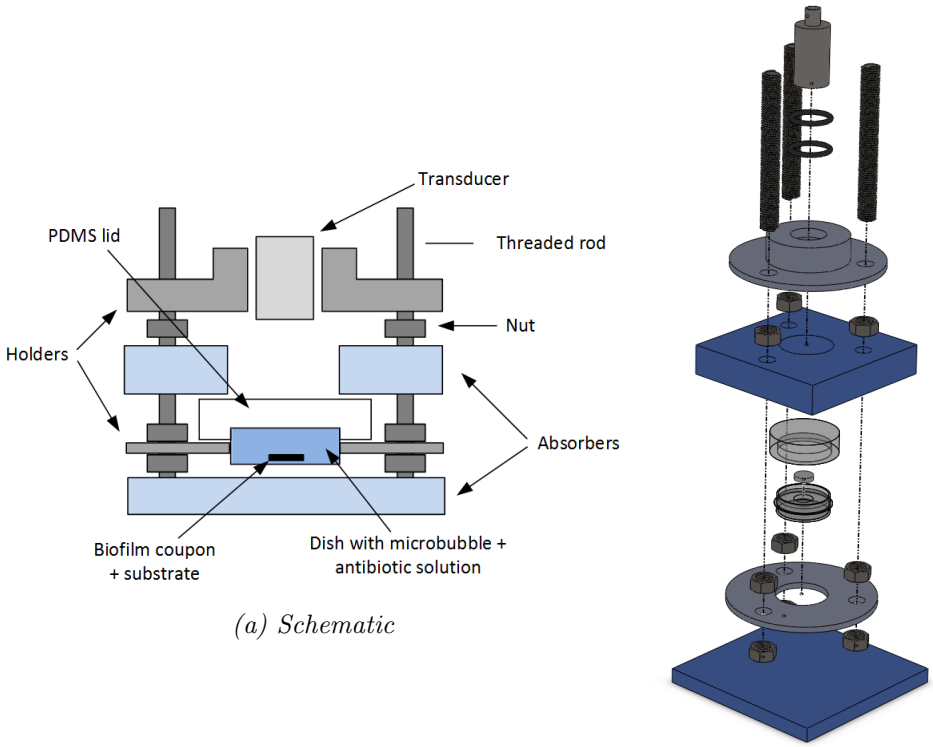

(a) Schematic

(b) Exploded view

Figure 6.1: Drawings of device used for exposing biofilms to a combination of microbubbles, antibiotics, and ultrasound

This device is placed inside a larger container whose dimensions only have to be slightly larger than the device itself. This means only around 3ℓ of degassed and sterilised water is required, compared to the much larger volume that would be required in a traditional water tank. A photograph of the device,

fully assembled, but outside of the larger container can be seen in fig. 6.2.

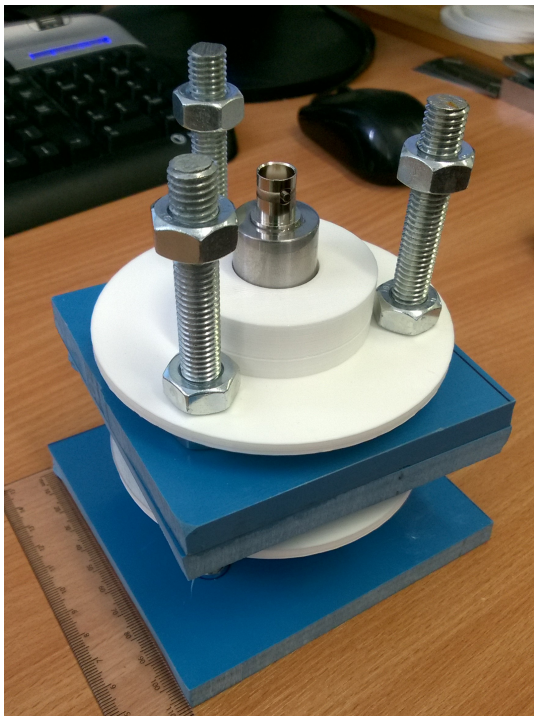

Figure 6.2: Photograph of fully assembled device without larger container

The US frequency was set at 1 MHz, chosen to be close to the resonance frequency of a reasonable proportion of the disperse population of bubbles [250]. Figure 6.3 shows the resonance frequency for lipid-shelled bubbles at various radii.

6.3 Computer modelling

The device, as described in the previous section, needed to be tested in a computer simulation to see if the biofilm is really only reached by the incident wave, without any interference from the reflected waves. Furthermore, since the initial laboratory experiment will not be conducted on real tissue, substitutes needed to be found.

A simplified, two-dimensional version of the device geometry was modelled in COMSOL Multiphysics, a finite element finite element analysis (FEA) package, to test the uniformity of the acoustic field and ensure that absorbers behaved as expected to reduce reflections. Figure 6.4 shows the geometry with appropriate labels (both of component and material). A material list is also given in table 6.1. The modelled geometry is a cross section of the device that does not include any threaded rods and nuts as they would only disperse the sound. Neither does it include the 3D printed holders as one is located above the US source and the other is located below the target. With the absorbers

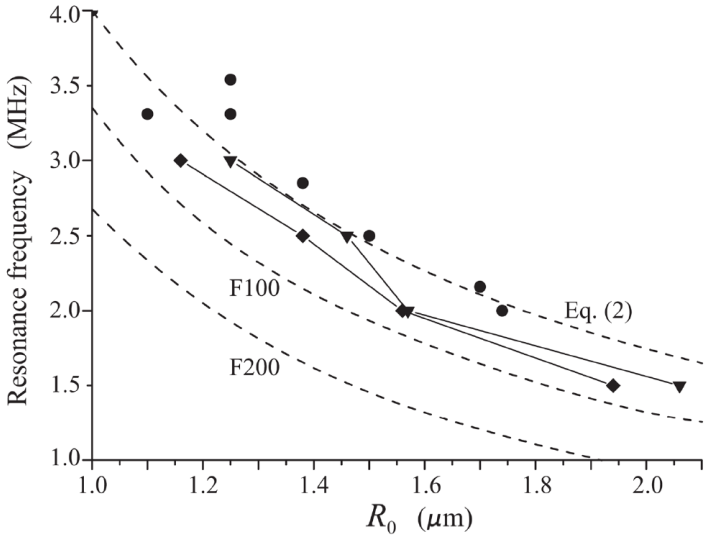

Figure 6.3: Effect of bubble radius on the resonance frequency of lipid-shelled microbubbles. The points on the graph represent the data from individual experiments, while the two dashed lines, labeled F100 and F200, represent the modelled resonance frequency of free bubbles at 100 and 200 kPa acoustic pressure, respectively. The dashed line labelled Eq. (2) represents the modelled resonance frequency of a lipid-shell microbubble. Graph taken from Donikov et al. [251]

appropriately positioned, reflections from these objects should not present a significant contribution to the incident sound.

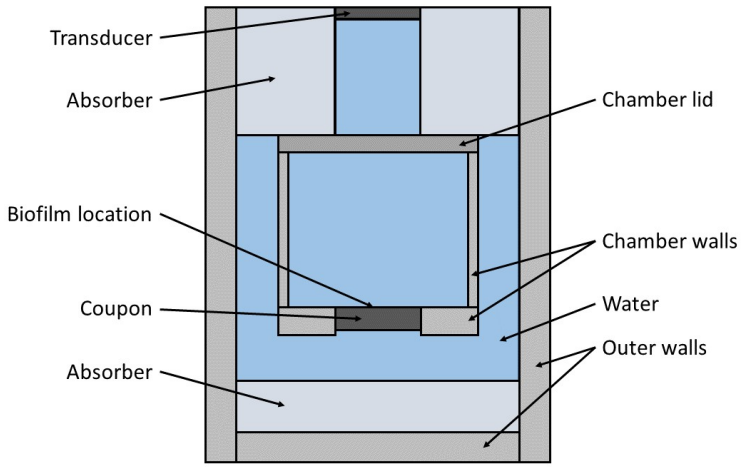

Figure 6.4: Geometry of simulated model

In order to resolve details of the 1 MHz wave propagating through the device, a triangular mesh with a minimum element size of 0.05 mm and a maximum of 0.1 mm was chosen. This gives between 14 and 28 elements per

Table 6.1: Components and materials modelled in the simulation

Component	Material	Density $[kg/m^3]$	Speed of sound $[m/s]$	Impedance [MRa]	Young's Modulus $[GPa]$	Poisson's ratio
Outer wall	PMMA	1190	2750	3.27	3	0.4
Inner wall	PMMA	1190	2750	3.27	3	0.4
Inner chamber bottom	Glass	2210	4540	10.03	72	0.2
Chamber lid	PDMS	970	1119	1.09	7.5E-4	0.49
Absorbers	Perfectly matched layer	-	-	-	-	
Water	Water	1000	1481	1.48	2.2	0.49
Transducer	Lead zirconate titanate (PZT)	7500	2380	17.85	-	-
Coupon	Polypropylene (PP)	900	2740	2.47	1.3	0.42
	Stainless steel (SS)	7850	6100	47.88	200	0.3
	Polystyrene (PS)	25	2340	0.06	3	0.12
	Polyvinyl chloride (PVC)	1760	2395	4.22	2.9	0.4
	Water	1000	1481	1.48	2.2	0.49

wavelength, which is enough to accurately resolve the simulation.

First, a frequency domain study was performed to find out which coupon material would be best to use as flesh/bone proxy. The four materials that the coupons were made of were polypropylene, polystyrene, polyvinyl chloride, and stainless steel. All were chosen due to their commercial availability. Water was used as a reference and to check if the model was behaving correctly. Figure 6.5 shows the normalised steady state acoustic pressure frequency response at 1 MHz of the device with these 5 materials for the coupon.

From the figure it can be seen that polypropylene lets most of the sound through and creates more travelling wave-like conditions, while with polystyrene and stainless steel most of the sound is reflected back creating a standing wave pattern. Polyvinyl chloride lies somewhere in the middle, with the sound being only partially reflected. This still creates a standing wave field in the space between the coupon and the transducer. When the coupon is replaced with water the sound is completely transmitted through the chamber, without any interference. In all five cases, there are no reflections coming from the bottom or the lateral surfaces suggesting that the absorbers, if placed in that position and work effectively, should prevent reflections.

To simulate flesh and soft tissue, polypropylene was chosen as soft tissue absorbs most of the sound. Soft tissue has a mean value for acoustic impedance of 1.63 MRayl, with the sound velocity of 1540 m/s, and density of 1.06 g/cm^3 [252]. Polypropylene has an acoustic impedance of 2.36 MRayl, with the sound velocity of 2660 m/s, and density of 0.89 g/cm^3 [222]. While not an exact match, it has the closest impedance out of the available materials. For modelling bone, stainless steel was chosen, despite the much higher acoustic impedance (45.7 MRayl compared to 7.71 MRayl mean, for bone [253]). The sound velocity of bone is between 3700 and 4400 m/s [254], while that of steel is 5790 m/s [221]. The velocities between the two materials are relatively

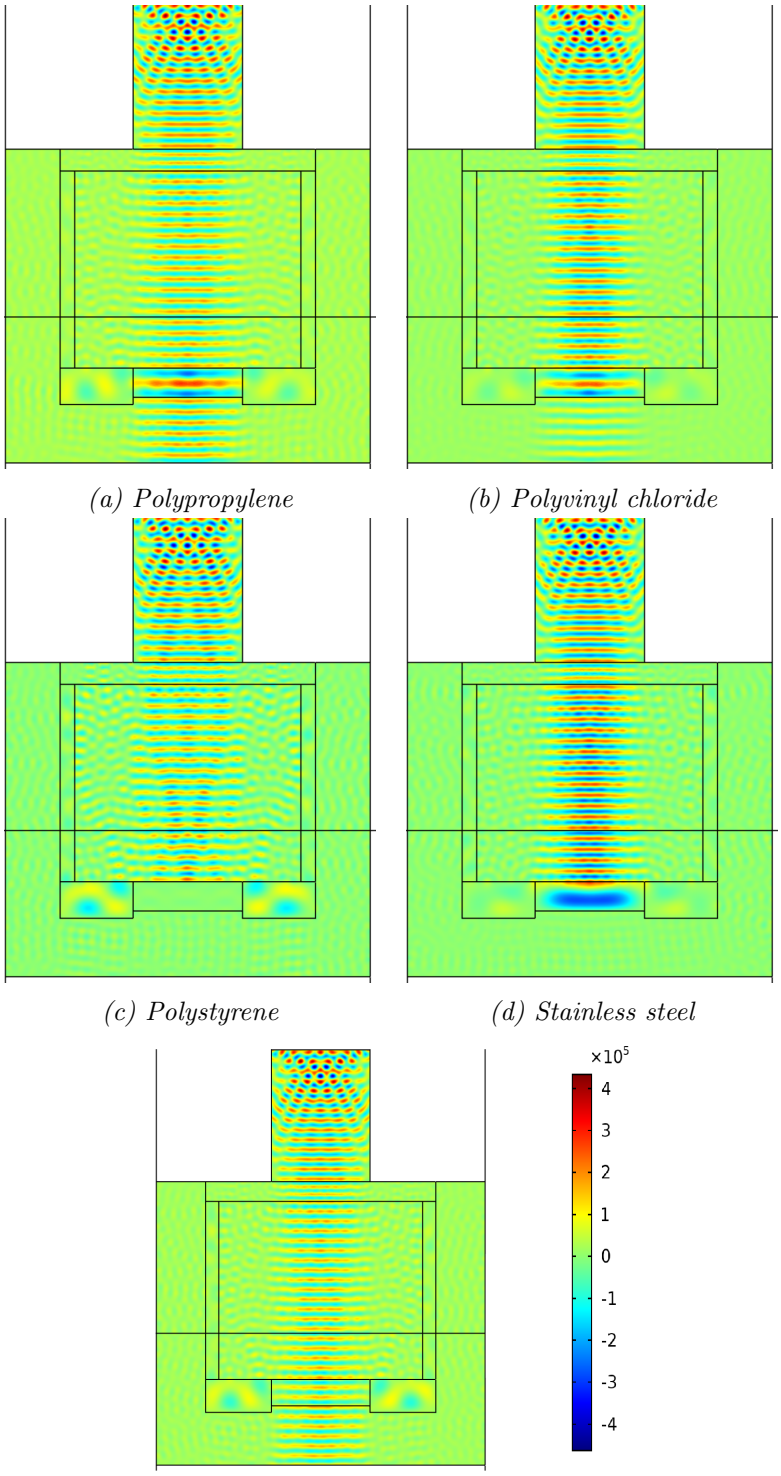

(a) Polypropylene *(b) Polyvinyl chloride*

(c) Polystyrene *(d) Stainless steel*

(e) Water

Figure 6.5: Normalised steady-state frequency results at 1 MHz for different coupon materials. The colourbar represents pressure in Pascals.

similar, and despite the difference in the impedance, it was decided that stainless steel was the best choice to represent bone. Furthermore, SS lies closer to the other extreme of the range, acting as an almost complete rigid boundary. This gives valuable insight as to how the method would work in this, more extreme, circumstance as well as help elucidate the effect of reflection (from a completely reflective material) on MB performance.

A final comparison was made between the two materials by looking at the normalised acoustic pressure on the surface of the coupon, as seen in figure 6.6. The pressure at the SS coupon surface is 30 times greater than that of the PP coupon. This is in line with the statement that the PP coupon creates conditions for a travelling wave, while the SS coupon creates a standing wave field with its high impedance. Furthermore, the PP coupon has areas of both positive and negative pressure, which shows this is not a hard boundary, while the SS coupon is, as the pressure in its surface is entirely positive.

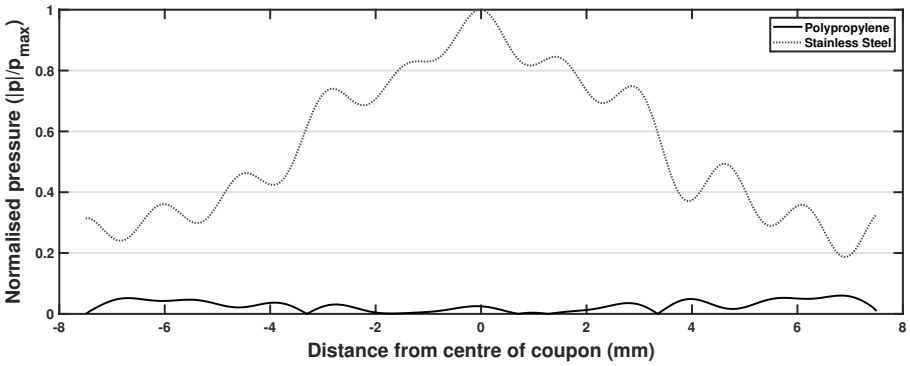

Figure 6.6: Simulated normalised acoustic pressure at the coupon surface for both polypropylene and stainless steel coupons. The values were normalised with respects to the highest acoustic pressure value from both cases (the maximum acoustic pressure with the stainless steel coupon)

6.4 Methods

Alongside the device design and manufacturing, the study involved the production of microbubbles and the establishment of the biofilm model.

6.4.1 Microbubble production

The gas microbubbles used in the experiments have a lipid shell surrounding the gas core. The shell can have a net charge associated with it, depending on the lipids used. In a neutral shell DSPC (1,2-distearoyl-*sn*-glycero-3-phosphocholine, obtained from Avanti Lipids, 18:0 PC (DSPC) — 850365) and PEG40s (polyoxyethylene (40) stearate, obtained from Sigma Aldrich, P3440), solubilised in chloroform at 25 and 10 mg/ml, respectively, are used. They are

mixed in a 9:1 molar ratio [255–257]. This ratio was later changed to 9:5 to accommodate for the possible antimicrobial properties of PEG40s [258].

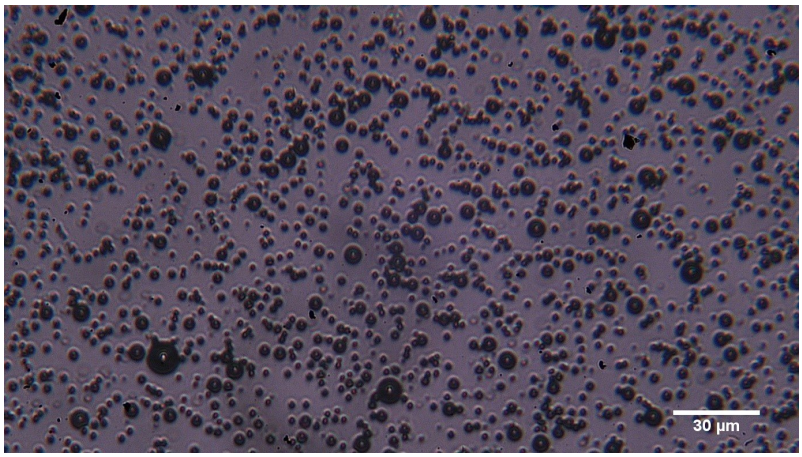

(a) Microscope Image of the lipid microbubbles

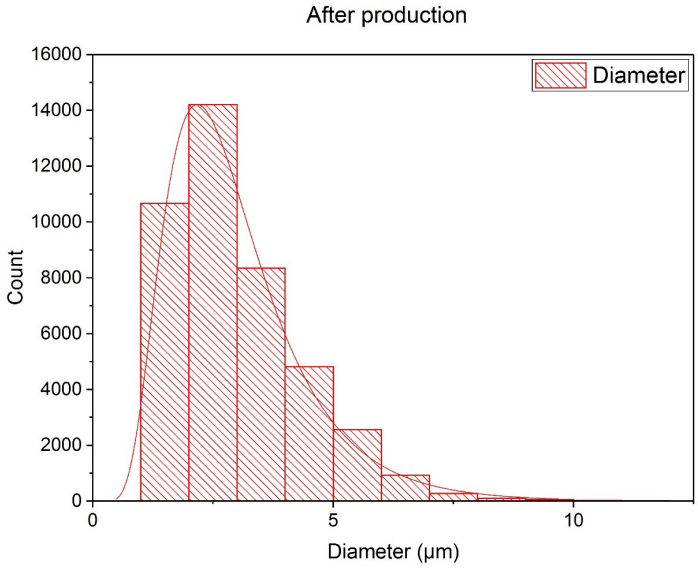

(b) Size distribution of the microbubbles at the time of production

Figure 6.7: Image and size distribution of microbubbles created using DSPC and PEG40s

Bubbles were made in 5 ml batches with a total lipid concentration of 4 mg/ml. First, the lipid solution was manually mixed, and then the vial was sealed with perforated parafilm. The solution was left overnight so the chloroform can evaporate. They were then resuspended in 5 ml of phosphate-buffered saline (PBS), and the mixture heated to 95 °C and stirred continuously for 30 min. They were then removed from the hot plate and a tip sonicator (Fisherbrand Model 120 Sonic Dismembrator with 3.1 mm diameter microtip) was immersed into the solution. It was run, at 20 kHz and 36 W, for 2 min 30

sec, in order to disperse the lipids. The tip was then placed at the air-liquid boundary and run at 84 W for 30 sec to form lipid-shelled bubbles. The vial containing the bubble suspension was placed on ice for 5 min to cool down, and were put on ice until they were used [259].

Because microbubbles have limited stability, they were always prepared on the day of the experiments, between 3 and 5 hours before experiments, but were kept on ice to slow down the gas diffusion process. Microbubbles were sized by placing them on a haemocytometer (Hausser scientific Neubauer Improved HL) and taking a minimum of a hundred images at different locations. The images were then processed with ImageJ [1] to get the count and size of each bubble. This process was then repeated at different time points (0, 1, 2, 5, 24 hours). The mean concentration of the microbubbles at the time of production was $1.19 \cdot 10^8$ bubbles/ml, while at the time when the experiments took place it was $5.97 \cdot 10^7$ bubbles/ml. The mean diameter at time of production was 2.9 μm with a SD of 2.4 μm, while 2 hours later, at the time the experiments took place the mean dimaeter was 3.97 μm with a SD of 4.1 μm. Figure 6.7a shows a representative image of the microbubbles created, while 6.7b shows the size distribution at the time of production.

6.4.2 Biofilm growth

Biofilms were grown inside a CDC biofilm reactor (Biosurface Technologies Corporation, Montana, US). It is a glass jar with an effluent valve placed 1/3 of the height from the bottom. On top sits a cover which holds 8 rods that are placed inside the reactor. These rods each contain holes for holding up to 3 coupons each. On these coupons the biofilm is grown. The bioreactor and its components can be seen in figure 6.8.

The strain of *Pseudomonas Aeruginosa* used for biofilm growth was NCTC 13359. Cultures of the strain were grown overnight in 3 ml of tryptic soy broth (TSB) media at room temperature. The bioreactor was sterilised and autoclaved, and the coupons were inserted into rods which were placed inside the reactor. The effluent valve of the bioreactor was then sealed. The next day the overnight culture was diluted so that it had an optic density (OD) of 1 and a volume of 2 ml. Approximately 400 ml of TSB medium was then added to the biofilm reactor - sufficient to leave the top coupon with a liquid-air interface. The 2 ml of OD 1 bacterial culture was then added.

The bioreactor was set on a combined hot-plate magnetic stirrer device, at a temperature of 37°C, and a rotational speed of approximately 200 rpm. The top of the biofilm was sealed with tinfoil. The biofilm was left to incubate on the hot-plate stirrer for 24 hours before being used in any experiment.

[1] By using the Analyse particles option.

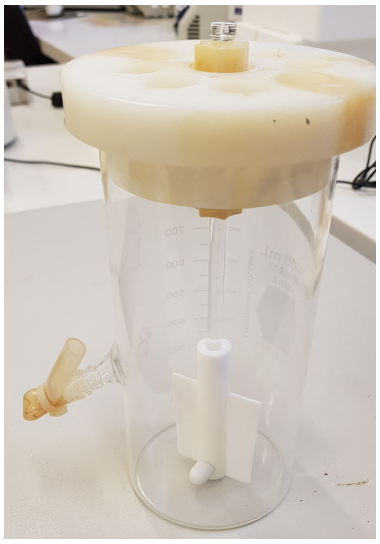

(a) Empty bioreactor

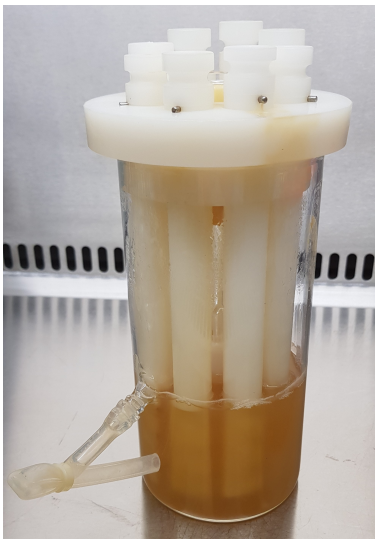

(b) Full bioreactor

(c) Empty rod

(d) Full rod

(e) Coupons - SS and PP

Figure 6.8: Images of the bioreactor and its components

6.4.3 Calibration of the acoustic field

The acoustic pressure field was characterised using a needle hydrophone (200 μm diameter needle, Precision Acoustics, Dorchester, UK), with the ultrasound stimulation setup (full device assembly and biofilm container, but with bottom surface removed to allow hydrophone access to target site) submerged in a tank filled with filtered and degassed water. Automated position-control software (UMS2, Precision Acoustics, Dorchester, UK) translated the hy-

drophone at desired incremental displacements beneath the stationary ultrasound stimulation setup, and transferred its response signals from an oscilloscope (Waverunner 64Xi, Teledyne LeCroy, Geneva, Switzerland) to a computer disk for analysis. Drive voltage (PP007-WR, LeCroy) and current (4100, Pearson Electronics, Palo Alto, CA, USA) probes were monitored to ensure proper system operation, and allow subsequent calculation of electrical impedance.

Calibration data were processed in MATLAB (The MathWorks Inc., Natick, MA, USA) using the following steps: (i) application of a high pass filter to remove any DC offset in the data traces, (ii) calculation of hydrophone A(f,x,y,z) and drive voltage V(f) Fourier transforms, and (iii) calculation of the transmitting voltage response (TVR) at each frequency and scan grid point (x,y,z): TVR(f,x,y,z) = A(f,x,y,z)/(V(f)S(f)) where S(f) is the hydrophone sensitivity. Water temperature was monitored with a glass thermometer, whose values were used to calculate sound speed for use in estimating hydrophone position.

Three types of calibration tests were performed in this study: (1) voltage-dependence of the acoustic peak pressure in the target plane at the transducer resonant frequency, to identify a range of acoustic pressure amplitudes suitable for microbubble stimulation; (2) axial scan of the peak pressure at the transducer resonant frequency and the maximum driving voltage, to evaluate the sensitivity of the system to variations in the distance between the US source and the target plane; and (3) planar scan of the acoustic pressure in the target plane at the optimal US frequency, to spatially characterise the properties of the ultrasound field to which bacteria and microbubbles are exposed.

It was desirable to choose a value for the peak-to-peak pressure at the position of the biofilm that is as high as possible while not causing inertial cavitation. Inertial cavitation, and associated microbubble collapse and fluid jetting, would potentially disrupt the biofilm and remove fragments of it without killing all bacteria [213]. The disrupted fragments would enter the local environment and potentially arrive at new sites viable for biofilm growth, thus negating the possible positive effects of the method [260]. Figure 6.9, taken from Dicker *et al.*, shows the threshold for inertial cavitation (shown as PT50) for an encapsulated bubble with a mean diameter of 1.42 ± 0.70 μm [255]. The lowest cavitation threshold reported in the paper for a 10 % PEG [2] microbubble shell was around 1.05 MPa peak negative pressure (PNP), at 2.75 MHz. The conditions described in the paper differ from the conditions chosen in the performed experiments, but because the cavitation threshold lowers as the frequency lowers [111, 261, 262], it was deemed appropriate to ensure that the peak-to-peak acoustic pressure at the biofilm location would be <1 MPa.

[2]The PEG lipid used in this study is different from the one used in our study. Here three PEG chains of three different molecular weights are considered: PEG 2000, PEG 3000, and PEG 5000.

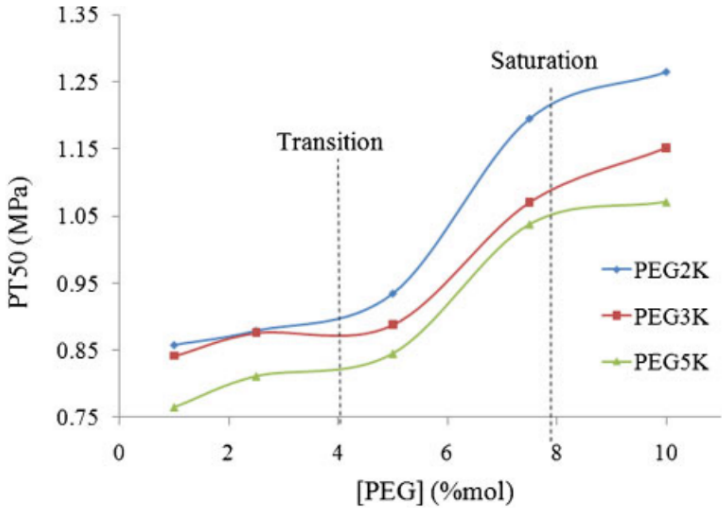

Figure 6.9: Inertial cavitation threshold (denoted as PT50) for a population of encapsulated microbubbles with a mean diameter of 1.42 µm as a function of the PEG composition in the bubble shell. Each line represents a different PEG polymer. The bubble shell also contained the DSPC polymer. Taken from Dicker et al. [255]

6.4.4 Experimental procedure

All experiments had one or more of the three elements present: ultrasound, microbubbles, and antibiotic. The benefit of having all three elements present was being tested. Experiments that didn't have some, or any of the elements were labelled as a control. Within these elements various parameters were tested.

Experiments were performed in a Class II safety cabinet. A biofilm coated coupon was inserted into the container which was then sealed with the PDMS lid (figure 6.1 shows the exact positioning of these components). A solution of microbubbles and antibiotic was injected into the sealed dish which displaced the air inside. The holes on the lid were then sealed. What was in the solution depended on the condition being tested (as discussed in section 6.4.5). The dish was then secured on the 3d printed dish holder. Absorbers and the spacing nuts were then placed on top of the dish. The assembly so far was placed inside the small water tank (base 15 x 15 cm, and height of 20 cm). The assembly was then completed by placing the transducer holder, with the transducer (Camasonics Ltd., 1 MHz, 15 mm diameter element) secured firmly in it. The bottom of the transducer protruded from the holder by 3 mm. Care was taken not to trap any exogenous bubbles inside the sound path.

The signal generator (Rigol, DG1022A) was set to emit a 1 MHz signal at 0.5 V_{pp}, and when pulsing was required, it was set to 100 kHz pulse repetition frequency (PRF), at 25% duty cycle. There is no standard protocol for sonication so the duty cycle was chosen to minimise the rise in temperature that

occurs when running continuously. The signal was fed to a power amplifier (T& C Power Conversion Inc., AG1020) which then output the signal to the transducer at 200 V_{pp}.

Once the treatment was finished on one side of the coupon, the device was disassembled and the coupon was turned around and placed back in the dish. The process was then repeated for the other side. Once the coupon was treated on both sides it was placed into a new rod which was then placed into medium inside a 50 ml Falcon tube to be incubated. If the experiment required antibiotics then they were mixed into the medium as well. The antibiotic concentration was kept in the range 4-8 $\mu g/ml$, which was observed to cause a 1 log reduction in bacterial number compared to the handled control. The tubes and rods (which included the coupons) were sealed with tinfoil and left in an incubator at 37 °C. The incubation period lasted for 24 hours.

Parallel to the experiments, controls were performed. The basic control is the handled control. The coupons were handled as if they were being treated but without any microbubbles or antibiotic. No solution was put in the dish during this procedure. After 3 coupons were in a clean rod, they were placed inside a falcon tube with TSB medium. No antibiotics were mixed with the medium. The second control - antibiotic control, repeats the same procedure, except the medium in the falcon tube now contains antibiotic. The last control performed on every bioreactor is an unhandled control. A rod is taken directly from the bioreactor, submerged into sterile water a few times to remove any planktonic bacteria, and placed into the medium. This serves as a comparison for the handled control to assess whether the procedure itself causes removal of bacteria. The results from this control are not analysed in detail as they only serve to discard experiments where the procedure removes too many bacteria. These control coupons came from the same bioreactor as the main experiment coupons, to ensure as similar biofilm conditions as possible.

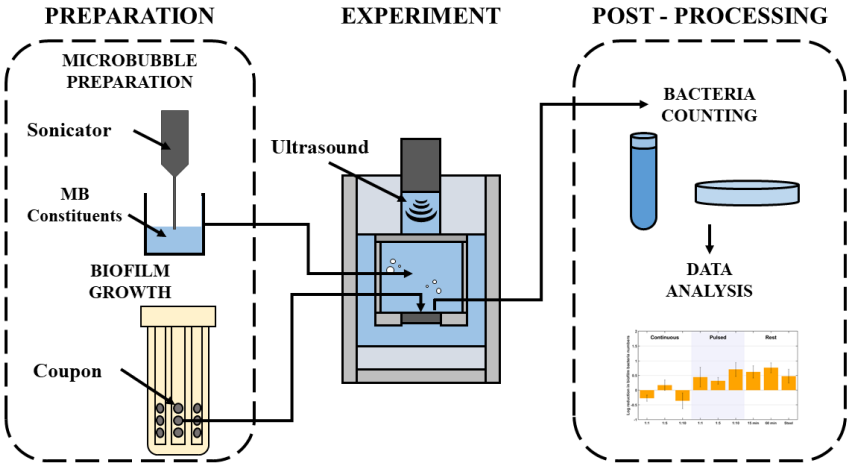

Figure 6.10: Schematic of the biofilm eradication experiments

For any other control (e.g. antibiotic and bubbles, or ultrasound and antibiotic), the procedure is the same as the main experiment, but parts are omitted if a condition is missing - the container is not placed inside the device if there is no ultrasound during the experiment, or no antibiotic or bubbles placed in the solution put into the container if those conditions are not needed.

Figure 6.10 shows a schematic of the experimental process, including the preparation and post-processing.

6.4.5 Different experimental parameters

A variety of conditions were tested to identify an effective biofilm treatment protocol. These include:

- Microbubble concentration,
- Continuous vs. pulsed ultrasound exposure,
- Effect of priming the biofilm with the bubble suspension before and in-between multiple exposures,
- Varying the recovery period between exposures,
- The physical properties of the substrate (acoustically transparent vs. acoustically reflective).

The literature does not agree on what ultrasound protocol is best for the application tested in this project. So far there have been many protocols suggested with no consensus on whether or not there exists one that works best (see section 2.6.1 for further detail). To that end multiple protocols were tested for best performance. The simplest one was continuous ultrasound exposure of bubbles for 5 min. This was labelled as "continous". The exposure was then changed to pulsed, with a 100 kHz PRF, at 25% duty cycle. The duration was kept at 5 minutes. It was labelled "pulsed".

Microbubble concentration can have a considerable effect on ultrasound dispersion, which in turn has an effect on the overall force exerted on the microbubbles [111]. The MB concentration was altered to observe the possible effects it might have on the overall reduction in bacterial numbers. The solution injected into the dish consisted of two components in equal parts: antibiotic in double concentration in sterile water, and the microbubble solution diluted in sterile water, if needed. When mixed, the antibiotic concentration ended up the same as in the incubation tubes. Three bubble concentrations were tested: undiluted bubbles (with the final mix then labelled "1:1"), bubbles diluted in 4 parts sterile water (labelled "1:5"), and bubbles diluted in 9 parts sterile water (labelled "1:10"). Table 6.2 shows the component ratios for each concentration.

A second ultrasound exposure was introduced to the protocol, as well as priming and resting times. The procedure now involved 15 min of priming

Table 6.2: Component ratios in microbubble solutions at different concentrations

MB ratio label	Water	:	MBs	:	Antibiotics
1:1	0	:	10	:	10
1:5	8	:	2	:	10
1:10	9	:	1	:	10

time (resting after the bubbles were injected into the dish), 5 min of pulsed US exposure, 15 min of rest, and 5 min of pulsed US exposure. The priming was introduced so that the bubbles have time to "latch" onto the biofilm for easier penetration when the ultrasound is turned on. Furthermore, prior work has shown that microbubble constituents have an effect on membrane fluidity, therefore the priming would allow an investigation into the potential for sensitising the bacterial cells prior to US stimulation [263]. This protocol was labeled "short rest". The resting times were then changed to allow extra time for the bubble/AB mix to act on the biofilm. The new procedure was then: 5 min for priming, 5 min for pulsed US exposure, 60 min for resting, and 5 min for the second US exposure. It was labelled "long rest".

Finally, the effects of substrate materials were tested, as the polypropylene coupon was replaced with stainless steel. The "long rest" procedure was used as it yielded the best results with PP. The coupons in procedures were labelled accordingly.

6.4.6 Counting the number of bacteria

After incubation the bacteria were counted using the Miles-Misra method [264]. The rods were removed from the TBS filled Falcon tubes and each individually washed by dipping into another Falcon tube half filled with sterile PBS, so any planktonic bacteria were removed. The coupons were then individually placed in a media filled 10 ml Falcon tube. The tubes were sealed and shaken at 2000 rpm for 10 minutes on a shaker.

TSB media (90 μl) was added to the first row of a 96-well plate (one column was reserved for each coupon). Blank media (90 μl) was added to 5 additional rows, making for 5 dilutions. To the first row, and into the appropriate well, 10 μl of the culture from the Falcon tubes containing the coupon was added. The medium-culture mix was diluted down by 10 μl each time using a multichannel pipette. A 10 μl sample of each dilution was taken from the 96-well plate and dropped directly onto an agar plate. For each dilution there were 3 repetitions. The inoculum was allowed to dry before it was incubated overnight at 37 °C. After incubation, the number of colonies visible was counted in the lowest dilution and multiplied up to gain an estimate of the number of colonies present in the biofilm on each coupon. To get the final number of bacteria/ml the average number of colonies for a dilution was

multiplied by 50 and by the dilution factor.

6.4.7 Data analysis

Each experiment contained 3 coupons for every control and condition. Since these values differ between coupons and especially different experiments which come from different bioreactors, a normalisation was performed.

To allow all of the datasets to be compared they needed to be normalised in a way that preserves the statistical properties of each dataset (mean, variance, etc.). To achieve this, the mean and variance was found for each condition (i.e. of the 3 values that were acquired for each condition). These values were normalised with respect to the mean value of the handled control. For the means this meant dividing by the value of the control mean, but for variance it meant dividing by the square of that value [265]. Once normalised, the values could then be averaged over multiple experiments. This produced the overall mean and the overall variance from which the standard deviation was found. The averaging process was done on the values from the same condition or control.

The process was repeated but with normalisation with respect to the mean value of the antibiotic control. This allowed quick inspection to see how well each condition performed both with respect to no treatment and only using antibiotic treatment.

While the second comparison was deemed more important as the experiments are testing if the combination of all three elements is better than just using antibiotics, the sub-inhibitory concentration of the antibiotic means any reduction in bacteria numbers is a relevant step towards finding a more effective treatment.

The values were displayed on the graph as a log reduction. This is a base 10 logarithm representation of the number of bacteria removed from the biofilm with respect to the control. It can be calculated as $LR = log_{10}(B/A)$, where B represents the bacteria numbers before treatment, and A represents bacteria numbers after treatment. A 1-log reduction represents a 10-fold decrease in numbers (i.e. 90%), while a 2-log reduction represents a 100-fold reduction (i.e. 99%).

For a more in-depth statistical analysis of distribution and significance, each value of any tested condition was normalised with respect to the mean value of the handled control. This includes other controls as well as any tested condition. The data could thus all be pooled together and compared as distributions. Each coupon represented one sample. For each condition at least three different bioreactors had to be used to ensure no biofilm outliers exist. This means a minimum of 9 sample points.

The significance between two distributions was assessed using the Mann-Whitney U-test, with a p-value of < 0.01. The usual Student's t-test, or its equivalent for checking the significance between normal solutions, was not used

as the data were not normally distributed. While there is a number of tests for normality of distributions, one of which was the Jarque-Bera test which was applied to these datasets, they are not usable in this scenario as each set has not sufficient data points. A more useful tool was to plot a histogram of the individual sets (like the antibiotic control one, seen in figure 6.11a, as it has 75 data points), or of all of the points pooled together. As they are normalised, for the main experiments they all fall between 0 and 1, representing total removal of biofilm or no removal at all, and since all of the data come from the same basic set-up, with only the conditions varying, they were all plotted on the same histogram (figure 6.11d).

The histograms in figure 6.11 show that the data follow a negative exponential distribution. This kind of distribution can be seen often in nature, and as such not having a normal distribution is not an unexpected result.

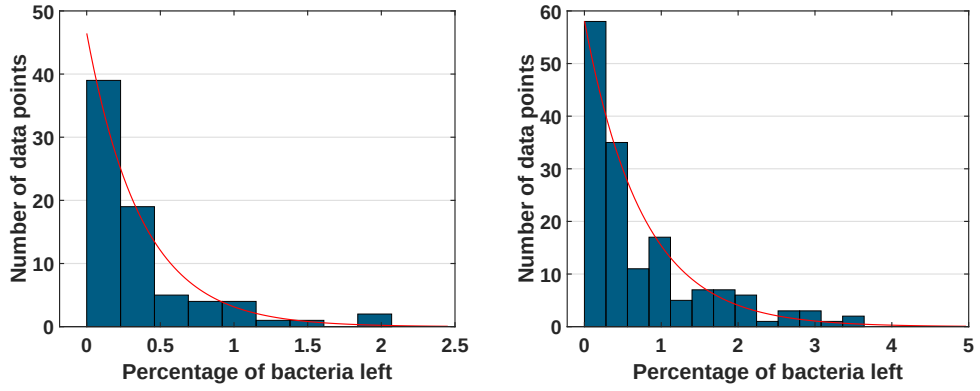

(a) Antibiotic control data

(b) All control data

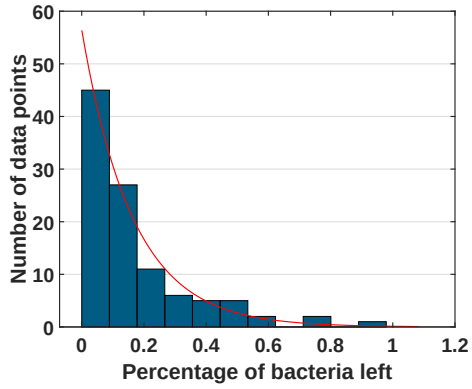

(c) All experiment data

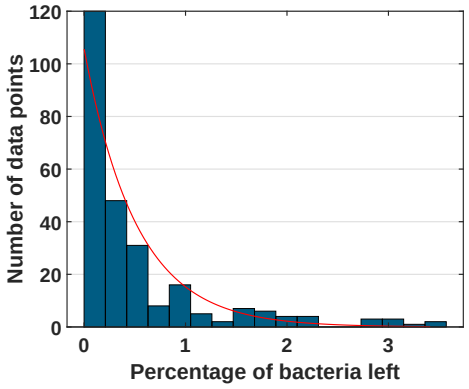

(d) All data

Figure 6.11: Distribution of experiment and control data. They are created by combining all of the data from the specific set (in case of b to d). The x-axis represents the ratio of bacteria left on the biofilm compared to the handled control. A negative exponential distribution curve was fitted to the data as well.

6.5 Results and discussion

6.5.1 Calibration data

The transducer (tested with the method described in section 6.4.3) had a peak output, at 200 V_{pp}, of 0.5 MPa. Figure 6.12 shows the increase in peak-to-peak acoustic pressure, as the input voltage increases. The increase within this range of input voltages is linear.

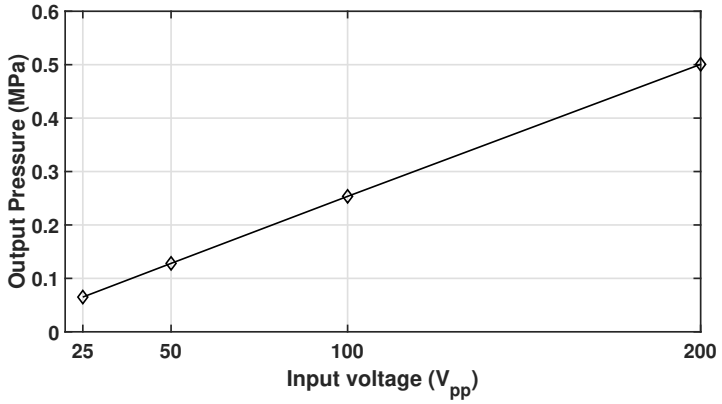

Figure 6.12: Peak-to-peak acoustic pressure response of transducer to an increase in input voltage

Figure 6.13 shows the normalised pressure at the measurement position as it moves away from the transducer along the centre line. The pressure is normalised with respect to the highest measurement in this experiment. As expected, the peak is not found in the measurement closest to the transducer, but some distance away, due to interferences from different points of the transducer plate [111]. After the initial rise, the pressure diminishes with increasing the distance from the transducer.

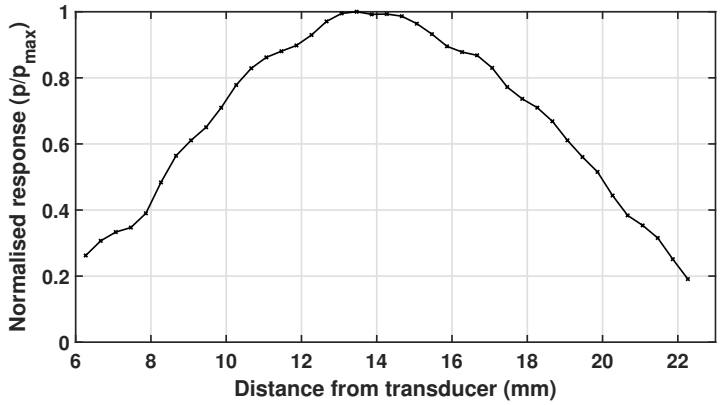

Figure 6.13: Normalised acoustic pressure response of transducer to a steady voltage input with increasing measurement distance

A distance of 8.6 mm from the transducer was chosen and a 2D scan was performed to find the normalised pressure distribution, which can be seen in figure 6.14. The distribution looks as expected - a peak in the middle and a taper off as the distance from that middle increases.

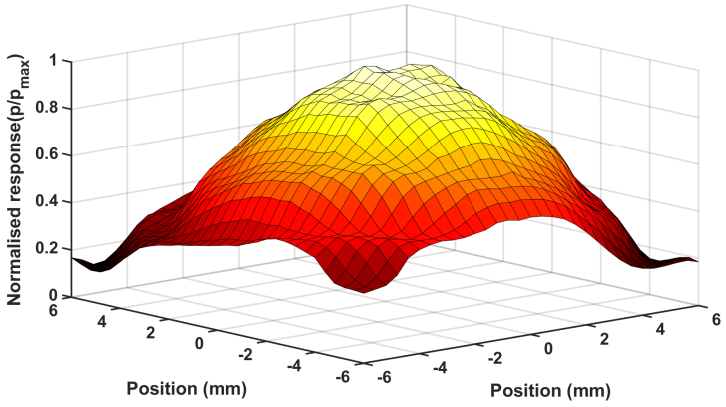

Figure 6.14: Peak-to-peak acoustic pressure response of transducer to an increase in input voltage

These three figures show that this transducer is capable of outputting 0.5 MPa peak-to-peak pressure. All tests, where distance from the transducer was fixed, were performed at a distance of 14.5 mm from the transducer.

6.5.2 Controls

To check the validity of the ultrasonic method, it had to be compared not only to a biofilm that had no treatment (but was handled the same way as if it did), but also to biofilms that were treated with only the constituent components of the method - ultrasound, antibiotics, and microbubbles. Since it was suspected the lipid components of the microbubble shell may have some effect on the biofilm [258] they were tested as well, as an additional control.

The AB only control was set to be the baseline which the combined method would compare to. The goal was that the combined method has at least a 3 log reduction compared to the handled method, and a 2 log reduction compared to the baseline control [3] From a total of 26 controls performed the antibiotics managed to kill 68% (0.5 log reduction) of the bacteria compared to the handled control. While antibiotics could kill the required 99.9% of bacteria for the biofilm to be declared dead, the dose here was kept small to allow for the effects of the combined method to show. The 0.5 log reduction suits this purpose. Since low AB dosages have therapeutic effects, such as less side-effects and smaller chances of the bacteria developing AMR they would be kept in the final version of the combined method.

[3]The 3 log reduction is equivalent of 99.9% eradication which is the standard for ensuring biofilm death. The 2 log reduction comes from the fact that the antibiotic alone provides a 1 log reduction.

Ultrasound alone had a small reduction in bacteria numbers compared to the handled control (23% or 0.1 log), but it did slightly better than the associated AB control (i.e. both controls came from the same biofilm reactor). Since there was only one US test done, this isn't enough to draw any significant conclusions, but the data suggest that using ultrasound alone isn't enough to provide effective treatment and the results showed no statistical significance.

Bubble controls were separated into three concentrations, described in section 6.4.5, as 1:1, 1:5, and 1:10. The same concentrations were used with the bubble constituent controls. Five out of the six controls had a bacteria count higher or approximately equal to that of the handled control, with the sole exception being the 1:5 bubble constituent control, which had a 50% (0.3 log) bacteria number reduction. Compared to the antibiotic controls from the same bioreactor, all six performed worse. This was to be expected as bubbles by themselves cannot penetrate the biofilm and eradicate it. While some studies do show an effect from bubbles on mammalian cells [263] it was suspected, and later confirmed with these results, that it would not be enough to cause a large reduction in bacteria numbers. Furthermore the standard deviations for these controls are quite high suggesting the control did not have a considerable effect on biofilm reduction and the overall spread seems to suggest no noticable effect at all.

Figure 6.15 shows the log reduction of bacteria numbers for single element controls. While the results show averaged data, it is important to note that all of the controls are compared, firstly, to the handled control of the same bioreactor (each consisting of 3 coupons), and then to the antibiotic control from the same bioreactor. To compare between bioreactors the controls were normalised with respect to the handled control and the antibiotic control respectively.

Subfigure a) shows the results normalised to the handled control and shows the overall effectiveness of the method, while subfigure b) shows the results normalised to the antibiotic control, which shows how better the method is than just using antibiotics. If any method is to succeed it needs to be sufficiently better than the antibiotic control. A goal improvement would be a further 2 log reduction

Further controls consisted of pairs of constituents - AB and US, US and MB, and AB and MB (in two bubble concentrations, 1:1 and 1:5).

Both US and MB, and US and AB had only one experiment, consisting of 3 coupons, done each, so not much can be inferred from the results, but the performed experiments had no positive reduction compared to either of the two controls, which is why no further repeats were done.

The AB and MB control was performed with two bubble concentrations - 1:1 and 1:5. For the higher bubble concentration, the bacteria number reduction compared to the handled control was 96% (1.4 log), which is only partial attributed to the antibiotic as the number reduction compared to the AB control is 58% (0.4 log). The weaker bubble concentration (1:5) did not have any

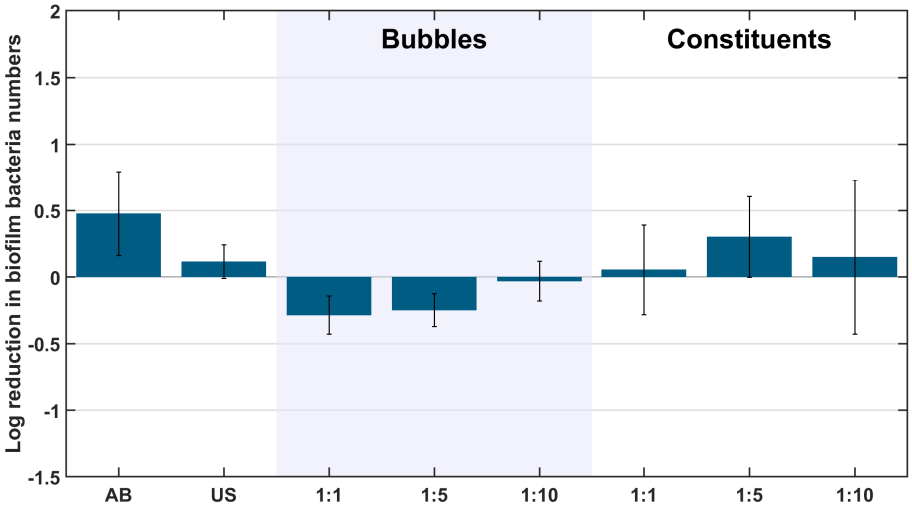

(a) Normalised to handled control

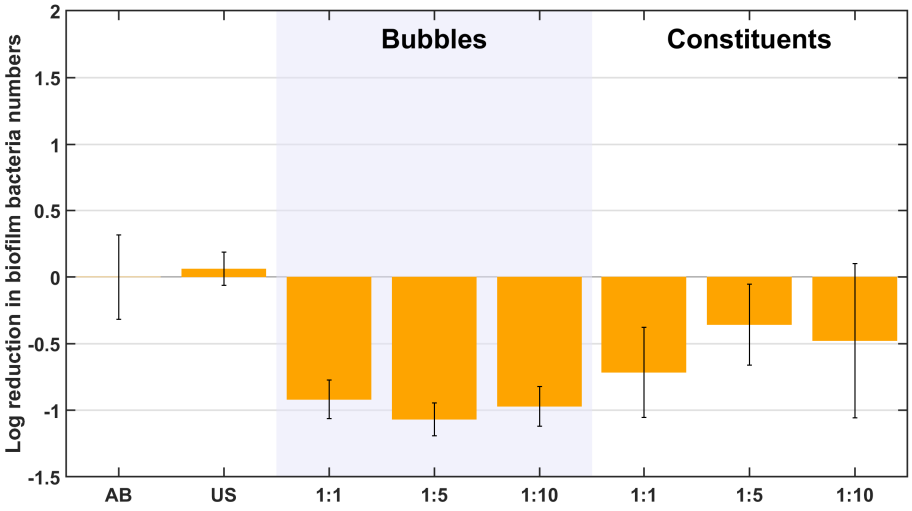

(b) Normalised to antibiotic control

Figure 6.15: Log reduction of bacteria numbers for single element controls

noticeable effect on the bacteria numbers, barely performing better than the handled control (20%, or 0.1 log) and much worse than the AB control (-140%, or -0.4 log).

Figure 6.16 depicts the log reductions for the three two element controls, compared to both handled and antibiotic controls.

6.5.3 Main experiments

High density microbubble clouds may absorb the US field and prevent it from pushing them to the biofilm surface, while at the same time creating a secondary shockwave, if driven at the bubble cloud's resonance [266–268]. This

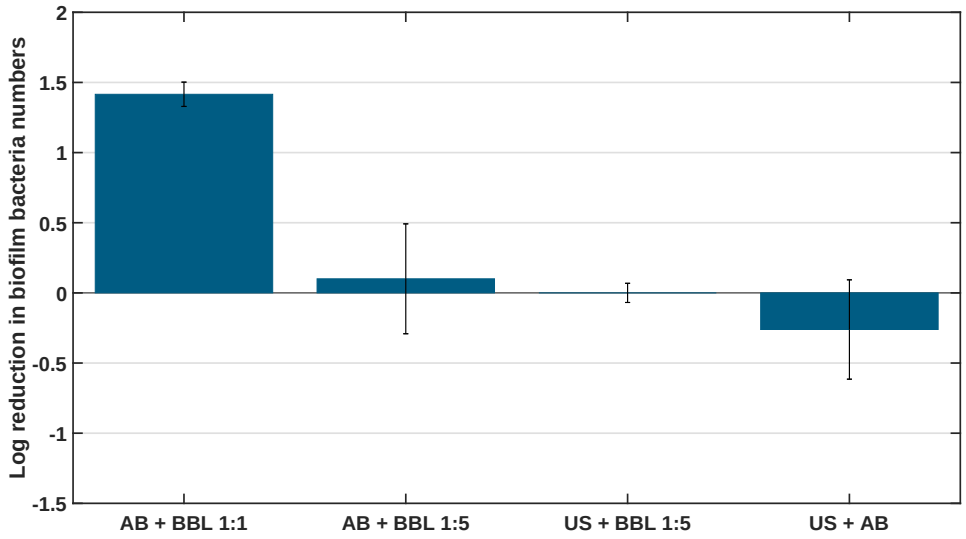

(a) Normalised to handled control

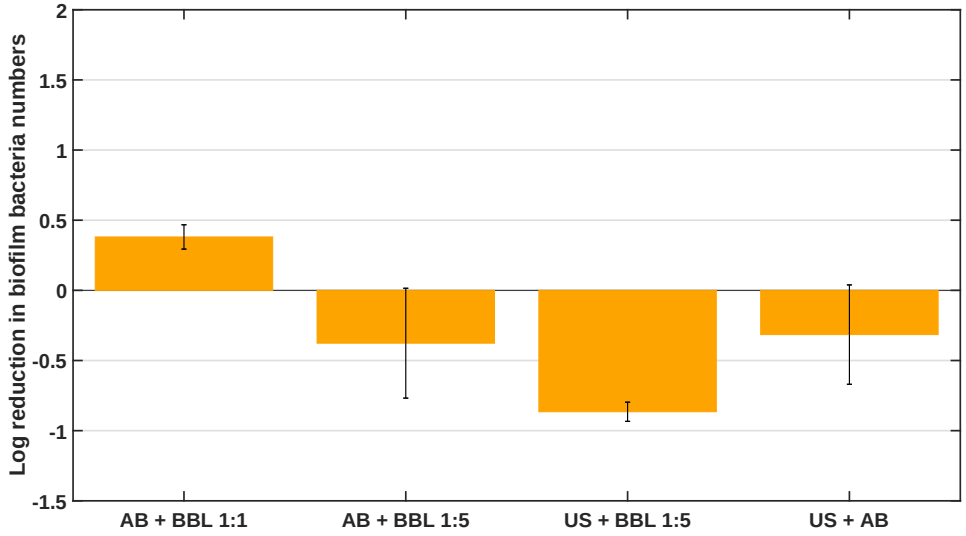

(b) Normalised to antibiotic control

Figure 6.16: Log reduction of bacteria numbers for two element controls.

can create a complicated ultrasound-microbubble interaction, which outcome is not a net movement towards the biofilm. At the same time, low density bubble clouds may not have enough bubbles to make any significant penetration into the biofilm for the antibiotic to act. The first set of experiments explore the effect on bubble concentration on the overall bacteria number reduction. In figure 6.17 the left unshaded area shows the results from the initial experiments. Only one of the three concentrations (1:5), managed to achieve any improvement over the antibiotic controls (as seen in subfigure b)), and even that was not statistically significant. The big difference between the two subfigures for each concentration shows that the antibiotic provided the highest contribution and the method contributed only a little, or not at all.

The second change to the method tried pulsing the US transducer at 25% duty cycle. This would reduce aggregation and coalescing of bubbles due to secondary Bjerknes forces [111]. Pulsing showed overall improvement on all three concentrations as now the method performed better than just the antibiotic. This can be seen in the middle, shaded section of figure 6.17b. When the concentration was reduced to 1:5 the number of remaining bacteria was higher than before, but with a further reduction to 1:10 the bacteria number dropped substantially by 0.7 log (80%) compared to the antibiotic control.

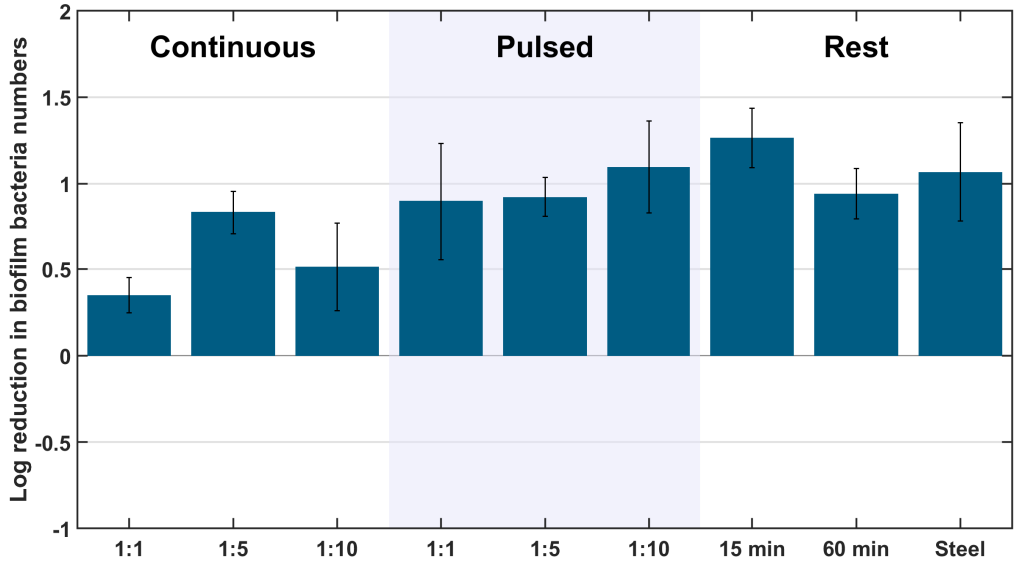

(a) Normalised to handled control

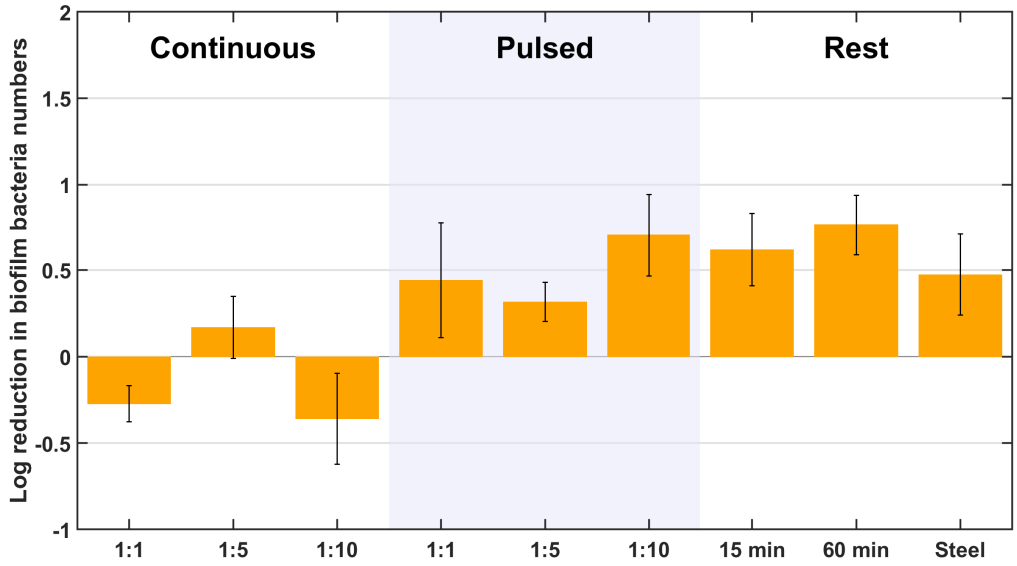

(b) Normalised to antibiotic control

Figure 6.17: Log reduction of bacteria numbers for experimental results.

Adding a 15 minutes priming period, and a 15 minutes rest period between the first and second sonification periods (so that the bubbles, and bubble constituents, have time interact with the biofilm), resulted in an increase in the bacteria number reduction, going from 0.3 log to 0.6 log (52% to 76%) for the same bubble concentration. This is seen in figure 6.17b in the right, unshaded area. When the rest period is increased to 60 minutes (the priming was reduced to 5 so as not to have the experiment last too long) the reduction is further increased to 0.76 log (83% better than using antibiotic alone).

Another big difference between the various rest periods is how large the contribution of the method was on the overall numbers compared to the antibiotic. In figure 6.17a the bacteria number reduction with respect to the handled control is shown, and when comparing it to the values in subfigure (b), it becomes apparent that in the case of a 15 minute rest, the antibiotic had a larger contribution than in the case of a 60 minute rest. This indicates that with the longer rest time, the method is less susceptible to the effectiveness variations of the antibiotic. This is presumably due to the longer time the antibiotic is allowed to penetrate to the inner layers of the biofilm.

In both cases, it is possible that the multiple exposures create new openings in the biofilm, or reopen closed ones, if enough time is given for the biofilm to regrow (e.g. *P. aeruginosa* PAO1 strain has a doubling time between 1 and 1.5 hours in minimal media [4] [269]). By increasing the rest period, antibiotics are allowed a longer time to reach the core of the biofilm. Presumably, for each biofilm, there is an optimum rest duration which allows as much time for the antibiotic to work inside the biofilm, without the openings closing up again. In the same vein, it is possible that even further exposures would reduce the bacteria numbers further, with each additional exposure multiplying the time available to the antibiotics to penetrate. The extended exposure to water and TSB might even activate the bacteria at the biofilm core, making them absorb the antibiotic, thus increasing the effectiveness of the method [215].

When polypropylene is exchanged with stainless steel, bacteria reduction number is lowered to only 0.5 log greater than antibiotic alone. This is still an improvement over using just antibiotic alone. A problem that might be presenting itself is that stainless steel, like bone, is very reflective, so combined with the incident wave, even if it is pulsed, it creates a standing wave. The bubbles are then, due to the sub resonance excitation, likely pushed towards the antinodes of the standing wave [270], instead of being pushed to the surface. This means only a small portion of the bubbles is actually being utilised as they may be trapped at different antinodes. The bottom antinode, however, may lie inside the biofilm, meaning the bubbles trapped in it would still have to penetrate the biofilm. This was enough to make the method around 66% (0.47 log) better than using antibiotic alone. Table 6.3 shows all of the experimental results for the methods mentioned below, including the bacteria

[4] Throughout the duration of the experiment, 80 minutes in total, the number of biofilms may drop by 50 %, which is a considerable decrease, but the absolute numbers are still high.

Table 6.3: Bacteria reduction rates for all performed experiments. The input voltage was 200 V_{pp} which produced a maximum peak-to-peak pressure of 0.5 MPa at the biofilm location. The frequency of the US was 1 MHz and every exposure was 5 minutes long. In experiments with rest periods, there was an exposure before and after. In case of pulsed US the wave was pulsed at 25% duty cycle with a 100 kHz PRF.

	Bacteria reduction ratio	
Experiment	Handled control	Antibiotic control
Continuous, ø, PP, 1:1	55% (0.34 log)	-87% (-0.27 log)
Continuous, ø, PP, 1:5	85% (0.82 log)	32% (0.17 log)
Continuous, ø, PP, 1:10	69% (0.51 log)	-129% (-0.36 log)
Pulsed, ø, PP, 1:1	87% (0.89 log)	64% (0.44 log)
Pulsed, ø, PP, 1:5	88% (0.92 log)	52% (0.32 log)
Pulsed, ø, PP, 1:10	92% (1.09 log)	80% (0.70 log)
Pulsed, 15 min, PP, 1:5	95% (1.26 log)	76% (0.62 log)
Pulsed, 60 min, PP, 1:5	88% (0.94 log)	83% (0.76 log)
Pulsed, 15 min, SS, 1:1	91% (1.07 log)	66% (0.47 log)

reduction ratio, in percentages and log, compared to the handled control and the antibiotic control.

All of the multiple exposure experiments (15 and 60 minutes with PP and 60 minutes with SS)) were both statistically significant compared to the antibiotic control. Table 6.4 shows the results from the Mann-Whitney U-test, including the truthfulness of the null hypothesis as well as the p-value.

Further statistical analysis can be done between the various methods themselves, comparing them to see if any stand out as definitively better than the rest. Table 6.5 shows the p-values for the Mann-Whitney U-test comparing all of the methods between themselves. Of the three most promising methods (pulsed, no rest, 1:10 concentration; pulsed, 15 min rest, 1:5 concentration;

Table 6.4: P-values and null hypothesis return on all experiments from Mann-Whitney U-test, with alpha was set to 0.01

Experiment	Null Hypothesis	P-value
Continuous, ø, PP, 1:1	False	0.9065
Continuous, ø, PP, 1:5	True	0.0077
Continuous, ø, PP, 1:10	True	0.0075
Pulsed, ø, PP, 1:1	True	0.0072
Pulsed, ø, PP, 1:5	False	0.0108
Pulsed, ø, PP, 1:10	True	0.0005
Pulsed, 15 min, PP, 1:5	True	0.0000
Pulsed, 60 min, PP, 1:5	True	0.0095
Pulsed, 15 min, SS, 1:1	True	0.0009

Table 6.5: P-values and null hypothesis return on all experiments from Mann-Whitney U-test, with alpha set to 0.01, where the datasets on the left have been compared to the datasets on the top. The shaded cells are the ones that indicate statistical significance.

		Continuous			Pulsed			Rest		
		1:1	1:5	1:10	1:1	1:5	1:10	15 min	60 min	Steel
Cont.	1:1	1	0.0038	0.0049	0.0006	0.0001	0.0001	0.0001	0.0001	0.0001
	1:5		1	0.6956	0.0948	0.6440	0.0085	0.0428	0.0032	0.0948
	1:10			1	0.1081	0.7800	0.0473	0.1420	0.0131	0.1825
Pulsed	1:1				1	0.8147	0.6496	0.5457	0.6665	0.9314
	1:5					1	0.2482	0.2973	0.2581	0.6048
	1:10						1	0.9816	0.3736	0.6495
Rest	15 min							1	0.3994	1
	60 min								1	0.6048
	Steel									1

and pulsed, 60 min rest, 1:5 concentration), none are statistically significant compared to the other. This suggest that the rest periods do not necessarily contribute anything towards the total bacteria number reduction, but rather the combination of active US insonification with the MBs and AB is what is driving the reduction in bacterial numbers.

Further improvements could be made to the method. The *P. Aeruginosa* biofilm has an overall negative charge, while Gentamicin is a neutrally charged, but polar molecule [271]. It is speculated that by introducing negatively charged bubbles, the antibiotic could be attracted to the charged bubble shell and be carried into the biofilm where it would then be absorbed by the bacteria (with both the bubbles and biofilm being negative the antibiotic would, ideally, get attracted to the bacteria). This only depends on the bubbles penetrating the biofilm despite having the same charge as the biofilm. The radiation forces from the ultrasound field should be strong enough to achieve that.

Nitric oxide (NO) causes a change in bacterial phenotype and can be used as a quorum sensing inhibitor for *P. Aeruginosa* [272]. When introduced into the system the communication between the bacteria inside the biofilm breaks down and the biofilm starts falling apart. A way of delivering NO into the biofilm would be by encapsulating it in a microbubble shell. Therefore, when the bubble reaches the biofilm core it can be caused to cavitate and release the NO, and thus disrupting the operation of the biofilm. This could be coupled with the idea of using charged bubbles to help with antibiotic delivery.

6.6 Conclusion

Biofilms present a serious threat to our ability to treat infections. The defences they have developed can drastically reduce the effectiveness of antibiotics, as well as slow their penetration down. For a lot of bacteria inside the biofilm this means that the concentration of antibiotic that reaches them will not be high enough to kill them. This gives them an opportunity to develop AMR which makes future generations of the biofilm even harder, if not impossible to kill.

Combining antibiotics with other methods that increase penetration and absorption can possibly overcome this problem. It is speculated that when microbubbles are injected into the system and sonicated with an ultrasonic probe they can penetrate the biofilm and through stable cavitation create openings (small perforation in the biofilm) through which the antibiotic can access the inner layers of the biofilm. This is the method that was tested in this chapter.

A device was developed that allowed for a cost-effective, quick, and reliable testing of this method that meets the requirements for testing in a microbiological lab environment. It could be easily assembled, sterilised, and only required around 1 litre of water to operate. It consisted of an ultrasonic transducer suspended above a sealed container which contained the biofilm, as well as the antibiotic and microbubble solution. The bottom and the sides of the device are lined with acoustic absorbers to prevent any reflections inside, this is what allows for its compact size. By using FEA, various materials were chosen to represent different types of tissue that would be present during treatment - polypropylene for soft tissue, and stainless steel for the hard bone tissue.

Multiple conditions were tested when exploring the combined method with the PP coupon: different bubble concentrations were used (1:1, 1:5, 1:10), they were insonified with a continuous and a pulsed (25% duty cycle) wave, a second insonification period was introduced, with the rest between the two that was, at first, 15 minutes, and then changed to 60 minutes. The best performing condition was then used for the SS test.

The highest bacteria reduction number was achieved by having two 5 minute insonification periods, in which pulsed waves were used, with a 60 minute rest period in between, with a 1:5 bubble concentration. This method achieved a 0.76 log (83%) reduction in numbers compared to using just an antibiotic. A much shorter treatment was also very successful; a single 5 minute exposure to pulsed ultrasound with a low bubble concentration of 1:10 produced a 0.7 log (80%) reduction compared to the antibiotic control. The method with a 15 minute rest period between two treatments and a 1:5 bubble concentration produced a 0.6 log (76%) reduction, suggesting that longer rest periods benefit the bacteria reduction effects. This same method had the best absolute reduction in bacterial numbers of 1.26 log (95 %) compared to using no treatment at all. This still does not meet the 3 log reduction needed to kill

the biofilm, but with an increase in antibiotic levels this could be achieved.

When stainless steel was used, alongside the 60 minute rest period method, it resulted in a 0.47 log (67%) reduction compared to the control. Due to the high impedance of the material a standing wave forms which traps bubbles in the antinodes reducing the effectivness in penetrating the biofilm.

There are still ways of improving the results, as charged bubbles could be utilised to carry the antibiotic, which has an opposite charge, into the biofilm, thus speeding up the diffusion process. The bubbles could also be filled with NO which is known to disrupt normal biofilm behaviours.

These results provide an important improvement over the current methods. By allowing lower, sub-inhibitory, antibiotic concentrations with an equally successful or better bacteria reduction rate the chances of a biofilm developing AMR are severely reduced. Additionally, by reducing the antibiotic concentration, their side-effects are reduced as well. This is especially important with the more aggressive antibiotics.

Chapter 7

Conclusion and future work

The body of work presented in this thesis consists of three projects centred around the idea that an ultrasonic sound wave can be used in conjunction with surfaces to manipulate objects. Each project presents a different aspect, and a different end purpose, of the basic idea of manipulation. The key contributions of this thesis are:

- The design, construction, and testing of a device that can be used for capturing specific cells from water or air samples by using ultrasound to push pathogens towards a specific antibody coated layer (Chapter 3),
- Development and evaluation of a more reliable method for capturing spores from a water sample for the purpose of detecting threats to human health (Chapter 4),
- Development and evaluation of a method for capturing basophils as a part of a bigger allergy diagnosis method (Chapter 5),
- Creation of a novel method for eradicating surface biofilm using a combination of ultrasonically activated microbubbles and antibiotics (Chapter 6).

7.1 Testing water and air quality

Anthrax spore capture is proving to be a challenge in the field. Various biosensors have been developed to meet the requirements of field testing, but they trade speed for accuracy or vice versa.

The device developed to address the issue of fast and easy pathogen detection, was based on the thin-reflector (TR) principle - the heights of the layeres from a layered resonator are tuned in such a way that the first structural mode of the device is excited, and the node from the ultrasound standing wave (USW) is positioned at the very edge of the reflector layer.

The device was meticulously characterised in chapter 3. The TR mode was combined with a *Bacillus globigii* (BG) specific antibody coating designed to

capture the spores. In chapter 4 the limit of detection of the device was tested and found to be 100 spores/ml which matched the goal set at the beginning of the project. The time it took for the test to complete was around 30 minutes.

There are multiple directions in which the project can be taken:

- The detection of captured spores needs to be implemented in a way that can be integrated into a portable system and is well established in the field. Polymerase chain reaction (PCR) is well suited for this task, as is portable Raman spectrometry which promises a low-cost and easy to use detection method powered which is sufficiently low power for battery powered systems.
- The device design can be streamlined and optimised for easier and more robust use, for e.g. the use of magnetic or lever clamps instead of screws, or the integration of the whole system into a "black box" that requires minimal user training.
- For use in situations where sterile conditions are needed a disposable and isolated fluid channel can be developed by utilising thin plastic films that couple with the fixed and permanent carrier layer and transducer.

7.2 Allergy testing

Allergy incidence is on the rise, but testing centres cannot provide fast enough responses in performing allergy tests. The golden standard test involves multiple experienced personnel exposing a patient over a period of days, a procedure which can produce extreme discomfort.

The TR device was adapted to capture basophils, the white blood cells responsible for allergic reactions, by changing the antibody coating to be basophil specific in chapter 5. It was optimised for flow by using purified basophil, after which the device was tested with lysed blood (whole blood where the erythrocytes and platelets have been removed) and the antibody coatings were imaged. The results proved promising with basophil captured in the thousands from 1 ml samples and over a period of 10 minutes with an additional 2 hours for processing. However, they were overall inconclusive as the stain was not basophil specific.

There is a straight path regarding what comes next:

- The tests are to be repeated and imaged with the appropriate stain to see how many basophils are truly captured.
- A proof of principle allergy test is to be performed in the device (by flowing allergens after the basophils have been captured).
- Blood component separation by using USWs is to be incorporated into the system in order to integrate every step of the method into a single, easy-to-use device.

7.3 Biofilm eradication

Diabetic foot ulcer are chronic wounds that develop as a consequence of diabetes. Their healing process is inhibited by bacterial structures called biofilms which provide additional defensive properties against antibiotics. The problem is compounded by the recent threat of anti-microbial resistance (AMR) that is developing in bacterial populations.

Bubbles react more strongly to ultrasound than cells so for the task of eradicating a biofilm, the objective of the last project, both a travelling and a standing ultrasonic wave was utilised to push microbubble (MB) into a *Pseudomonas Aeruginosa* (*P. Aeruginosa*) biofilm to open up paths for the antibiotics, introduced with the bubbles, to penetrate the biofilm and increase their effectiveness.

A new device was designed in chapter 6 to meet the specifications of a biofilm eradication method: easy to manufacture, use and sterilise; quick to assemble and disassemble; compatible with use in a microbiology lab; and does not need hgih amounts of water (<5l). It was used to test a variety of conditions in order to optimise the method for biofilm eradication. By using a pulsed wave for 5 minutes to insonify a low concentration of MB (1 part MB mixture in 20) in conjunction with a sub-inhibitory concentration of antibiotics a reduction in bacteria numbers 80 % greater than using antibiotics alone was achieved. This is less than the target of 99.99 %, but this goal could be achievable with certain improvements.

There are two main improvements in the method that are considered at this point:

- The biofilm has an overall negative charge, while the antibiotic has a slight positive charge. By introducing a negatively charged MBs it might be possible to "lead" the antibiotic into the biofilm expediting its release.
- The air inside the MBs can be replaced with nitric oxide (NO) that would dissolve into the biofilm core in order to disrupt its normal functioning.
- Once the bacteria reduction is increased to a desired number the device can be redesigned so that it can be used in clinical settings.

7.4 Final words

Acoustic manipulation can be a powerful tool, but requires careful optimisation in order to succeed. When used correctly it can offer an alternative to well established techniques in a multitude of areas, three of which were explored in this thesis.

The design of the devices and the overall methods were guided by the idea that they must be easy to use, cheap, and fast. Only by meeting all three can the devices expect to find any real-world implementation.

The aim of the thesis was to develop devices and methods that utilise ultrasound to enhance surface mediated interactions and that can show an improvement over the methods currently in place. In spore detection, the device was able to perform as well as other commercial alternatives, but at faster speeds, with a possibility of further integration with fast and reliable sensing technologies. With basophil detection, while the results were inconclusive, they showed a promising capture number, at the fraction of the cost of alternative methods and with simpler instructions. Finally, a different device built for the purpose of eradication of surface biofilms showed that an a significant improvement over antibiotics alone can be made while simultaneously reducing the dosage of the antibiotic. This would ensure less chance of the bacteria developing AMR, a critical issue in the world today.

Appendix A

MATLAB code for generating particle paths

```
1
2  H=100;           % Height of channel (um)
3  D = 62;          % Length of channel (mm)
4  dt = 0.1;        % Time step (s)
5  va = 6.94;       % Average velocity (mm/s) found from
       experimental data
6  R = 50;          % Half height of channel (um)
7  V = [-2*va/R^2 0 2*va]; % Values for parabolic
       velocity profile
8
9  hv = 3/60;       % Drop rate
10
11 for jj = 1:100
12     h0=jj;           % starting height in um
13     d0 = 0;          % starting distance in mm
14     v0 = polyval(V,round(h0-50));          % given as
           function(round(height))
15     ii = 1;
16     h(jj) = {h0};
17     d(jj) = {d0};
18     v(jj) = {v0};
19     while h{jj} > 0
20         d{jj}(ii+1) = d{jj}(ii)+v{jj}(ii)*dt;
21         h{jj}(ii+1) = h{jj}(ii) - hv*dt;
22         v{jj}(ii+1) = polyval(V,round(h{jj}(ii+1)-50)
               ); % function(round(h(ii+1)))
23         ii = ii+1;
24     end
25 end
```

```
%% Figure of all the spore paths with the x-axis having a non-standard distance

figure
ax(1) = axes('position', [0.5 0.15 0.4 0.8]);    % This starts the distribution process
for jj=100:-1:1
    plot(d{jj},h{jj},'HandleVisibility','off')
    hold on
end
line([62 62],[0 100], 'LineStyle','--','LineWidth',1.5)
ax(2) = copyobj(ax(1), gcf);                % From here
set(ax(2), 'position', [0.1 0.15 0.4 0.8]);
set(ax(1), 'box', 'off', 'ycolor', 'none','xscale','log');
set(ax(2), 'box', 'off');
set(ax(1), 'xlim', [500 max(d{100})]);
set(ax(2), 'xlim', [0 500]);
linkaxes(ax, 'y');                          % To here it is for the
                                            % non-uniform
                                               distribution
                                                of axis
                                               values
set(ax(1),'YGrid','on')
set(ax(2),'Ygrid','on')
ylabel(ax(2),'Height of spore inside channel (\mu m)')
xl = xlabel('Distance along the channel (mm)');
set(xl,'Position',[650 -8])
ylim([0 100])
hold off
legend('Length of channel')

set(ax,'fontsize',14,'fontWeight','bold','Linewidth',2)
set(findall(gcf,'type','text'),'fontSize',14,'fontWeight','bold')
ax=gca;
```

References

[1] W.H.O. *Burden of disease and cost-effectiveness estimates*. 2012. URL: http://www.who.int/water_sanitation_health/diseases/burden/en/ (visited on Aug. 31, 2015).

[2] T. Clasen et al. "Interventions to improve water quality for preventing diarrhoea: systematic review and meta-analysis". In: *BMJ* 334 (7597 Apr. 2007), p. 782.

[3] S. Gundry, R. Conroy, and J. Wright. "A systematic review of the health outcomes related to household water quality in developing countries". In: *J Water Health* 2 (1 Mar. 2004), pp. 1–13.

[4] T. Mattila-Sandhols and G. Wirtanen. "Biofilm formation in the industry: A review". In: *Food Rev Int* 8 (4 1992), pp. 573–603.

[5] A.V. Kneese and B.T. Bower. *Managing water quality: eonomics, technology, institutions*. Rff Press, 1984.

[6] O. Lazcka, F.J. Del Campo, and F.X. Muñoz. "Pathogen detection: A perspective of traditional methods and biosensors". In: *Biosens Bioelectron* 22 (2007), pp. 1205–1217.

[7] World Health Organization. *Guidelines for drinking-water quality*. 4th edition. 2017. URL: https://www.who.int/water_sanitation_health/publications/drinking-water-quality-guidelines-4-including-1st-addendum/en/ (visited on Jan. 13, 2019).

[8] Y. Alamanos et al. "A community waterborne outbreak of gastroenteritis attributed to Shigella sonnei". In: *Epidemiology and Infection* 125.3 (2000), 499–503.

[9] J.B. Kaper, J.G. Morris, and M.M. Levine. "Cholera". In: *Clinical Microbiology Reviews* 8.1 (1995), pp. 48–86.

[10] J.P. Nataro and J.B. Kaper. "Diarrheagenic *Escherichia coli*". In: *Clinical Microbiology Reviews* 11.1 (1998), pp. 142–201.

[11] *Stool exudates in a patient with shigellosis*. 2006. URL: https://commons.wikimedia.org/w/index.php?curid=611972 (visited on Feb. 16, 2018).

[12] Thames Water. *How we look after your water*. 2016. URL: https://www.thameswater.co.uk/help-and-advice/water-quality/how-we-look-after-your-water (visited on Jan. 23, 2019).

[13] P.A.C. Braga et al. "Bacterial identification: from the agar plate to the mass spectrometer". In: *RSC Adv.* 3 (4 2013), pp. 994–1008.

[14] World Health Organisation. *Drinking water*. Feb. 7. URL: https://www.who.int/news-room/fact-sheets/detail/drinking-water (visited on Jan. 23, 2019).

[15] A.E. Yousef. "Principles of bacteria detection". In: ed. by M. Zourob, S. Elwary, and A. Turner. 1st. New York, USA: Springer, 2008. Chap. Detection of bacterial pathogens in different matrices: Current practices and challenges, pp. 31–48.

[16] S. Zhang et al. "Predicting detection limits of enzyme-linked immunosorbent assay (ELISA) and bioanalytical techniques in general". In: *Analyst* 139 (2 2014), pp. 439–445.

[17] M. Carrera et al. "Difference between the spore sizes of *Bacillus anthracis* and other *Bacillus* species". In: *Journal of Applied Microbiology* 102.2 (2007), pp. 303–312.

[18] R.C. Spencer. "*Bacillus anthracis*". In: *Journal of Clinical Pathology* 56.3 (2003), pp. 182–187.

[19] Bacillus anthracis *spore*. 2002. URL: https://phil.cdc.gov/Details.aspx?pid=10123 (visited on Feb. 16, 2018).

[20] J.H. Carr. Bacillus anthracis *bacteria*. URL: https://phil.cdc.gov/Details.aspx?pid=1811 (visited on Feb. 16, 2018).

[21] W.S. Albrink et al. "Human inhalation anthrax: a report of three fatal cases". In: *The American journal of pathology* 36.4 (1960), p. 457.

[22] M.N. Swartz. "Recognition and Management of Anthrax — An Update". In: *New England Journal of Medicine* 345.22 (2001), pp. 1621–1626.

[23] L. Baillie and T.D. Read. "*Bacillus anthracis*, a bug with attitude!" In: *Current Opinion in Microbiology* 4.1 (2001), pp. 78 –81.

[24] S. Shafazand et al. "Inhalational Anthrax: Epidemiology, Diagnosis, and Management". In: *Chest* 116.5 (1999), pp. 1369 –1376.

[25] S.A. Plotkin et al. "An epidemic of inhalation anthrax, the first in the twentieth century: I. Clinical features". In: *The American Journal of Medicine* 29.6 (1960), pp. 992 –1001.

[26] J.C. Holty et al. "Systematic review: A century of inhalational anthrax cases from 1900 to 2005". In: *Annals of Internal Medicine* 144.4 (2006), pp. 270–280.

[27] S.R. Klee et al. "Evaluation of different methods to discriminate Bacillus anthracis from other bacteria of the Bacillus cereus group". In: *Journal of Applied Microbiology* 100.4 (2006), pp. 673–681.

[28] V.I. Klichko et al. "Anaerobic induction of Bacillus anthracis hemolytic activity". In: *Biochemical and Biophysical Research Communications* 303.3 (2003), pp. 855 –862.

[29] X. Hu et al. "Sympatric soil communities of Bacillus cereus sensu lato: population structure and potential plasmid dynamics of pXO1- and pXO2-like elements". In: *FEMS Microbiology Ecology* 70.3 (2009), pp. 344–355.

[30] L.M. Irenge and J.-L. Gala. "Rapid detection methods for Bacillus anthracis in environmental samples: a review". In: *Applied Microbiology and Biotechnology* 93.4 (Feb. 2012), pp. 1411–1422.

[31] D. King et al. "Performance Assessment of Three Commercial Assays for Direct Detection of Bacillus anthracis Spores". In: *Journal of Clinical Microbiology* 41.7 (2003), pp. 3454–3455.

[32] C.F. Fronczek and J.-Y. Yoon. "Biosensors for Monitoring Airborne Pathogens". In: *Journal of Laboratory Automation* 20.4 (2015), pp. 390–410.

[33] J. Moldenhauer. "Principles of bacteria detection". In: ed. by M. Zourob, S. Elwary, and A. Turner. 1st. New York, USA: Springer, 2008. Chap. Overview of Rapid Microbiological Methods, pp. 49–79.

[34] A.P.F. Turner, I. Karube, and G.S. Wilson, eds. *Biosensors: Fundamentals and Applications*. 1st. Oxford, UK: Oxford University Press, 1987.

[35] M. Shichiri et al. "Telemetry Glucose Monitoring Device With Needle-Type Glucose Sensor: A Useful Tool for Blood Glucose Monitoring in Diabetic Individuals". In: *Diabetes Care* 9.3 (1986), pp. 298–301.

[36] C. von Pirquet. "Allergie". In: *Munchen Med Wchnschr* 53 (1906), pp. 1457–1458.

[37] P.G.H. Gell and R.R.A. Coombs. *Clinical Aspects of Immunology.* 24-25 Broad Street, Oxford, UK: Blackwell Scientific Publications Ltd., 1963.

[38] A.B. Kay. "Allergy and Allergic Diseases". In: *New England Journal of Medicine* 344.1 (2001), pp. 30–37.

[39] S. ROMAGNANI. "Human T_H1 and T_H2 subsets: doubt no more". In: *Immunol. Today* 12 (1991), pp. 256–257.

[40] D. Fraser et al. *Nelson biology 12*. Toronto, Ont: Nelson Education, 2012, p. 473.

[41] J.O. Warner et al. “Allergy practice worldwide: a report by the World Allergy Organization Specialty and Training Council”. In: *International archives of allergy and immunology* 139.2 (2006), pp. 166–174.

[42] D.H. Smith et al. “A National Estimate of the Economic Costs of Asthma”. In: *American Journal of Respiratory and Critical Care Medicine* 156.3 (1997), pp. 787–793.

[43] E. von Mutius et al. “Prevalence of asthma and atopy in two areas of West and East Germany.” In: *American Journal of Respiratory and Critical Care Medicine* 149.2 (1994), pp. 358–364.

[44] E. von Mutius et al. “Increasing prevalence of hay fever and atopy among children in Leipzig, East Germany”. In: *The Lancet* 351.9106 (1998), pp. 862 –866.

[45] G.A.W. Rook and J.L. Stanford. “Give us this day our daily germs”. In: *Immunology Today* 19.3 (1998), pp. 113 –116.

[46] E. Sepp et al. “Intestinal microflora of Estonian and Swedish infants”. In: *Acta Paediatrica* 86.9 (1997), pp. 956–961.

[47] B. Björksten et al. “The intestinal microflora in allergic Estonian and Swedish 2-year-old children”. In: *Clinical and Experimental Allergy* 29.3 (1999), pp. 342–346.

[48] J.L. Cho et al. “Allergic asthma is distinguished by sensitivity of allergen-specific CD4+ T cells and airway structural cells to type 2 inflammation”. In: *Science Translational Medicine* 8.359 (2016), 359ra132–359ra132.

[49] R.A. Settipane and D.R. Charnock. *Nonallergic rhinitis*. Ed. by J.N. Baraniuk and D.J. Shusterman. 1st. Boca Raton: CRC Press, 2016. Chap. Epidemiology of Rhinitis: Allergic and Nonallergic.

[50] B. Lipworth et al. “An algorithm recommendation for the pharmacological management of allergic rhinitis in the UK: a consensus statement from an expert panel”. In: *NPJ primary care respiratory medicine* 27.1 (2017), p. 3.

[51] T. Zuberbier et al. “EAACI/GA^{2}LEN/EDF/WAO guideline: management of urticaria”. In: *Allergy* 64.10 (2009), pp. 1427–1443.

[52] B.Y.-H. Thong and T.-C. Tan. “Epidemiology and risk factors for drug allergy”. In: *British Journal of Clinical Pharmacology* 71.5 (2011), pp. 684–700.

[53] G. Du Toit et al. “Randomized Trial of Peanut Consumption in Infants at Risk for Peanut Allergy”. In: *New England Journal of Medicine* 372.9 (2015), pp. 803–813.

[54] World Allergy Organization. *White book on allergy*. Ed. by R. Pawanakar et al. Milwaukee, Wisconsin, USA: WAO, 2011. URL: https://www.worldallergy.org/UserFiles/file/WAO-White-Book-on-Allergy_web.pdf (visited on Jan. 27, 2019).

[55] C. Mayorga et al. "In vitro diagnosis of immediate allergic reactions to drugs: an update". In: *J Investig Allergol Clin Immunol* 20.2 (2010), pp. 103–109.

[56] A.B. Kay. "Allergy and Allergic Diseases". In: *New England Journal of Medicine* 344.2 (2001), pp. 109–113.

[57] H.H. Jacobi et al. "Histamine immunocytochemistry: a new method for detection of basophils in peripheral blood". In: *Journal of Immunological Methods* 237.1 (2000), pp. 29 –37.

[58] U. Blank, F.H. Falcone, and G. Nilsson. "The history of mast cell and basophil research – some lessons learnt from the last century". In: *Allergy* 68.9 (2013), pp. 1093–1101.

[59] K.D. Stone, C. Prussin, and D.D. Metcalfe. "IgE, mast cells, basophils, and eosinophils". In: *Journal of Allergy and Clinical Immunology* 125.2, Supplement 2 (2010), S73 –S80.

[60] F.H. Falcone, H. Haas, and B.F. Gibbs. "The human basophil: a new appreciation of its role in immune responses". In: *Blood* 96.13 (2000), pp. 4028–4038.

[61] C.E.H. Grattan. "Basophils in Chronic Urticaria". In: *Journal of Investigative Dermatology Symposium Proceedings* 6.2 (2001), pp. 139 – 140.

[62] C. Ballard. *Basophil, eosinophil, and lymphocyte*. 1974. URL: https://phil.cdc.gov/Details.aspx?pid=15133 (visited on Feb. 16, 2018).

[63] L. Hall-Stoodley, J.W. Costerton, and P. Stoodley. "Bacterial biofilms: from the natural environment to infectious diseases". In: *Nature reviews microbiology* 2.2 (2004), p. 95.

[64] C.E. Zobell. "The effect of solid surfaces upon bacterial activity". In: *Journal of bacteriology* 46.1 (1943), p. 39.

[65] S. Singh et al. "Understanding the mechanism of bacterial biofilms resistance to antimicrobial agents". In: *The open microbiology journal* 11 (2017), p. 53.

[66] S. Maleki et al. "Alginate Biosynthesis Factories in *Pseudomonas fluorescens*: Localization and Correlation with Alginate Production Level". In: *Applied and Environmental Microbiology* 82.4 (2016), pp. 1227–1236.

[67] A. Taglialegna, I. Lasa, and J. Valle. "Amyloid Structures as Biofilm Matrix Scaffolds". In: *Journal of Bacteriology* 198.19 (2016), pp. 2579–2588.

[68] H.-C. Flemming, T.R. Neu, and D.J. Wozniak. "The EPS Matrix: The "House of Biofilm Cells"". In: *Journal of Bacteriology* 189.22 (2007), pp. 7945–7947.

[69] L. Laganenka and V. Sourjik. "Autoinducer 2-Dependent *Escherichia coli* Biofilm Formation Is Enhanced in a Dual-Species Coculture". In: *Applied and Environmental Microbiology* 84.5 (2018).

[70] M.R. Parsek and P.K. Singh. "Bacterial Biofilms: An Emerging Link to Disease Pathogenesis". In: *Annual Review of Microbiology* 57.1 (2003), pp. 677–701.

[71] P.D. Marsh and E. Zaura. "Dental biofilm: ecological interactions in health and disease". In: *Journal of Clinical Periodontology* 44.S18 (2017), S12–S22.

[72] M. Jamal et al. "Bacterial Biofilm: Its Composition, Formation and Role in Human Infections". In: *Research & Reviews: Journal of Microbiology and Biotechnology. Research and Reviews* 4.3 (2015).

[73] S.L. Chua et al. "Dispersed cells represent a distinct stage in the transition from bacterial biofilm to planktonic lifestyles". In: *Nature communications* 5 (2014), p. 4462.

[74] H. Wu et al. "Strategies for combating bacterial biofilm infections". In: *International journal of oral science* 7.1 (2015), p. 1.

[75] R.A. Cooper, T. Bjarnsholt, and M. Alhede. "Biofilms in wounds: a review of present knowledge". In: *Journal of Wound Care* 23.11 (2014), pp. 570–582.

[76] T.-F. Mah et al. "A genetic basis for Pseudomonas aeruginosa biofilm antibiotic resistance". In: *Nature* 426.6964 (Nov. 2003), pp. 306–310.

[77] J.G. Leid et al. "The Exopolysaccharide Alginate Protects *Pseudomonas aeruginosa* Biofilm Bacteria from IFN-γ-Mediated Macrophage Killing". In: *The Journal of Immunology* 175.11 (2005), pp. 7512–7518.

[78] W.-C. Chiang et al. "Extracellular DNA Shields against Aminoglycosides in Pseudomonas aeruginosa Biofilms". In: *Antimicrobial Agents and Chemotherapy* 57.5 (2013), pp. 2352–2361.

[79] M. Hentzer, L. Eberl, and M. Givskov. "Transcriptome analysis of *Pseudomonas aeruginosa* biofilm development: anaerobic respiration and iron limitation". In: *Biofilms* 2.1 (2005), 37–61.

[80] W. Hengzhuang et al. "In Vivo Pharmacokinetics/Pharmacodynamics of Colistin and Imipenem in *Pseudomonas aeruginosa* Biofilm Infection". In: *Antimicrobial Agents and Chemotherapy* 56.5 (2012), pp. 2683–2690.

[81] N. Høiby et al. "The clinical impact of bacterial biofilms". In: *International journal of oral science* 3.2 (2011), p. 55.

[82] R.M. Donlan and J.W. Costerton. "Biofilms: Survival Mechanisms of Clinically Relevant Microorganisms". In: *Clinical Microbiology Reviews* 15.2 (2002), pp. 167–193.

[83] J.B. Lyczak, C.L. Cannon, and G.B. Pier. "Lung Infections Associated with Cystic Fibrosis". In: *Clinical Microbiology Reviews* 15.2 (2002), pp. 194–222.

[84] C. Attinger and R. Wolcott. "Clinically Addressing Biofilm in Chronic Wounds". In: *Advances in Wound Care* 1.3 (2012), pp. 127–132.

[85] N.A. Richmond, A.D. Maderal, and A.C. Vivas. "Evidence-based management of common chronic lower extremity ulcers". In: *Dermatologic Therapy* 26.3 (2013), pp. 187–196.

[86] R.G. Frykberg and J. Banks. "Challenges in the treatment of chronic wounds". In: *Advances in wound care* 4.9 (2015), pp. 560–582.

[87] J.W. Walsh et al. "Association of diabetic foot ulcer and death in a population-based cohort from the United Kingdom". In: *Diabetic Medicine* 33.11 (2016), pp. 1493–1498.

[88] national Institute for Health and Care Excellence (NICE). *Guidelines for drinking-water quality*. 2016. URL: `https://www.nice.org.uk/guidance/ng19/chapter/introduction` (visited on Feb. 6, 2019).

[89] M. Malone et al. "The prevalence of biofilms in chronic wounds: a systematic review and meta-analysis of published data". In: *Journal of Wound Care* 26.1 (2017), pp. 20–25.

[90] M. Hill and N.R. Harris. "Principles of bacteria detection". In: ed. by Mohammed Zourob, Souna Elwary, and Anthony Turner. 1st. New York, USA: Springer, 2008. Chap. Ultrasonic Microsystems for bacterial cell manipulation, pp. 909–928.

[91] M. Hill, Shen Y., and J.J. Hawkes. "Modelling of layered resonators for ultrasonic separation". In: *Ultrasonics* 40 (2002), pp. 385–392.

[92] A. Lenshof et al. "Acoustofluidics 5: Building microfluidic acoustic resonators". In: *Lab Chip* 12 (2012), pp. 684–695.

[93] H. Bruus. "Acoustofluidics 9: Modelling and applications of planar resonant devices for acoustic particle manipulation". In: *Lab Chip* 12 (2012), pp. 1417–1426.

[94] A. Lenshof, C. Magnusson, and T. Laurell. "Acoustofluidics 8: Applications of acoustophoresis in continuous flow microsystems". In: *Lab Chip* 12 (2012), pp. 1210–1223.

[95] J.J. Hawkes et al. "Ultrasonic deposition of cells on a surface". In: *Biosens Bioelectron* 19 (2004), pp. 1021–1028.

[96] S.P. Martin et al. "Spore and micro-particle capture on an immunosensor surface in an ultrasound standing wave system". In: *Biosens Bioelectron* 21 (2005), pp. 758–767.

[97] P. Glynne-Jones et al. "Robust acoustic particle manipulation: A thin-reflector design for moving particles to a surface". In: *J Acoust Soc Am* 126 (2009), EL75–EL79.

[98] A. Kund. "Über eine neue Art akustischer Staubfiguren und über die Anwen- dung derselben zur Bestimmung der Schallgeschwindigkeit in festen Körpern und Gasen". In: *Annalen der Physik* 203 (1866), pp. 497–523.

[99] J.W. Rayleigh. "On the circulation of air observed in Kundt's tubes, and on some allied acoustical problems". In: *Philosophical Transactions of the Royal Society of London* (1884), pp. 1–21.

[100] J.W. Rayleigh. "On the pressure of vibrations". In: *Philosophical Magazine* 3 (1902), pp. 338–346.

[101] L.V. King. "On the acoustic radiation pressure on spheres". In: *Royal Society of London Proceedings Series A*. Vol. 147. 1934, pp. 212–240.

[102] K. Yosioka and Y. Kawasima. "Acoustic radiation pressure on a compressible sphere". In: *Acta Acust united Ac* 5 (1955), pp. 197–173.

[103] L.P. Gor'kov. "On the forces acting on a small particle in an acoustical field in an ideal fluid". In: *Dokl. Akad. Nauk SSSR* 140 (Mar. 1962), pp. 88–92.

[104] A. Doinikov. "Acoustic radiation pressure on a rigid sphere in a viscous fluid". In: *Proc. R. Soc. Lond. A*. 1994.

[105] A. Doinikov. "Acoustic radiation force on a spherical particle in a viscous heat- conducting fluid. I. general formula". In: *J. Acoust. Soc. Am.* 101 (1997), pp. 713 –721.

[106] M. Settnes and H. Bruus. "Forces acting on a small particle in an acoustical field in a viscous fluid". In: *Phys Rev E* 85 (2012). 016327.

[107] H. Bruus. "Acoustofluidics 1: Governing equations in microfluidics". In: *Lab Chip* 11 (2011), pp. 3742–3751.

[108] H. Bruus. "Acoustofluidics 2: Perturbation theory and ultrasound resonance modes". In: *Lab Chip* 12 (2012), pp. 20–28.

[109] H. Bruus. "Acoustofluidics 7: The acoustic radiation force on small particles". In: *Lab Chip* 12 (2012), pp. 1014–1021.

[110] M. Ohlin. "Ultrasonic Fluid and Cell Manipulation". PhD thesis. Department of Applied Physics, KTH Royal Institute of Technology, 2015.

[111] T.G. Leighton. *The Acoustic Bubble*. London, UK: Academic Press, 1994.

[112] H. Gu et al. "Using Biofunctional Magnetic Nanoparticles to Capture Vancomycin-Resistant Enterococci and Other Gram-Positive Bacteria at Ultralow Concentration". In: *Journal of the American Chemical Society* 125.51 (2003), pp. 15702–15703.

[113] J. Suehiro et al. "Selective detection of bacteria by a dielectrophoretic impedance measurement method using an antibody-immobilized electrode chip". In: *Sens. Actuator B-Chem.* 119 (2006), pp. 319–326.

[114] D. Bavli, N. Emanuel, and Y. Barenholz. "Real-time monitoring of E. coli O157 and Salmonella enterica serovar Typhimurium in water using ultrasound and latex-based immunoassay". In: *Anal. Methods* 6 (2 2014), pp. 395–403.

[115] L. Tengelsen et al. "Coordinated Response to Reports of Possible Anhtrax Contamination, Idaho, 2001". In: *Emerg Infect Dis* 8.10 (2002), pp. 1093–5.

[116] C. Ash et al. "Comparative Analysis of Bacillus anthracis, Bacillus cereus, and Related Species on the Basis of Reverse Transcriptase Sequencing of 16S rRNA". In: *International Journal of Systematic and Evolutionary Microbiology* 41.3 (1991), pp. 343–346.

[117] C.K. Marston et al. "Molecular approaches to identify and differentiate Bacillus anthracis from phenotypically similar Bacillus species isolates". In: *BMC Microbiology* 6.1 (Mar. 2006), p. 22.

[118] EeJ. Stewart. "Growing Unculturable Bacteria". In: *Journal of Bacteriology* 194.16 (2012), pp. 4151–4160. DOI: 10.1128/JB.00345-12.

[119] R.W. Titball, P.C. Turnbull, and R.A. Hutson. "The monitoring and detection of Bacillus anthracis in the environment". In: *Society for Applied Bacteriology symposium series* 20 (1991), 9S—18S.

[120] D.A. Rasko et al. "Bacillus anthracis comparative genome analysis in support of the Amerithrax investigation". In: *Proceedings of the National Academy of Sciences* (2011).

[121] E. Engvall and P. Perlman. "Enzyme-linked immunosorbent assay (ELISA). Quantitative assay of immunoglobulin G." In: *Immunochem* 8.9 (1971), pp. 871–884.

[122] *Official Method 996.08 Salmonella in selected foods, BAX automated system. The official method of analysis*. 18th. AOAC International. Gaithersburg, MD, USA, 2005.

[123] A. Kuehn et al. “Development of Antibodies against Anthrose Tetrasaccharide for Specific Detection of Bacillus anthracis Spores”. In: *Clinical and Vaccine Immunology* 16.12 (2009), pp. 1728–1737.

[124] H. Yu. “Comparative studies of magnetic particle-based solid phase fluorogenic and electrochemiluminescent immunoassay”. In: *Journal of Immunological Methods* 218.1 (1998), pp. 1 –8.

[125] R.E. Biagini et al. “Comparison of a Multiplexed Fluorescent Covalent Microsphere Immunoassay and an Enzyme-Linked Immunosorbent Assay for Measurement of Human Immunoglobulin G Antibodies to Anthrax Toxins”. In: *Clinical and Vaccine Immunology* 11.1 (2004), pp. 50–55.

[126] B.J. Hindson et al. “Autonomous Detection of Aerosolized Biological Agents by Multiplexed Immunoassay with Polymerase Chain Reaction Confirmation”. In: *Analytical Chemistry* 77.1 (2005), pp. 284–289.

[127] D.D. Williams and C.L. Turnbough. “Surface Layer Protein EA1 Is Not a Component of Bacillus anthracis Spores but Is a Persistent Contaminant in Spore Preparations”. In: *Journal of Bacteriology* 186.2 (2004), pp. 566–569.

[128] K. Mullis et al. “Specific Enzymatic Amplificatino of DNA In Vitro: The Polymerase Chain Reaction”. In: *Cold Spring Harb Symp Quant Biol.* 1986, pp. 263–273.

[129] A. Niemz, T.M. Ferguson, and D.S. Boyle. “Point-of-care nucleic acid testing for infectious diseases”. In: *Trends in Biotechnology* 29.5 (2011), pp. 240 –250.

[130] L. Garibyan and N. Avashia. “Polymerase Chain Reaction”. In: *J Invest Dermatol* 133 (2013).

[131] H. Wang et al. “Simultaneous Capture, Detection, and Inactivation of Bacteria as Enabled by a Surface-Enhanced Raman Scattering Multifunctional Chip”. In: *Angewandte Chemie International Edition* 54.17 (), pp. 5132–5136.

[132] C. Ash and M.D. Collins. “Comparative analysis of 23S ribosomal RNA gene sequences of Bacillus anthracis and emetic Bacillus cereus determined by PCR-direct sequencing”. In: *FEMS Microbiology Letters* 94.1-2 (1992), pp. 75–80.

[133] K.S. Blackwood et al. “Reassessment of Sequence-Based Targets for Identification of Bacillus Species”. In: *Journal of Clinical Microbiology* 42.4 (2004), pp. 1626–1630.

[134] P. Keim et al. “The genome and variation of Bacillus anthracis”. In: *Molecular Aspects of Medicine* 30.6 (2009), pp. 397 –405.

[135] C. Ryu et al. "Sensitive and Rapid Quantitative Detection of Anthrax Spores Isolated from Soil Samples by Real-Time PCR". In: *Microbiology and Immunology* 47.10 (2003), pp. 693–699.

[136] C.T. Sacchi et al. "Sequencing of 16S rRNA Gene: A Rapid Tool for Identification of *Bacillus anthracis*". In: *Emerg Infect Dis* 8.10 (2002), pp. 1117–23.

[137] W. Hurtle et al. "Detection of the Bacillus anthracis gyrA Gene by Using a Minor Groove Binder Probe". In: *Journal of Clinical Microbiology* 42.1 (2004), pp. 179–185.

[138] T. Notomi et al. "Loop-mediated isothermal amplification of DNA". In: *Nucleic Acids Research* 28.12 (2000), e63.

[139] B. hatano et al. "LAMP Using a Disposable Pocket Warmer for Anthrax Detection, a Highly Mobile and Reliable Method for Anti-Bioterrorism". In: *Jpn.J.Infect.Dis.* 63 (2010), pp. 36–40.

[140] *Schematic drawing of PCR cycle*. Wikimedia. 2014. URL: `https://en.wikipedia.org/wiki/Polymerase_chain_reaction#/media/File:Polymerase_chain_reaction.svg` (visited on Apr. 5, 2016).

[141] D. Ivnitski et al. "Biosensors for detection of pathogenic bacteria". In: *Biosens Bioelectron* 14 (1999), pp. 599–624.

[142] M.A. Cooper. "Label-free screening of bio-molecular interactions". In: *Anal Bioanal Chem* 377.5 (Nov. 2003), pp. 834–842.

[143] X. Zhang et al. "Rapid Detection of an Anthrax Biomarker by Surface-Enhanced Raman Spectroscopy". In: *Journal of the American Chemical Society* 127.12 (2005). PMID: 15783231, pp. 4484–4489.

[144] Y. Li, W.A. Dick, and O.H. and Touvinen. "Fluorescence microscopy for visualization of soil microorganisms — a review". In: *Biol Fertility Soils* (2004).

[145] E. Barsoukov and J.R. Macdonald. "Impedance spectroscopy Theory". In: Hoboken, New Jersey, USA: John Wiley & Sons Ltd., 2005. Chap. Experiment and Application.

[146] Z. Muhhamemad-Tahir and E.C. Alocilja. "A conductometric biosensor for biosecurity." In: *Biosens Bioelectron* 18 (2003), pp. 813–819.

[147] Y. Haik et al. "Principles of bacteria detection". In: ed. by M. Zourob, S. Elwary, and A. Turner. 1st. New York, USA: Springer, 2008. Chap. Magnetic techniques for Rapid Detection of Pathogens, pp. 415–458.

[148] J. Gao, H. Gu, and B. Xu. "Multifunctional Magnetic Nanoparticles: Design, Synthesis, and Biomedical Applications". In: *Accounts of Chemical Research* 42.8 (2009), pp. 1097–1107.

[149] D.L. Gatto-Menking et al. “Sensitive detection of biotoxoids and bacterial spores using an immunomagnetic electrochemiluminescence sensor”. In: *Biosensors and Bioelectronics* 10.6 (1995), pp. 501 –507.

[150] R. Zhou, P. Wang, and H.-C. Chang. “Bacteria capture, concentration and detection by alternating current dielectrophoresis and self-assembly of dispersed single-wall carbon nanotubes”. In: *Electrophoresis* 27.7 (2006), pp. 1376–1385.

[151] P. Ohlsson et al. “Integrated Acoustic Separation, Enrichment, and Microchip Polymerase Chain Reaction Detection of Bacteria from Blood for Rapid Sepsis Diagnostics”. In: *Analytical Chemistry* 88.19 (2016), pp. 9403–9411.

[152] M. Zourob et al. “Optical Leaky Waveguide Sensor for Detection of Bacteria with Ultrasound Attractor Force”. In: *Analytical Chemistry* 77.19 (2005), pp. 6163–6168.

[153] Z. Mandralis et al. “Enhanced synchronized ultrasonic and flow-field fractionation of suspensions”. In: *Ultrasonics* 32.2 (1994), pp. 113 – 122.

[154] H. Bohm et al. “Viability of plant cell suspensions exposed to homogenous ultrasonic fields of different energy density and wave type”. In: *Ultrasonics* 38 (2000), pp. 629–632.

[155] J.J. Hawkes, M.S. Limaye, and W.T. Coakley. “Filtration of bacteria and yeast by ultrasound-enhanced sedimentation”. In: *Journal of Applied Microbiology* 82.1 (1997), pp. 39–47.

[156] D. Carugo et al. “A thin-reflector microfluidic resonator for continuous-flow concentration of microorganisms: a new approach to water quality analysis using acoustofluidics”. In: *Lab Chip* 14 (Aug. 2014), pp. 3830–3842.

[157] Y. Ai, C.K. Sanders, and B.L. Marrone. “Separation of Escherichia coli Bacteria from Peripheral Blood Mononuclear Cells Using Standing Surface Acoustic Waves”. In: *Analytical Chemistry* 85.19 (2013), pp. 9126–9134.

[158] M. Antfolk et al. “Focusing of sub-micrometer particles and bacteria enabled by two-dimensional acoustophoresis”. In: *Lab Chip* 14 (15 2014), pp. 2791–2799.

[159] B. Hammarström, T. Laurell, and J. Nilsson. “Seed particle-enabled acoustic trapping of bacteria and nanoparticles in continuous flow systems”. In: *Lab Chip* 12 (21 2012), pp. 4296–4304.

[160] P. Jenkins, R.A. Barnes, and W.T. Coakley. “Detection of meningitis antigens in buffer and body fluids by ultrasound-enhanced particle agglutination”. In: *Journal of Immunological Methods* 205.2 (1997), pp. 191 –200.

[161] M.A. Sobanski et al. "Ultrasound enhanced detection of individual meningococcal serogroups by latex immunoassay". In: *Journal of Clinical Pathology* 55.1 (2002), pp. 37–40.

[162] S.J. Gray et al. "Ultrasound-Enhanced Latex Immunoagglutination and PCR as Complementary Methods for Non-Culture-Based Confirmation of Meningococcal Disease". In: *Journal of Clinical Microbiology* 37.6 (1999), pp. 1797–1801.

[163] A.W. Poon, C.S. Goodman, and R.J. Rubin. "In vitro and skin testing for allergy: comparable clinical utility and costs". In: *The American journal of managed care* 4.7 (July 1998), 969—985.

[164] S.H. Sicherer and H.A. Sampson. "Food allergy: A review and update on epidemiology, pathogenesis, diagnosis, prevention, and management". In: *Journal of Allergy and Clinical Immunology* 141 (1 Jan. 2018), pp. 41–58.

[165] P. Demoly et al. "International Consensus on drug allergy". In: *Allergy* 69.4 (), pp. 420–437.

[166] A. Muraro et al. "EAACI Food Allergy and Anaphylaxis Guidelines: diagnosis and management of food allergy". In: *Allergy* 69.8 (), pp. 1008–1025.

[167] K. Brockow et al. "General considerations for skin test procedures in the diagnosis of drug hypersensitivity". In: *Allergy* 57.1 (), pp. 45–51.

[168] F.M. Khan et al. "Basophil activation test compared to skin prick test and fluorescence enzyme immunoassay for aeroallergen-specific Immunoglobulin-E". In: *Allergy, Asthma & Clinical Immunology* 8.1 (Jan. 2012), p. 1.

[169] "Guidelines for the Diagnosis and Management of Food Allergy in the United States: Report of the NIAID-Sponsored Expert Panel". In: *Journal of Allergy and Clinical Immunology* 126.6, Supplement (2010). Guidelines for the Diagnosis and Management of Food Allergy in the United States: Report of the NIAID-Sponsored Expert Panel, S1 –S58.

[170] D.L. Neuman-Sunshine et al. "The natural history of persistent peanut allergy". In: *Annals of Allergy, Asthma & Immunology* 108.5 (2012), 326 –331.e3.

[171] D.M. Fleischer and A.W. Burks. "Pitfalls in Food Allergy Diagnosis: Serum IgE Testing". In: *The Journal of Pediatrics* 166.1 (2015), pp. 8 –10. ISSN: 0022-3476.

[172] H.A. Sampson. "Food allergy. Part 2: Diagnosis and management". In: *Journal of Allergy and Clinical Immunology* 103.6 (1999), pp. 981 –989.

[173] P. Bousquet et al. "Provocation Tests in Diagnosing Drug Hypersensitivity". In: *Current Pharmaceutical Design* 14.27 (2008), pp. 2792–2802.

[174] "Drug Allergy: An Updated Practice Parameter". In: *Annals of Allergy, Asthma & Immunology* 105.4 (2010), 259 –273.e78.

[175] R. Mirakian et al. "BSACI guidelines for the management of drug allergy". In: *Clinical & Experimental Allergy* 39.1 (), pp. 43–61.

[176] W. Aberer et al. "Drug provocation testing in the diagnosis of drug hypersensitivity reactions: general considerations". In: *Allergy* 58.9 (), pp. 854–863.

[177] E.C. McGowan and S. Saini. "Update on the Performance and Application of Basophil Activation Tests". In: *Current Allergy and Asthma Reports* 13.1 (Feb. 2013), pp. 101–109.

[178] M. L. Sanz et al. "Flow cytometric basophil activation test by detection of CD63 expression in patients with immediate-type reactions to betalactam antibiotics". In: *Clinical & Experimental Allergy* 32.2 (), pp. 277–286.

[179] S. Sato et al. "Basophil Activation Marker CD203c Is Useful in the Diagnosis of Hen's Egg and Cow's Milk Allergies in Children". In: *Int Arch Allergy Immunol* 152 (Suppl 1 June 2010), pp. 54–61.

[180] L. Heinzerling et al. "The skin prick test – European standards". In: *Clinical and Translational Allergy* 3.1 (Feb. 2013), p. 3.

[181] A. Verstege et al. "The predictive value of the skin prick test weal size for the outcome of oral food challenges". In: *Clinical & Experimental Allergy* 35.9 (), pp. 1220–1226.

[182] S. Celik-Bilgili et al. "The predictive value of specific immunoglobulin E levels in serum for the outcome of oral food challenges". In: *Clinical & Experimental Allergy* 35.3 (), pp. 268–273.

[183] S. Sato, N. Yanagida, and M. Ebisawa. "How to diagnose food allergy". In: *Current Opinion in Allergy and Clinical Immunology* 18.3 (June 2018), pp. 214–221.

[184] H.A. Sampson et al. "Standardizing double-blind, placebo-controlled oral food challenges: American Academy of Allergy, Asthma & Immunology–European Academy of Allergy and Clinical Immunology PRACTALL consensus report". In: *Journal of Allergy and Clinical Immunology* 130.6 (2012), pp. 1260 –1274.

[185] P. Demoly et al. "Determining the negative predictive value of provocation tests with beta-lactams". In: *Allergy* 65.3 (), pp. 327–332.

[186] H.A. Sampson and D.G. Ho. "Relationship between food-specific IgE concentrations and the risk of positive food challenges in children and adolescents". In: *Journal of Allergy and Clinical Immunology* 100.4 (1997), pp. 444 –451.

[187] S. Allan Bock. "Prospective Appraisal of Complaints of Adverse Reactions to Foods in Children During the First 3 Years of Life". In: *Pediatrics* 79.5 (1987), pp. 683–688.

[188] A.F. Santos et al. "Basophil activation test discriminates between allergy and tolerance in peanut-sensitized children". In: *Journal of Allergy and Clinical Immunology* 134.3 (2014), pp. 645 –652.

[189] A. Rubio et al. "Benefit of the basophil activation test in deciding when to reintroduce cow's milk in allergic children". In: *Allergy* 66.1 (), pp. 92–100.

[190] P. Valenti et al. "Lactoferrin Decreases Inflammatory Response by Cystic Fibrosis Bronchial Cells Invaded with Burkholderia Cenocepacia Iron-Modulated Biofilm". In: *International Journal of Immunopathology and Pharmacology* 24.4 (2011), pp. 1057–1068.

[191] D.D. Rhoads, R.D. Wolcott, and S.L. Percival. "Biofilms in wounds: management strategies". In: *Journal of Wound Care* 17.11 (2008), pp. 502–508.

[192] M.C.B. Ammons, L.S. Ward, and G.A. James. "Anti-biofilm efficacy of a lactoferrin/xylitol wound hydrogel used in combination with silver wound dressings". In: *International Wound Journal* 8.3 (), pp. 268–273.

[193] D. Kim et al. "Clinical Assessment of a Biofilm-disrupting Agent for the Management of Chronic Wounds Compared With Standard of Care: A Therapeutic Approach". In: *Wounds: a compendium of clinical research and practice* 30 (5 May 2018), pp. 120–130.

[194] James A. Shapiro. "THINKING ABOUT BACTERIAL POPULATIONS AS MULTICELLULAR ORGANISMS". In: *Annual Review of Microbiology* 52.1 (1998), pp. 81–104.

[195] W C Fuqua, S C Winans, and E P Greenberg. "Quorum sensing in bacteria: the LuxR-LuxI family of cell density-responsive transcriptional regulators." In: *Journal of Bacteriology* 176.2 (1994), pp. 269–275.

[196] B. LaSarre and M.J. Federle. "Exploiting Quorum Sensing To Confuse Bacterial Pathogens". In: *Microbiology and Molecular Biology Reviews* 77.1 (2013), pp. 73–111.

[197] M. Cardinal et al. "Serial surgical debridement: A retrospective study on clinical outcomes in chronic lower extremity wounds". In: *Wound Repair and Regeneration* 17.3 (), pp. 306–311.

[198] C.M. Waters et al. "Enzymatic degradation of in vitro *Staphylococcus aureus* biofilms supplemented with human plasma". In: *Infect Drug Resist* 9 (Apr. 2016), pp. 71–78.

[199] David Lebeaux, Jean-Marc Ghigo, and Christophe Beloin. "Biofilm-Related Infections: Bridging the Gap between Clinical Management and Fundamental Aspects of Recalcitrance toward Antibiotics". In: 78.3 (2014), pp. 510–543.

[200] J.C. Carmen et al. "Ultrasonic-enhanced gentamicin transport through colony biofilms of Pseudomonas aeruginosa and Escherichia coli". In: *Journal of Infection and Chemotherapy* 10.4 (2004), pp. 193 –199. ISSN: 1341-321X.

[201] A.M. Rediske et al. "Ultrasonic Enhancement of Antibiotic Action on Escherichia coli Biofilms: an In Vivo Model". In: *Antimicrobial Agents and Chemotherapy* 43.5 (1999), pp. 1211–1214.

[202] C.M. Runyan et al. "Low-frequency ultrasound increases outer membrane permeability of *Pseudomonas aeruginosa*". In: *The Journal of General and Applied Microbiology* 52.5 (2006), pp. 295–301.

[203] W.G. Pitt and S.A. Ross. "Ultrasound Increases the Rate of Bacterial Cell Growth". In: *Biotechnology Progress* 19.3 (2003), pp. 1038–1044.

[204] Z. Qian, P. Stoodley, and W.G. Pitt. "Effect of low-intensity ultrasound upon biofilm structure from confocal scanning laser microscopy observation". In: *Biomaterials* 17.20 (1996), pp. 1975 –1980.

[205] J. Liu, T.N. Lewis, and M.R. Prausnitz. "Non-Invasive Assessment and Control of Ultrasound-Mediated Membrane Permeabilization". In: *Pharmaceutical Research* 15.6 (June 1998), pp. 918–924.

[206] Y. Cai et al. "A Review of the Combination Therapy of Low Frequency Ultrasound with Antibiotics". In: *BioMed Research International* 2017, 2317846 (2017).

[207] W. Jiang et al. "Low-intensity pulsed ultrasound treatment improved the rate of autograft peripheral nerve regeneration in rat". In: *Scientific Reports* 6.22773 (2016).

[208] T. Nishikawa et al. "A study of the efficacy of ultrasonic waves in removing biofilms". In: *Gerodontology* 27.3 (2010), pp. 199–206.

[209] M. Alhede et al. "Phenotypes of Non-Attached Pseudomonas aeruginosa Aggregates Resemble Surface Attached Biofilm". In: *PLOS ONE* 6.11 (Nov. 2011), pp. 1–12. URL: `https://doi.org/10.1371/journal.pone.0027943`.

[210] S. Carding et al. "Dysbiosis of the gut microbiota in disease". In: *Microbial Ecology in Health and Disease* 26.1 (2015), p. 26191.

[211] P.R. Birkin, D.G. Offin, and T.G. Leighton. "An activated fluid stream – New techniques for cold water cleaning". In: *Ultrasonics Sonochemistry* 29 (2016), pp. 612 –618. ISSN: 1350-4177.

[212] R.P. Howlin et al. "Removal of Dental Biofilms with an Ultrasonically Activated Water Stream". In: *Journal of Dental Research* 94.9 (2015), pp. 1303–1309.

[213] P. R. Birkin et al. "Cold water cleaning of brain proteins, biofilm and bone – harnessing an ultrasonically activated stream". In: *Phys. Chem. Chem. Phys.* 17 (32 2015), pp. 20574–20579.

[214] N. He et al. "Enhancement of Vancomycin Activity against Biofilms by Using Ultrasound-Targeted Microbubble Destruction". In: 55.11 (2011), pp. 5331–5337. DOI: 10.1128/AAC.00542-11.

[215] Y. Dong et al. "Synergy of ultrasound microbubbles and vancomycin against Staphylococcus epidermidis biofilm". In: *Journal of Antimicrobial Chemotherapy* 68.4 (2013), pp. 816–826.

[216] R.K. Kasimanickam et al. "Prevention and treatment of biofilms by hybrid- and nanotechnologies". In: *Int J Nanomedicine* 8 (2013), pp. 2809–19.

[217] E. Ronan et al. "USMB-induced synergistic enhancement of aminoglycoside antibiotics in biofilms". In: *Ultrasonics* 69 (2016), pp. 182 –190.

[218] D. Carugo and P. Glynne-Jones. *Online industrial water quality analysis system for rapid and accurate detection of pathogens*. Tech. rep. Aquality Project, 2012.

[219] M. Hill, Y. Shen, and J.J. Hawkes. "Modelling of layered resonators for ulrasonic separation". In: *Ultrasonics* 40 (1-8 2002).

[220] M. Hill and R.J.K Wood. "Modelling in the design of flow-through ultrasonic separator". In: *Ultrasonics* 38 (2000), pp. 662–665.

[221] Onda Corporation. *Acoustic properties of solids*. Apr. 2003. URL: http://www.ondacorp.com/images/Solids.pdf (visited on July 18, 2016).

[222] Onda Corporation. *Acoustic properties of plastics*. Apr. 2003. URL: http://www.ondacorp.com/images/Plastics.pdf (visited on July 18, 2016).

[223] Corning. *MACOR - Machinable glass ceramic for industrial applications*. 2012. URL: https://www.corning.com/media/worldwide/csm/documents/71759a443535431395eb34ebead091cb.pdf (visited on June 24, 2018).

[224] AZO Materials and Granta Design Ltd. *Cellulose Acetate - material properties*. June 2002. URL: https://www.azom.com/properties.aspx?ArticleID=1461 (visited on July 14, 2018).

[225] Lingbo Kong et al. "Monitoring the Kinetics of Uptake of a Nucleic Acid Dye during the Germination of Single Spores of *Bacillus* Species". In: *Anal. Chem.* 82.20 (Oct. 2010), pp. 8717–8724.

[226] Katerina Ragkousi et al. “Analysis of Nucleoid Morphology during Germination and Outgrowth of Spores of *Bacillus* Species”. In: *J. Bacteriol.* 182.19 (Oct. 2000), pp. 5556–5562.

[227] A. Mathys et al. “Flow cytometric assessment of *Bacillus* spore response to high pressure and heat”. In: *Innov Food Sci Emerg Technol* 8 (2007), pp. 519–527.

[228] A. Magge et al. “Analysis of dye binding by and membrane potential in spores of Bacillus species”. In: *Journal of Applied Microbiology* 106.3 (2009), pp. 814–824.

[229] ThermoFisher Scientific. *Fluorescein (FITC)*. URL: https://www.thermofisher.com/uk/en/home/life-science/cell-analysis/fluorophores/fluorescein.html# (visited on July 16, 2018).

[230] Sigma-Aldrich. *Auramine O - Product information*. URL: https://www.sigmaaldrich.com/content/dam/sigma-aldrich/docs/Sigma/Product_Information_Sheet/a9655pis.pdf (visited on July 16, 2018).

[231] ThermoFisher Scientific. *Alexa Fluor 555 Dye*. URL: https://www.thermofisher.com/uk/en/home/life-science/cell-analysis/fluorophores/alexa-fluor-555.html# (visited on July 16, 2018).

[232] *Nexterion Slide E Protein Application*. 1.3. Schott. Oct. 2017. URL: https://www.schott.com/nexterion/english/products/functional-coatings/epoxysilane-coating.html.

[233] *Nexterion Slide H Protein Application*. 3.0. Schott. Oct. 2017. URL: https://www.schott.com/nexterion/english/products/functional-coatings/3d-hydrogel-coating.html.

[234] Tetracore. *Rabbit Anti-B.globigii IgG*. URL: http://www.tetracore.com/antibody-products/abinfo/TC_7009.html (visited on July 24, 2018).

[235] M. McDonnel, P. Glynne-Jones, and M. Hill. *Target capture rate*. Personal Comunication. Sept. 2014.

[236] A.D. Edelstein et al. “Advanced methods of microscope control using μManager software”. In: *J Biol Methods* 1.2 (2014), e10.

[237] B. Massey. *Mechanics of fluids*. Special Indian Edition, 8th. London: Taylor and Francis, 2010. Chap. 6, p. 213.

[238] M. Carrera, R.O. Zandomeni, and J.-L. Sagripanti. “Wet and dry density of *Bacillus anthracis* and other *Bacillus* species”. In: *Journal of Applied Microbiology* 105.1 (2008), pp. 68–77.

[239] Water Dynamic and Kinematic Viscosity. *Rabbit Anti-B.globigii IgG*. URL: https://www.engineeringtoolbox.com/water-dynamic-kinematic-viscosity-d_596.html (visited on Jan. 6, 2019).

[240] B. Massey. *Mechanics of fluids*. Special Indian Edition, 8th. London: Taylor and Francis, 2010. Chap. 6, pp. 191–195.

[241] K Haisch et al. "Purification of morphologically and functionally intact human basophils to near homogeneity". In: *Journal of Immunological Methods* 226.1 (1999), pp. 129 –137.

[242] S. Sekula-Neuner et al. "Allergen Arrays for Antibody Screening and Immune Cell Activation Profiling Generated by Parallel Lipid Dip-Pen Nanolithography". In: *Small* 8.4 (2012), pp. 585–591.

[243] R. Kumar et al. "Click-Chemistry Based Allergen Arrays Generated by Polymer Pen Lithography for Mast Cell Activation Studies". In: *Small* 12.38 (2016), pp. 5330–5338.

[244] P. Bohec et al. "Acoustophoretic purification of platelets: Feasibility and impact on platelet activation and function". In: *Platelets* 0.0 (2017), pp. 1–7.

[245] UK Department of Health and Social Care. *UK 5 Year Antimicrobial Resistance (AMR) Strategy 2013-2018, Annual progress report*. 2016. URL: `https://www.gov.uk/government/collections/antimicrobial-resistance-amr-information-and-resources` (visited on Jan. 14, 2019).

[246] NICE guideline. *Diabetic foot problems: prevention and management*. Aug. 2015. URL: `https://www.nice.org.uk/guidance/ng19/chapter/introduction` (visited on Jan. 14, 2019).

[247] N. Høiby et al. "Antibiotic resistance of bacterial biofilms". In: *International Journal of Antimicrobial Agents* 35.4 (2010), pp. 322 –332.

[248] E.B.M. Breidenstein, C. de la Fuente-Núñez, and R.E.W. Hancock. "*Pseudomonas aeruginosa*: all roads lead to resistance". In: *Trends in Microbiology* 19.8 (2011), pp. 419 –426.

[249] Dario Carugo et al. "Biologically and acoustically compatible chamber for studying ultrasound-mediated delivery of therapeutic compounds". In: *Ultrasound in Med. & Bio.* 41.7 (2015), pp. 1927–1937.

[250] N. de Jong et al. "Ultrasonic characterization of ultrasound contrast agents". In: *Medical & Biological Engineering & Computing* 47.8 (Aug. 2009), pp. 861–873.

[251] Alexander A. Doinikov, Jillian F. Haac, and Paul A. Dayton. "Resonance frequencies of lipid-shell microbubbles in the regime of nonlinear oscillations". In: *Ultrasonics* 49.2 (2009), pp. 263 –268.

[252] G.D. Ludwig. "The Velocity of Sound through Tissues and the Acoustic Impedance of Tissues". In: *The Journal of the Acoustical Society of America* 22.6 (1950), pp. 862–866.

[253] A. Saïed et al. "Spatial distribution of anisotropic acoustic impedance assessed by time-resolved 50-MHz scanning acoustic microscopy and its relation to porosity in human cortical bone". In: *Bone* 43.1 (2008), pp. 187 –194.

[254] H. Sievänen et al. "Ultrasound Velocity and Cortical Bone Characteristics In Vivo". In: *Osteoporosis International* 12.5 (May 2001), pp. 399–405.

[255] S. Dicker et al. "Determination of microbubble cavitation threshold pressure as function of shell chemistry". In: *Bubble Science, Engineering & Technology* 2.2 (2010), pp. 55–64.

[256] J. Owen et al. "The Role of PEG-40-stearate in the Production, Morphology, and Stability of Microbubbles". In: *Langmuir Article ASAP* ().

[257] R.H. Abou-Saleh et al. "Poly(ethylene glycol) Lipid-Shelled Microbubbles: Abundance, Stability, and Mechanical Properties". In: *Langmuir* 30.19 (2014), pp. 5557–5563.

[258] J. Chirife et al. "In vitro antibacterial activity of concentrated polyethylene glycol 400 solutions." In: *Antimicrobial agents and chemotherapy* 24.3 (1983), pp. 409–412.

[259] Joshua Owen et al. "A versatile method for the preparation of particle-loaded microbubbles for multimodality imaging and targeted drug delivery". In: *Drug Delivery and Translational Research* 8.2 (Apr. 2018), pp. 342–356.

[260] M. Jamal et al. "Bacterial biofilm and associated infections". In: *Journal of the Chinese Medical Association* 81.1 (2018), pp. 7 –11. ISSN: 1726-4901.

[261] "Section 7—Discussion of the Mechanical Index and Other Exposure Parameters". In: *J Ultrasound Med* 19.2 (2000), pp. 143–168.

[262] Christy K. Holland and Robert E. Apfel. "An improved theory for the prediction of microcavitation thresholds". In: *IEEE Transactions on Ultrasonics, Ferroelectrics, and Frequency Control* 36.2 (Mar. 1989), pp. 204–208.

[263] D. Carugo et al. "Modulation of the molecular arrangement in artificial and biological membranes by phospholipid-shelled microbubbles". In: *Biomaterials* 113 (2017), pp. 105 –117.

[264] A.A. Miles, S.S. Misra, and J.O. Irwin. "The estimation of the bactericidal power of the blood". In: *Epidemiology & Infection* 38.6 (1938), pp. 732–749.

[265] David M. Lane. *Online Statistics Education: A Multimedia Course of Study*. 2015. URL: `http://onlinestatbook.com/2/summarizing_distributions/transformations.html` (visited on June 7, 2018).

[266] Yoichiro Matsumoto and Shin Yoshizawa. "Behaviour of a bubble cluster in an ultrasound field". In: *International Journal for Numerical Methods in Fluids* 47.6-7 (), pp. 591–601.

[267] E.A. Brujan et al. "The final stage of the collapse of a cloud of bubbles close to a rigid boundary". In: *Ultrasonics Sonochemistry* 18.1 (2011), pp. 59 –64.

[268] Z. Xu et al. "Effects of acoustic parameters on bubble cloud dynamics in ultrasound tissue erosion (histotripsy)". In: *The Journal of the Acoustical Society of America* 122.1 (2007), pp. 229–236.

[269] A.E. LaBauve and M.J. Wargo. "Growth and Laboratory Maintenance of *Pseudomonas aeruginosa*". In: *Curr Protoc Microbiol* (May 2012).

[270] Anthony Eller. "Force on a Bubble in a Standing Acoustic Wave". In: *The Journal of the Acoustical Society of America* 43.1 (1968), pp. 170–171.

[271] IUPHAR/BPS Guide to PHARMACOLOGY. *Gentamicin compound summary.* URL: `https://pubchem.ncbi.nlm.nih.gov/compound/gentamicin#section=Top` (visited on Dec. 6, 2018).

[272] Nicolas Barraud et al. "Involvement of Nitric Oxide in Biofilm Dispersal of *Pseudomonas aeruginosa*". In: *J Bacteriol* 188.21 (Nov. 2006), pp. 7344–7353.